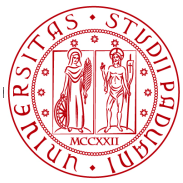

UNIVERSITÀ
DEGLI STUDI
DI PADOVA

Sede Amministrativa: Università degli Studi di Padova

Dipartimento di Scienze Chimiche

SCUOLA DI DOTTORATO DI RICERCA IN SCIENZE MOLECOLARI
INDIRIZZO: SCIENZE CHIMICHE
CICLO XXIII

AGING OF CULTURAL HERITAGE MATERIALS: A PHYSICO-CHEMICAL APPROACH TO CONSERVATION SCIENCE.
STUDIES ON PAPER, PARCHMENT, PIGMENTS AND DYES

Direttore della Scuola: Ch.mo Prof. Maurizio Casarin
Coordinatore d'indirizzo: Ch.mo Prof. Maurizio Casarin
Supervisore: Ch.ma Prof.ssa Marina Brustolon

Dottoranda : Daria Confortin

One day the Son of the Merchant came to the Prince, and said boldly:
"Comrade, my studies are over.
I am now setting out on my travels to seek my fortunes on the sea.
I have come to bid you good-bye."
-The Kingdom of cards, Rabindranath Tagore-

INDEX

ABSTRACT

In this doctoral dissertation, photochemical and, in some cases, thermal aging (natural and accelerated) of materials from cultural heritage (paper, parchment, linseed oil paints, pigments and dyes) are studied with a number of both destructive and non-destructive experimental techniques such as Electron Paramagnetic Resonance (EPR)[1], Nuclear Magnetic Resonance-MObile Universal Surface Explorer (NMR-MOUSE)[2], High Performance Liquid Chromatography-Photo Diode Array (HPLC-PDA)[3], Liquid Chromatography-Mass Spectrometry (LC-MS)[4], Fiber Optics Reflectance Spectroscopy (FORS)[3,1], Attenuated Total Reflectance-Infrared spectroscopy (ATR-IR)[5], micro-fading-meter[3] and Xenotest exposure device[3].

My research activity was carried out in collaboration with the Chemical Sciences Department of the University of Padua, the Netherlands Institute for Cultural Heritage (Amsterdam) and the Image Permanence Institute (Rochester Institute of Technology, NY) and thanks to the accessibility to the Van Gogh Museum collection.

In chapters one and two, an introduction to the history of colorants and to colorimetry and a description of the degradation reactions induced by light and by common gaseous pollutants are presented.

In chapters three, four and five, the results of my research activity are analyzed. In particular, in chapter three of my doctoral dissertation, Writing Materials, the dependence of chemical-physical properties of paper and parchment on aging is investigated with an NMR device called MOUSE. NMR-MOUSE is an instrument of great potential in the field of conservation science because it enables the measurement of nuclear relaxation times of various materials in situ and without sampling. Nuclear relaxation times are directly related to the chemical-physical nature of materials and were proved to be markers of the state of conservation of paper. As for parchment, nuclear relaxation times enabled to distinguish between samples from the XX century and XVIII century. For both materials, different environments for water (bound or free molecules) could be recognized.

---

[1] Instrument belongings to the EPR group (Prof. Marina Brustolon), Departement of Chemical Sciences, University of Padua.
[2] Instrument belongings to the University of Padua (Centro di Servizi Interdipartimentale, ex CUGAS).
[3] Instrument belongings to the Netherlands Institute for Cultural Heritage (ICN, Amsterdam).
[4] Instrument belongings to the group of analytical chemistry (Prof. Franco Magno), Departement of Chemical Sciences, University of Padua.
[5] Instrument belongings to Departement of Chemical Sciences, University of Padua.

In chapter four, Pigments and Dyes, a number of EPR spectra of known and unknown pigments is provided. In addition, the effect of different pigments or dyes on polymerization of linseed oil paints is revealed with NMR-MOUSE. EPR spectroscopy was demonstrated to be effective in discriminating different pigments or classes of pigments with micro-invasive sampling. Relaxation times of linseed oil paints were demonstrated to be sensitive to the presence of pigments and an interpretation of the results in terms of different rates or degree of polymerization was given.

In chapter five, Dyes in Aqueous Solution and on Paper: Discoloration and Fading of Crystal Violet, which represents the main body of my doctoral research activity, an extensive analysis (HPLC-PDA, LC-MS, FORS, EPR, micro-fading assessments, Xenotest exposure device) of the photo-fading and thermal aging of an early synthetic dye (Crystal Violet) in aqueous solution and on paper is presented. The interest on the subject stems from the discoloration occurred on a group of Van Gogh drawings and letters all produced in 1888 in Arles and all made with a type of purple ink which was demonstrated to contain crystal violet and other structurally related derivatives (triarylmethane dyes). In particular, a seemingly brown drawing belonging to this group and entitled Montmajour (Arles, 1888. Van Gogh Museum) shows purple shades on the edges where the ink has been protected from light under the frame.

Another example, although not belonging to the Arles group, is a menu (Paris, 1886. Van Gogh Museum) drawn and written by Van Gogh with purple ink, as can be inferred from a reproduction made in 1958. Nevertheless, in a picture of the menu taken in 2001 it can be seen that the writings and part of the drawings had disappeared entirely. Interestingly, although FORS analysis revealed the presence of ink containing triarylmethane dyes, in this case no brown discoloration was visible.

With the aim of shedding light on aging mechanisms and discoloration of inks containing crystal violet on paper, accelerated aging experiments were conducted for pure crystal violet both in aqueous solution and on paper. Various experimental parameters were taken into consideration: the spectral range of the light source (UV or Vis), the paper substrate (pure cellulose paper, lignin paper, printing paper), temperature and the presence or absence of oxygen during irradiation.

Moreover, a purple ink containing methyl violet (a mixture of crystal violet and some of its demethylated derivatives) was reconstructed (by Judith Geerts, student of the University of Amsterdam, according to a recipe by Sigmund Lehner, 1909) and its

thermal (100 °C) and photo fading (UV light and natural sun light) was studied on different paper substrates (cellulose paper, lignin paper and protein-sized paper). The effect of various ink additives (gum arabic, sucrose and oxalic acid), of Fe(III) (as an example of photo-catalyst often present as an impurity in paper) and of common gaseous pollutants such as NO_2 and O_3, on the color of dyed (or written) samples of paper was also taken into consideration.

A group of ten historical samples of methyl violet from the ICN dye collection was also analyzed with HPLC-PDA, with the aim of comparing actual dye samples with both the model samples described in this doctoral dissertation and with the purple ink of the 'Montmajour' drawing (Arles, 1888. Van Gogh Museum).

Successively, some dyes and pigments (cochineal ink, indigo blue ink, indigo carmine, copper logwood synthesized from $CuSO_4$ or $Cu(AcO)_2$ and chromium logwood) used in the XIX century as alternative ingredients for purple inks were deposited on paper and artificially aged with UV light or heat. A colorimetric analysis of the samples was conducted before and after aging.

Finally, a group of letters from the XIX century (Birgit Reissland, private collection) was analyzed with FORS and the presence of dyes closely related to crystal violet was detected.

The analysis presented in chapter five of this doctoral dissertation has thus demonstrated that the synthetic dye methyl violet was widely used after its introduction to the market in 1866. Moreover, the poor lightfastness of crystal violet was explained to be due to demethylation and oxidation reactions. A series of degradation products was identified with HPLC-PDA and LC-MS both for crystal violet in aqueous solution and on paper after exposure to UV in the presence of oxygen. HPLC-PDA analysis of a sample of purple ink from the 'Montmajour' drawing (Arles, 1888. Van Gogh Museum) was in good agreement with the results of these model samples. The complete fading observed on the Menu was reproduced and explained as due to light exposure (UV or visible).

According to my experimental results, the first stage of the degradation mechanism consists of a series of demethylation reactions eventually leading to pararosaniline, a red dye corresponding to fully demethylated crystal violet. Afterwards, oxidation at the central carbon atom forms colorless (or slightly yellow) ketones responsible both for the fading of crystal violet and for a sensitization effect on dye degradation. The presence

of oxidized derivatives of Crystal Violet has also been demonstrated. As for the position of the oxygen attack, it has been hypothesized the formation of N-oxides of crystal violet or of its demethylated derivatives.

Heat (50 °C, 40% relative humidity) was shown to play a minor role in the fading of crystal violet on paper whereas visible light alone was enough for the dye to fade visibly. Interestingly enough, considering the fact that anoxic protection is in use, crystal violet did fade on paper following the exposure to UV light in the absence of oxygen as well.

The substrate (cellulose paper, lignin paper or printing paper), although it was not responsible for the nature of (colored) degradation products, played a role in determining the relative amounts products formed and the final color of the dye layer.

Interestingly, both artificial aging (UV light) and natural aging (sun light) of samples of paper dyed with an ink containing methyl violet and other additives led to different colors than in the presence of pure crystal violet. In particular, the colors obtained were brownish-grey and bluish-grey, in the presence or in the absence of Fe(III) respectively. Moreover, the addition of Fe(III) or of ink additives (such as sucrose and oxalic) alone to paper, caused the formation of yellow or brown discoloration after exposure to sunlight. ATR-IR analysis of the yellow areas revealed the formation of carbonyl groups from cellulose and Fe(III). On the basis of the results of the aging tests of the reconstructed ink, an hypothesis for the brown discoloration of the Montmajour drawing is provided.

Exposure to such a pollutant as NO_2 of purple ink containing methyl violet applied on different paper substrates (cellulose paper, lignin paper and protein-sized paper) produced a strong darkening of ink which turned bluish-black or black on all substrates. On cellulose paper, pure crystal violet faded to light blue. LC-MS analysis of the dyes extracted from this sample revealed the formation of at least one nitrosamine, due to the attack of the gas at one of the nitrogen atoms of the dye molecule. Exposure to O_3 did not lead to a significant color change of Crystal Violet on paper.

Accelerated aging experiments on pigments and dyes used as alternative ingredients for purple inks have brought about significant discoloration effects. Among others, copper logwood produced from copper sulphate and logwood extract showed a color shift from blue to reddish-brown after aging (in particular after thermal aging) and indigo carmine has faded entirely after exposure to UV light.

These experimental results therefore demonstrate the importance of reliable reconstructions of museum objects where the co presence of various components (e.g. additives, impurities, different paper substrate) can lead to peculiar interactions or color effects. To this regard, cooperation between natural scientists, art historians, conservators and restorers should be pursued both in order to get a complete characterization of a piece of artwork and so as not to misinterpret partial data coming from a single research field.

ABSTRACT

La presente tesi di dottorato riguarda lo studio dei fenomeni di invecchiamento naturale e accelerato di tipo foto-chimico (e in alcuni casi termico), di materiali di interesse artistico (carta, pergamena, colori a olio, pigmenti e coloranti) attraverso numerose tecniche sperimentali, sia distruttive che non, quali Electron Paramagnetic Resonance (EPR)[1], Nuclear Magnetic Resonance-MObile Universal Surface Explorer (NMR-MOUSE)[2], High Performance Liquid Chromatography-Photo Diode Array (HPLC-PDA)[3], Liquid Chromatography-Mass Spectrometry (LC-MS)[4], Fiber Optics Reflectance Spectroscopy (FORS)[3,1], Attenuated Total Reflectance-Infrared spectroscopy (ATR-IR)[5], micro-fading-meter[3] e camera per test di invecchiamento solare accelerato Xenotest[3].

La mia attività di ricerca è stata svolta in collaborazione con il Dipartimento di Scienze Chimiche dell'Università degli Studi di Padova, il Netherlands Institute for Cultural Heritage di Amsterdam (ICN) e l'Image Permanence Institute (Rochester Institute of Technology, New York) e grazie all'accessibilità alla collezione del Museo Van Gogh di Amsterdam.

Il primo e il secondo capitolo forniscono una introduzione alla storia dei coloranti e alla colorimetria e una descrizione delle reazioni di degrado indotte dalla luce e da comuni gas inquinanti.

Nei capitoli numero tre, quattro e cinque, vengono invece presentati i risultati della mia attività di ricerca. In particolare, nel terzo capitolo della mia tesi di dottorato, intitolato 'Materiali Scrittori', viene analizzata la dipendenza di proprietà chimico-fisiche della carta e della pergamena dall'invecchiamento, attraverso l'uso di una sonda NMR nota come MOUSE. Lo strumento NMR-MOUSE ha dimostrato di avere grandi potenzialità nel campo della scienza della conservazione in quanto permette di misurare i tempi di rilassamento nucleari di svariati materiali in situ e senza alcun campionamento. I tempi di rilassamento nucleari dipendono dalla natura chimico-fisica

---

[1] Strumento di proprietà del gruppo EPR (Prof. Marina Brustolon), Dipartimento di Scienze Chimiche, Università degli Studi di Padova.
[2] Strumento di proprietà dell'Università degli Studi di Padova (Centro di Servizi Interdipartimentale, ex CUGAS).
[3] Strumento di proprietà del Netherlands Institute for Cultural Heritage (ICN, Amsterdam).
[4] Strumento di proprietà del gruppo di chimica analitica (Prof. Franco Magno) , Dipartimento di Scienze Chimiche, Università degli Studi di Padova.
[5] Strumento di proprietà del Dipartimento di Scienze Chimiche, Università degli Studi di Padova.

dei materiali ed è stato dimostrato come costituiscano anche degli indicatori dello stato di conservazione della carta. Per quanto riguarda la pergamena, i tempi di rilassamento nucleari hanno permesso di discriminare fra campioni del XX secolo e del XVIII secolo. Inoltre, per entrambi i materiali, lo strumento NMR-MOUSE ha permesso di individuare due intorni chimico-fisici per le molecole d'acqua costituenti i materiali stessi. Si tratta, nel primo caso, di molecole d'acqua libere (acqua liquida) e, nel secondo, di molecole legate chimicamente al substrato cellulosico o proteico.

Nel quarto capitolo, intitolato 'Pigmenti e Coloranti', sono riportati svariati spettri EPR di pigmenti e coloranti, la cui natura chimica era nota solo in alcuni casi. Inoltre, con lo strumento NMR-MOUSE è stato osservato l'effetto della presenza di diversi pigmenti o coloranti sulla polimerizzazione dell'olio di lino. La spettroscopia EPR si è dimostrata efficace nel discriminare fra diversi pigmenti o classi di pigmenti anche con campionamenti micro-invasivi. Inoltre, i tempi di rilassamento nucleari di colori a base di olio di lino si sono dimostrati essere dipendenti dalla presenza dei pigmenti e i risultati sono stati interpretati in termini di diverse velocità o gradi di polimerizzazione.

Il quinto capitolo, intitolato 'Dyes in Aqueous Solution and on Paper: Discoloration and Fading of Crystal Violet', rappresenta il corpo principale di questa tesi di dottorato e consiste in un'estesa analisi (HPLC-PDA, LC-MS, FORS, EPR, valutazioni di *micro-fading*, camera per test di invecchiamento solare accelerato Xenotest) dei processi di invecchiamento foto-indotto e termico di uno dei primi coloranti organici sintetici, il crystal violet, in soluzione acquosa e su carta. L'interesse per questo argomento ha origine dall'osservazione dei fenomeni di alterazione cromatica che interessano un gruppo di disegni e lettere di Van Gogh, tutti prodotti ad Arles nel 1888 con un inchiostro viola che è stato dimostrato contenere crystal violet o altri coloranti strutturalmente correlati (coloranti del triafenilmetano). In particolare, il 'Montmajour' (Arles, 1888. Van Gogh Museum), un disegno apparentemente di colore marrone e appartenente al detto gruppo, mostra delle tracce di inchiostro viola sui bordi del foglio, dove l'inchiostro è stato protetto dalla luce sotto la cornice.

Un altro esempio, anche se non appartenente al gruppo di Arles, è costituito da un menù (Parigi, 1886. Museo Van Gogh) scritto e disegnato da Van Gogh con un inchiostro viola, come è stato possibile stabilire da una riproduzione dell'opera risalente al 1958. Tuttavia, in una foto del 2001 si può constatate come il testo e parte del disegno fossero completamente sbiaditi. E' interessante notare come in questo caso, benché da

un’analisi con spettroscopia FORS siano state rilevate tracce di coloranti del trifenilmetano, non si è osservato l’imbrunimento dell’inchiostro tipico del ‘Montmajour’.

Con l’obiettivo di far luce sui meccanismi di invecchiamento e di alterazione cromatica degli inchiostri contenenti crystal violet su carta, sono stati condotti degli esperimenti di invecchiamento accelerato di crystal violet puro, sia in soluzione acquosa che su carta. Numerosi parametri sperimentali sono stati presi in considerazione: l’intervallo spettrale della sorgente di luce (UV o visibile), il substrato cartaceo (di pura cellulosa, contenente lignina o da fotocopie), la temperatura e la presenza (o assenza) di ossigeno durante l’irraggiamento.

Inoltre, è stato riprodotto (da parte di Judith Geerts, studentessa dell’Università di Amsterdam) un inchiostro viola a base di methyl violet (a base cioè di una miscela di crystal violet e alcuni dei suoi prodotti di demetilazione) secondo una ricetta di Sigmund Lehner (1909) e il suo degrado foto-indotto (luce UV e luce solare naturale) e termico (100 °C) è stato studiato su diversi substrati cartacei (carta di cellulosa, carta di lignina e carta collata con proteine). Inoltre, sono stati presi in considerazione anche gli effetti, sul colore di campioni di carta tinta, di alcuni additivi utilizzati negli inchiostri (gomma arabica, saccarosio e acido ossalico), del Fe(III) (come esempio di foto-catalizzatore spesso presente nella carta come impurezza) e di comuni gas inquinanti, quali NO_2 e O_3.

E’ stato analizzato via HPLC-PDA anche un gruppo di dieci campioni storici di methyl violet provenienti dalla collezione dell’ICN al fine di poter confrontare campioni reali di coloranti sia con i campioni modello descritti nella presente tesi di dottorato che con un campione dell’inchiostro viola del disegno ‘Montmajour’ (Arles, 1888. Museo Van Gogh).

Successivamente, sono stati depositati su carta e invecchiati artificialmente (con luce UV o per trattamento termico) alcuni pigmenti e coloranti (inchiostro a base di cocciniglia o indaco, carminio d’indaco, colorante a base di estratto di campeggio e cromo e colorante a base di estratto di campeggio e rame sintetizzato a partire da $CuSO_4$ o $Cu(AcO)_2$) utilizzati nel XIX secolo come ingredienti per la produzione di inchiostri viola in alternativa al crystal violet.

Infine, è stato analizzato con la spettroscopia FORS un gruppo di lettere del XIX secolo (Birgit Reissland, collezione privata) ed è stata rivelata la presenza di coloranti strettamente correlati al crystal violet.

L'analisi presentata nel quinto capitolo della presente tesi di dottorato ha quindi dimostrato che l'uso del colorante sintetico methyl violet era molto diffuso dopo la sua introduzione nel mercato avvenuta nel 1866. Inoltre, la scarsa resistenza alla luce del crystal violet è stata spiegata come dovuta a reazioni di demetilazione e ossidazione. Una serie di prodotti di degrado è stata identificata con HPLC-PDA e LC-MS per il crystal violet esposto a luce UV in presenza di ossigeno, sia in soluzione acquosa che su carta. L'analisi HPLC-PDA di un campione di inchiostro viola prelevato dal disegno 'Montmajour' (Arles, 1888. Museo Van Gogh) si è dimostrata in accordo con i risultati dei campioni modello appena descritti. Lo sbiadimento completo osservato nel menù è stato riprodotto e spiegato come il risultato dell'esposizione alla luce (UV o visibile).

Sulla base dei miei risultati sperimentali, il primo stadio del meccanismo di degrado consiste di una serie di reazioni di demetilazione che porta come ultimo stadio alla pararosaniline, un colorante rosso corrispondente alla completa demetilazione del crystal violet. Successivamente, l'ossidazione in corrispondenza dell'atomo di carbonio centrale forma chetoni incolore (o debolmente gialli), responsabili sia dello sbiadimento del crystal violet che di un effetto di sensibilizzazione del colorante rispetto al degrado foto-indotto. E' anche stata rivelata la presenza di derivati ossidati del crystal violet. Per quanto riguarda la posizione dell'attacco da parte dell'ossigeno, è stata ipotizzata la formazione di N-ossidi del crystal volet o dei suoi prodotti di demetilazione.

Si è dimostrato anche come il calore (50 °C, 40% umidità relativa) abbia un ruolo secondario nel degrado del crystal violet su carta mentre l'esposizione a sola luce visibile è stata sufficiente a sbiadire completamente il colorante. Particolarmente interessante, considerato che la protezione in ambiente anossico è una delle tecniche di conservazione adottate nei musei, è il fatto che il crystal violet ha mostrato evidenti segni di sbiadimento anche a seguito di esperimenti di esposizione a luce UV in assenza di ossigeno.

Il substrato cartaceo (carta di cellulosa, di lignina o da fotocopie), benché non responsabile per la natura dei prodotti di degrado (colorati) rivelati, ha determinato le quantità relative dei prodotti formati e il colore assunto dallo strato di colorante.

E’ interessante notare come sia l’invecchiamento artificiale (luce UV) che quello naturale (alla luce del sole) di campioni di carta tinti con l’inchiostro contenente methyl violet e altri additivi, abbiano dato origine a colorazioni diverse da quella ottenuta in presenza di crystal violet puro. In particolare, i colori ottenuti sono un grigio-bruno o un grigio-blu, rispettivamente in presenza e assenza di Fe(III). Inoltre, la sola aggiunta di Fe(III) o additivi (tipo saccarosio o acido ossalico) alla carta ha causato la formazione di macchie gialle o brune dopo l’esposizione alla luce solare. L’analisi ATR-IR delle aree ingiallite ha rivelato la formazione di gruppi carbonilici a partire da cellulosa e Fe(III). Sulla base dei risultati dei test di invecchiamento dell’inchiostro ricostruito, è stato possibile formulare un’ipotesi per spiegare le cause del colore bruno apparso sul ‘Montmajour’.

L’esposizione ad un inquinante quale il biossido di azoto (NO_2) dell’inchiostro a base di methyl violet applicato su diversi substrati cartacei (di cellulosa, di lignina o collati con proteine) ha prodotto un forte scurimento dell’inchiostro, che è diventato nero-blu o nero, in tutti i substrati cartacei. Per quanto riguarda invece il crystal violet puro, si è ottenuto uno sbiadimento ad azzurro chiaro su carta di pura cellulosa. L’analisi LC-MS di quest’ultimo campione ha rivelato la presenza di almeno una nitrosoammina dovuta all’attacco del gas su uno degli atomi di azoto della molecola di colorante. L’esposizione ad ozono (O_3) non ha invece prodotto una variazione significativa del colore del crystal violet puro su carta.

Gli esperimenti di invecchiamento accelerato sui pigmenti e i coloranti utilizzati come ingredienti alternativi per la preparazione di inchiostri viola, hanno condotto a importanti alterazioni cromatiche. Fra gli altri, il colorante a base di estratto di campeggio e rame prodotto da solfato di rame ha mostrato una variazione di colore dal blu al bruno rossiccio a seguito dell’invecchiamento (termico in particolare) e il carminio d’indaco è sbiadito interamente dopo esposizione alla luce UV.

Questi risultati sperimentali, quindi, hanno dimostrato l’importanza di avere a disposizione affidabili ricostruzioni degli oggetti museali, dove la compresenza di varie componenti (ad esempio additivi, impurezze, diversi substrati cartacei) può portare a particolari interazioni chimiche o influenzare il colore percepito. A questo proposito, sarebbe auspicabile la cooperazione fra scienziati, storici dell’arte, conservatori e restauratori, al fine di poter ottenere una caratterizzazione completa di un’opera d’arte e così da non malinterpretare i dati parziali provenienti da un singola campo di ricerca.

CHAPTER ONE

COLORANTS AND COLORIMETRY

A brief history of pigments and dyes

Colors represent a fundamental part of our everyday life: they are almost ubiquitous in nature and they are used by people both for functional and aesthetic purposes. Colors are often associated to specific meanings, and are used not only for their aesthetic valence but also to convey precise messages. Colorants constitute the base materials through which colors have been handled for ages.

In this work the term 'colorant' will be used with a general meaning of coloring matter, being this either a dye or a pigment. The distinction between dyes and pigments lies on their application method: dyes are generally soluble in the medium whereas pigments are insoluble and are applied as a dispersion rather than a solution.

People started to make use of colors by means of natural colorants as early as prehistoric times, when they used to depict figurative scenes or to make fascinating hand stencils on cave walls using natural inorganic pigments such as colored earths. In prehistoric times natural dyes extracted from plants were also used, as it is demonstrated for instance in some dyed fabrics found in salt-mines of Hallstatt in Austria [Joosten et al.].

The first known synthetic pigment (3100 BC) was developed by the ancient Egyptians who made up for the scarcity of natural blue minerals with a copper compound known as Egyptian Blue [Campanella et al.]. Egyptians were probably responsible also for the invention of ink which they used to write on papyrus. The oldest known book is the so called Prisse d'Avennes papyrus (2600 BC), written in a black ink made of a dispersion of lampblack in water [Delamare et al.].

On the contrary, synthetic dyes were only produced starting from the mid-19th century. Before that date, fabrics were dyed with natural dyes extracted from plants or animals. Examples are the purple extract of murex - considered by Vitruvius the most precious and the most pleasant to the eye and used in the antiquity almost exclusively for the Roman Emperors' robes-, indigo blue (*Indigofera Tinctoria*), cochineal red (extracted from the homologous insect), the red dyes from brazilwood (*Caesalpinia echinata*) or madder (*Rubia tinctoria*) and the woad blue (*Isatis Tinctoria*) diffused in the Middle Age. Interestingly, in the 12th century an effective dyeing method with woad

was discovered and it was therefore possible to dye fabrics bright blue. Consequently, a taste for blue was developed and the traditional association of the color red with royalty lessened in favour of blue. Indeed, in that period the mantle of the Virgin in paintings and the robes of the King of France became blue [Delamare et al.].

In the 18th century, when the basics of chemistry as a scientific discipline had been finally established, chemists were able to produce new synthetic pigments. The first one was a deep blue pigment called Prussian blue which was actually accidentally synthesized by a paint manufacturer and a pharmacist in Berlin in 1704. Thanks to its coloring strength it has had a widespred diffusion since its introduction onto the market in 1710. Moreover, in 1781 it was first produced the zinc white, a substitute for the poisonous lead white, and in 1797 Vauquelin discovered in a red-orange mineral (crocoite, also known as Siberian lead red) a new element which he called chromium, from the Greek for color. The extraordinary capacity of chromium to produce many different colored salts was soon observed and by the mid-19th century a number of chromium pigments were available on the market (green, yellow, orange pigments).

It was in the 19th century that the first synthetic dye was synthesized by William Henry Perkin. It was a purple aniline derivative named Mauve which was patented in 1856 and then successfully introduced onto the market. For this achievement, which would have huge effects on colorant industry and fashion, Perkin was awarded a prize on the occasion of the Great London Exhibition in 1862. At the opening of the exhibition, Queen Victoria paid tribute to Perking wearing ‘rich mauve (lilac) velvet, trimmed with three rows of lace’ as E. Sheppard reported in his Memorials of St James’s Palace.

Since then, many chemists focused their research activity on the production of new synthetic dyes; at the beginning aniline constituted the privileged starting material and indeed such a definition as aniline dye was used as a synonymous with synthetic dye for decades. Nevertheless, other classes of dyes were soon discovered, e.g. triarylmethane dyes, azo dyes and carbonyl dyes [Christie]. By the end of the 19th century, synthetic dyes had been permanently introduced into the palettes of artists, notable examples being Van Gogh and Gauguin.

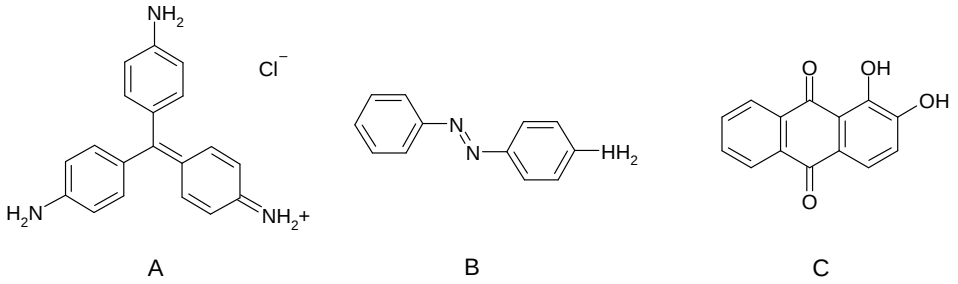

Figure 1: examples of A. triarylmethane dyes (Pararosaniline), B. azo dyes (Aniline Yellow) and C. carbonyl dyes (Alizarin).

When Perkin accidentally discovered the first synthetic dye, little knowledge of organic chemistry was available and the relation between color and chemical structure was still unknown. From that time onward, many studies were devoted to color chemistry. The work published in 1866 by the German F. A. Kekulè on the structure of benzene molecule was definitely one of the major contributions to the development of organic chemistry and it set the basis for the study both of new synthetic routes to colorants and of the relation between color and chemical structure of organic dyes. In 1867 C. Graebe and C. T. Liebermann suggested that dyes were unsatured compounds on the basis of their observation that the color of many dyes entirely faded if treated with reducing agents. Later in 1876, O. Witt developed the first theory on the relation between color of molecules and their chemical structure. Witt proposed that a dye structure consisted of two entities which he called chromophore and auxochrome, connected by a conjugated system of double bonds. According to Witt, it was the presence of the auxochrome which allowed the conjugated double bonds-chromophore system to become colored. Any specific combination of chromophores and auxochromes was called chromogen. Only later it was found that the system of conjugated double bonds may be linear or cyclic and that chromophores and auxochromes corresponded to electron-withdrawing (electron-acceptor) groups – e.g. nitro (-NO_2), azo (-N=N-), carbonyl (-C=O), ammonium (-NR_3^+), carboxyl (-CO_2H) groups – and electron-donating groups – e.g. amino (-NR_2) or hydroxyl (-OH) groups – respectively. Moreover, it was observed that the higher the electron-withdrawing power of the chromophores (or the higher the electron-releasing power of the auxochrome, or the longer the conjugated system) the larger the red shift (also known as bathochromic shift) of the absorption spectrum of the dye. A shift toward the opposite direction (blue shift) is called hypsochromic.

Although brighter colored and easier available in a number of different hues than inorganic pigments, most organic synthetic dyes soon turned out to be very fugitive and of poor lightfastness. In particular, many works of art have shown discoloration and fading of their coloring matter, being this for example oil paint, ink, pastel or dyed fabrics. As a consequence, the works of art at issue have undergone transformation from their original appearance and look different from what they were meant to be.

It is therefore of much interest to study the causes and the mechanisms of (synthetic) dye degradation and the discoloration or fading effects that degradation brings about. This is the way to develop the analytical procedures for assessing the original color from the degradation products, and for finding the best conservation practices.

Color spaces and color measurements [Feller 2001], [Zollinger], [Christie], [Minolta].

Although colors are tightly related to feelings and psychological perception, the need for color communication and color comparison led to extensive scientific studies on color measurement methods. As a result, a number of color spaces were developed consisting of reference systems where colors are expressed with some kind of univocal notation, such as numbers.

Colorimetry systems can be divided into three main groups: physical, perceptual and psychophysical systems. Physical systems describe colors on a purely physical basis, making use of absorption and reflection spectra of colorants (subtractive color mixtures). The color of subtractive color mixtures arises from the selective absorption of some wavelengths of the incident light by the colored object. The rest of the light is either transmitted or reflected (depending on whether the object is transparent or opaque) and can be described with absorption or reflectance spectra respectively. According to physical colorimetry systems, colors are described through their spectral features: the wavelength of the maximum of absorbance (λ_{max}), the intensity of the spectrum (molar extinction coefficient ε) at its maximum of absorbance and the shape of the absorption band [Zollinger], [Christie]. Roughly, the hue (red, yellow, green, blue, purple…) is related to the wavelength of the maximum of absorbance of the colorant (or, generally, the object) at issue, the intensity (or strength) of the color is related to the molar extinction coefficient and the width (and steepness) of the absorption band determines the brilliance or vividness (vivid or dull colors) of the color of a colorant. For example, absorption bands located in the range from 430-380 nm,

480-550 nm, 550-600 nm or 600-700 nm correspond to orange, red, violet or blue objects respectively. Interestingly, green objects are always characterized by two absorption bands at 400-450 nm and 580-700 nm. Moreover, very sharp absorption bands correspond to brilliant colors whereas wide bands correspond to dull colors. Limiting cases are achromatic colors black, grey and white: their common characteristic is that they don't show preferential absorption at any wavelength (and therefore the adjective achromatic). In particular, black and white objects absorb respectively all light of any wavelength or no light altogether whereas grey objects absorb the same amount of light at any wavelength (figure 2).

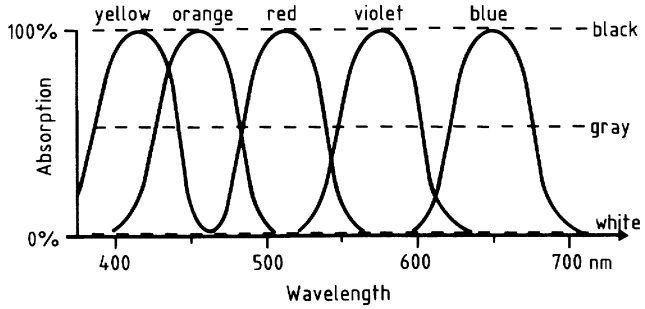

Figure 2: correspondence between absorption bands and perceived colors.

It should be noted that the physical systems, based on the absorption spectra alone, do not provide sufficient information on the color perceived, as one should take into account the sensitivity of the human vision. This latter is wavelength dependent, with a maximum at 555 nm.

Perceptual systems are based on visual appearance and on the measurement of sensations in color vision. In such a system, colors are expressed through three parameters called hue, saturation and brightness (or lightness) (HSB parameters). Placing colors on a three-dimension solid having different hue values along its outer rim, different saturation values along its radius and different brightness values along its vertical axis, the color space illustrated in figure 3 is obtained.

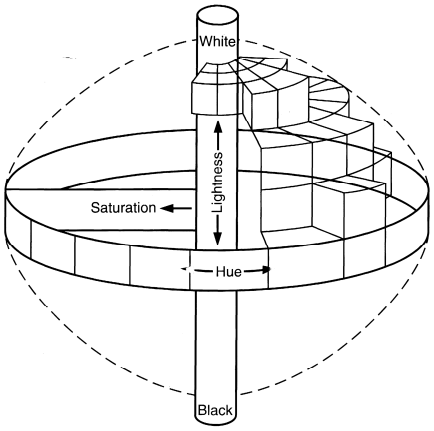

Figure 3: example of a perceptual system: HSB color space. In this figure, the brightness parameter (B) is called lightness.

The vertical axis corresponds to the so-called achromatic colors, that is colors going from black (minimum lightness) on the bottom side of the axis through grey to white (maximum lightness) on the top side of the axis. Saturation represents the distance of a color from the achromatic axis. It is worth noting that the HSB parameters have been chosen in such a way that equidistant colors in the color space correspond to equal perceptual differences (uniform color spacing). Nevertheless, truly uniform color spaces have not been developed yet. The earliest example of HSB system was developed by the American painter A. H. Munsell between 1905 and 1910.

Psychophysical systems are based on the stimuli generated in the human eye by visible light of various intensities and wavelengths and they are suitable for describing additive color mixtures. The color of additive color mixtures is the result of the summation of lights of different wavelengths. Most of the psychophysical systems were developed by the *Commission International de l'Eclairage* (CIE) and are based on visual matching of the light transmitted or reflected from an object to an observer by means of an additive mixture of three (primary) colors (red, green and blue). Light reflected or transmitted from an object to an observer depends both on the illuminant and on the object itself. The color perceived depends both on the reflected or transmitted light reaching the eye of the observer and on the response of the eye itself (its sensitivity to each wavelength). The CIE defined a number of standard illuminants; examples of the principal ones are illuminants A, B, C and D65.

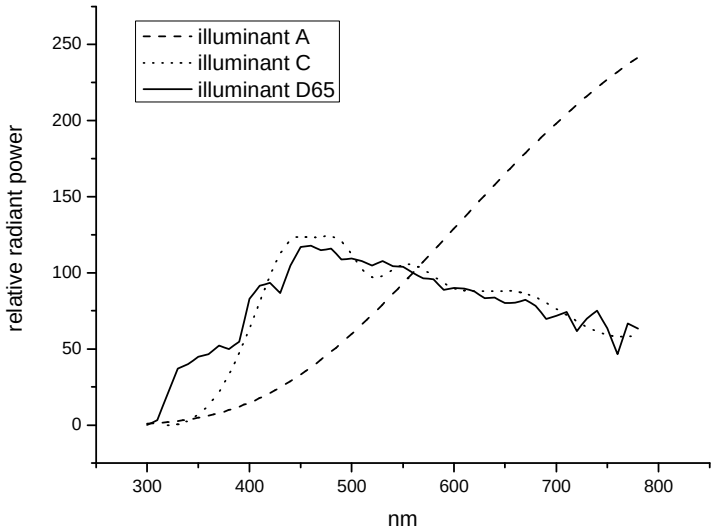

Figure 4: spectral radiant power of illuminants A, B, C and D65 as defined by the CIE commission.

Illuminant A represents the color temperature of an incandescence light at 2856 K and illuminants B and C were defined as mean noon sunlight (obtained by filtering a tungsten lamp, 4874 K) and average daylight (obtained by filtering with blue filters illuminant A, 6774 K) respectively. None of these illuminants includes as much UV light as the sunlight does, though, and for this reason they are not efficient for color measurements of fluorescent materials. Indeed, fluorescent materials owe their color also to the absorption of UV radiation followed by emission of visible light (fluorescence). Illuminant D65 (corresponding to average daylight with 6500 K color temperature) was thus introduced to compensate for this lack of radiant power in the UV range of illuminants B and C. At present, illuminant D65 is the most widely used, although no real light source simulates well enough its spectral distribution. D65 will be the illuminant used in this work. On the other hand, illuminant B is nowadays dismissed. The relative spectral radiant power[1] distributions of illuminants A, C and D65 are shown in figure 4.

The CIE also deduced the spectral sensitivity of the human eye by measuring the (average) relative amounts of red, green and blue lights needed to match the light at each wavelength of the visible spectrum. Experimental results were used to calculate the so-called standard observer color-matching functions ($\bar{x}(\lambda)$, $\bar{y}(\lambda)$ and $\bar{z}(\lambda)$), which roughly correspond to the sensitivity of the eye in the red, green and blue regions.

[1] The spectral radiant power represents the total radiant energy emitted by a source of electromagnetic radiation per unit time.

Given the radiant power distribution S(λ) of the illuminant and the color-matching functions, a set of three color descriptors X, Y and Z called tristimulus values can be obtained as follows:

$$X = k\sum S(\lambda)R(\lambda)\bar{x}(\lambda)\Delta\lambda \tag{1}$$

$$Y = k\sum S(\lambda)R(\lambda)\bar{y}(\lambda)\Delta\lambda \tag{2}$$

$$Z = k\sum S(\lambda)R(\lambda)\bar{z}(\lambda)\Delta\lambda \tag{3}$$

where Δλ is the wavelength interval used, R(λ) is the reflectance spectrum of the colored sample at issue and k is a normalizing factor to make Y equal to 100 for the white standard light. In this way, in the XYZ color space the descriptor Y has the special meaning of representing the lightness. Chromaticity coordinates x, y and z are usually preferred to tristimulus values X, Y and Z and are calculated as follows:

$$x = \frac{X}{X+Y+Z} \tag{4}$$

$$y = \frac{Y}{X+Y+Z} \tag{5}$$

$$z = \frac{Z}{X+Y+Z} = 1-(x+y) \tag{6}$$

To describe a color univocally, the lightness Y and two chromaticity coordinates (x and y) are needed. Plotting the chromaticity coordinates for each wavelength in the visible spectrum, a horseshoe-shaped chromaticity plane is obtained (figure 5). When the third dimension Y is added, a so-called color space is obtained.

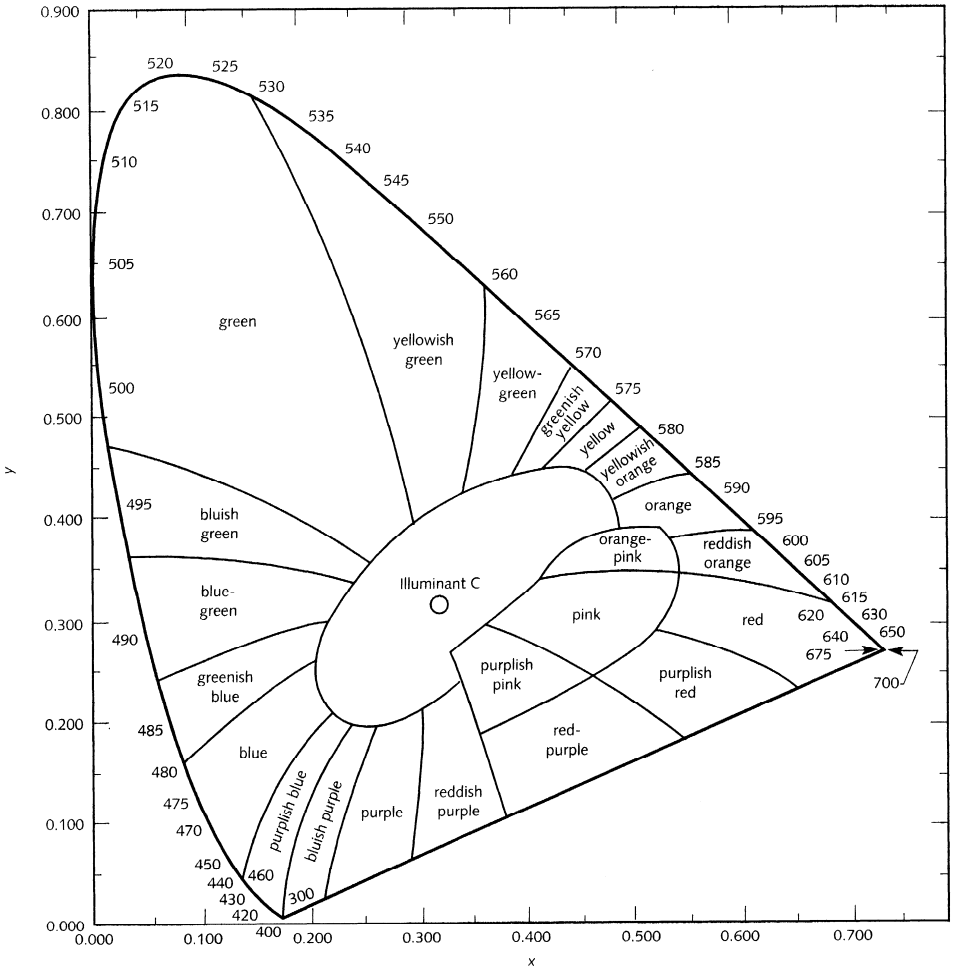

Figure 5: xy chromaticity plane, showing the correspondence between chromaticity coordinates and colors.

The outline of the color space (spectrum locus) is formed by the purest and most saturated colors of the color space, i.e. a color lying on the outline corresponds to light of a specific wavelength. Purple colors (lying on the bottom part of the outline) cannot be associated to any monochromatic radiation as the perception of a purple color needs at least the mixing of two monochromatic radiations, one in the red and the other in the blue-violet[2] region. Purple colors are called "non-spectral colors". The area in the chromaticity plane surrounding the illuminant point (achromatic point) is constituted by neutral colors with a very low saturation. It is worth noting that the xyY color space is not visually uniform as it was instead the case in perceptual HSB system[3].

[2] Violets roughly correspond to the colors lying in the regions called purplish blue and bluish purple in the chromaticity diagram in figure 5.

[3] Although truly uniform color spaces have not been developed yet, some of them are referred to as uniform because they are more uniform then the xy chromaticity plane.

With the aim of creating a more uniform color space, the CIE defined in 1976 the $L^*a^*b^*$ color space (or CIELAB color space). In the $L^*a^*b^*$ color space (figure 6) the chromaticity of colors is defined with the parameters a^* (roughly a measure of the degree of redness or greenness) and b^* (roughly a measure of the degree of yellowness or blueness) and the lightness is expressed by L^*. Red or yellow colors correspond to positive values of a* or b* respectively whereas green and blue colors correspond to negative values of a* or b* respectively.

$L^*a^*b^*$ color values are defined as follows:

$$L^* = 116(Y/Y_n)^{1/3} - 16 \tag{7}$$

$$a^* = 500[(X/X_n)^{1/3} - (Y/Y_n)^{1/3}] \tag{8}$$

$$b^* = 200[(Y/Y_n)^{1/3} - (Z/Z_n)^{1/3}] \tag{9}$$

where the subscript n refers to the tristimulus values of a perfect reflecting diffuser for the illuminant and observer used.

The concept of uniformity of color spaces is linked to the need for comparing colors: in a perfectly uniform color space one can define a so-called color-difference equation that enables to calculate the color difference ΔE between any two points in the color space as a function of their colorimetric values. In reality, truly uniform color spaces have not been developed yet and meaningful comparisons are only possible between similar colors. For instance, one unit of color difference in the green region is perceptually different from one unit of color difference in the red region. Therefore care is needed when using the recommended 1976 CIE $L^*a^*b^*$ color-different equation (eq. 10).

$$\Delta E^*_{ab} = [(\Delta L^*)^2 + (\Delta a^*)^2 + (\Delta b^*)^2]^{1/2} \tag{10}$$

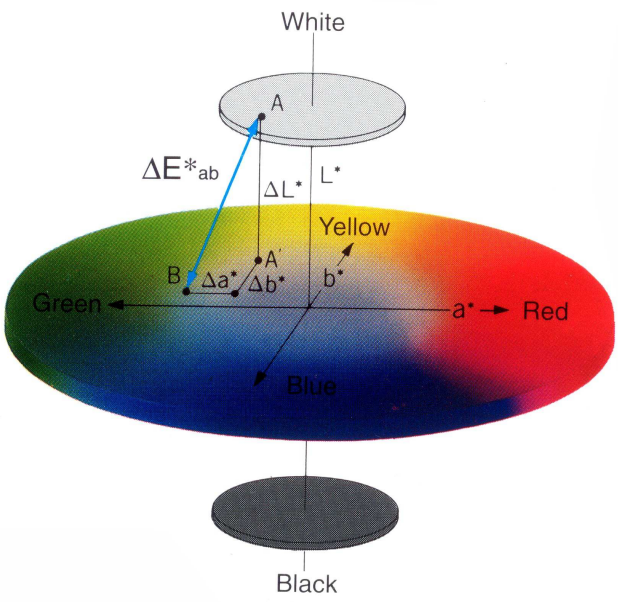

Figure 6: L*a*b* color space.

At this point, it should be noted that the parameter ΔE does not give any information about the direction of the color change. To this end, the CIE 1976 hue angle (h_{ab}) and chroma (C^*_{ab}) were defined as follows (eq. 11 and 12 and figure 7).

$$h_{ab} = \tan^{-1}(b^* / a^*) \tag{11}$$

$$C^*_{ab} = [(a^*)^2 + (b^*)^2]^{1/2} \tag{12}$$

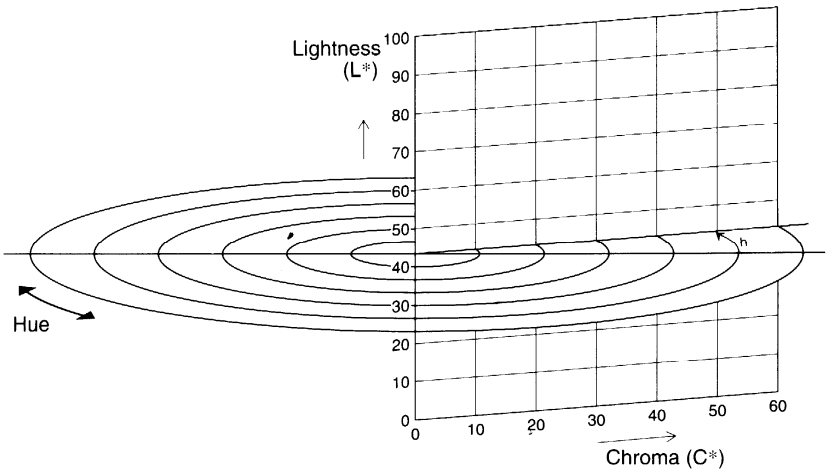

Figure 7: L*C*h color space.

This work is concerned with subtractive color mixtures, being them transparent solutions or (approximately) opaque surfaces. The subtractive color synthesis is mainly

due to two optical phenomena[4]: absorption and scattering of incident light. In transparent colored materials there is only absorption whereas turbid colored materials show both absorption and scattering. UV-Vis spectra of transparent materials are therefore measured in transmittance mode and the absorbance depends, to a first approximation, on the concentration of the absorbing species, according to the Lambert-Beer law. On the contrary, UV-Vis spectra of opaque materials (turbid materials that do not transmit any light) are to be measured in reflectance mode and a more complex dependence of absorbance on concentration holds true. In this case, absorption spectra can be calculated from reflectance spectra making use of the Kubelka-Munk theory. In fact, reflectance spectra are transformed into the so-called Kubelka-Munk units (K/S) according to equation (13) and spectra similar to absorption ones are obtained.

Kubelka-Munk theory is useful for describing optical properties of materials which both absorb and scatter light. In particular, according to the Kubelka-Munk theory, the absorption coefficient K (at each wavelength) over the scattering coefficient S (at each wavelength) ratio can be expressed as a function of the reflectance R (at each wavelength), as shown in equation (13).

$$K(\lambda)/S(\lambda) = [1-R(\lambda)]^2/2R(\lambda) \qquad (13)$$

In this work the Kubelka-Munk theory will be applied to the dye-paper system, where dye and paper will be considered the main light-absorbing and light-scattering agents respectively. In the calculations, the approximation is made that paper is opaque (i.e. paper does not transmit light). Although in reality paper is translucent and absorbs light (this is particularly true for lignin paper which shows an absorption in the blue region due to its yellow color), the Kubelka-Munk equation (13) can still be used for qualitative purposes, such as identification of dyes and comparison of the color of similar samples (dye-paper systems).

[4] Other phenomena might be present: among others, specular reflection in glossy materials and interference in pearlescent or iridescent materials. These phenomena will not be taken into account in this work since they are not present in the samples studied.

CHAPTER TWO
DEGRADATION INDUCED BY LIGHT OR COMMON GASEOUS POLLUTANTS

Mechanisms of photo-induced fading [Braun et al.] [Allen et al.].

For a material to undergo photo-induced fading, it is required that its constituting chemical species absorb light, i.e. they acquire radiant energy. In alternative, it is also possible that the radiant energy acquired by other chemical species is passed to the material in question through a sensitization process which will be taken into account later in this chapter.

UV-visible light is absorbed by molecules or complexes in materials when an electronic transition between the ground state and an excited state is allowed. Electronic states are classified depending on their spin state, i.e. the multiplicity of states allowed by their spin angular moment. The latter is characterized by the total spin quantum number S and the multiplicity is equal to 2S+1. When all electrons are paired S is equal to zero. Since the multiplicity of such states is equal to one, they are called singlet states and are denoted S_i, being the suffix i (=0, 1, 2,...) related to the successive energy levels of the states (figure 1, molecule D or A). On the contrary, if an electronic state is characterized by spin multiplicity equal to three (two unpaired electrons, S=1), then the state is said to be a triplet and it is denoted T_i. Generally, the ground state of a molecule is a singlet (S_0), but important exceptions exist, such as molecular oxygen with a triplet ground state (T_0). All other parameters being the same, the higher the multiplicity, the lower the energy of a state (Hund's rule of the maximum multiplicity).

According to the usual monoelectronic approximation, an electronic transition is described as a jump of an electron between two orbitals, generally from a bonding (or from a non-bonding) orbital to an anti-bonding one. For organic molecules absorbing in the visible range of the spectrum (π- conjugated systems) the two orbitals are generally the highest occupied molecular orbital (HOMO), and the lowest unoccupied one (LUMO). Each electronic state has an underlying vibrational structure and a transition between a given vibrational level of a given electronic state to a vibrational level of a different electronic state is called vibronic transition. Absorption bands are the results of the superimposition of all possible vibronic transition. The selection rules for an electronic transition depend on the symmetry of the two spatial electron wavefunctions

involved, and on their spin states. In electric dipole transitions, such as the electronic ones, the spin magnetic moment can not change, and therefore only the transitions conserving the spin state are allowed (generally $S_0 \rightarrow S_1$). ISC (InterSystemCrossing) is possible when a spin-orbit perturbation is present, and in this case an interconversion between singlet and triplet can happen. Therefore, electronic transitions between a singlet and a triplet state (e.g. $S_0 \rightarrow T_1$) are spin-forbidden and, to a first approximation are not allowed. Nevertheless, spin-forbidden transitions (e.g. $S_1 \rightarrow T_1$) are in fact observed when a spin-orbit perturbation is present. These transitions (also known as intersystem crossing), however, have a low probability and are therefore very low in intensity [Turro].

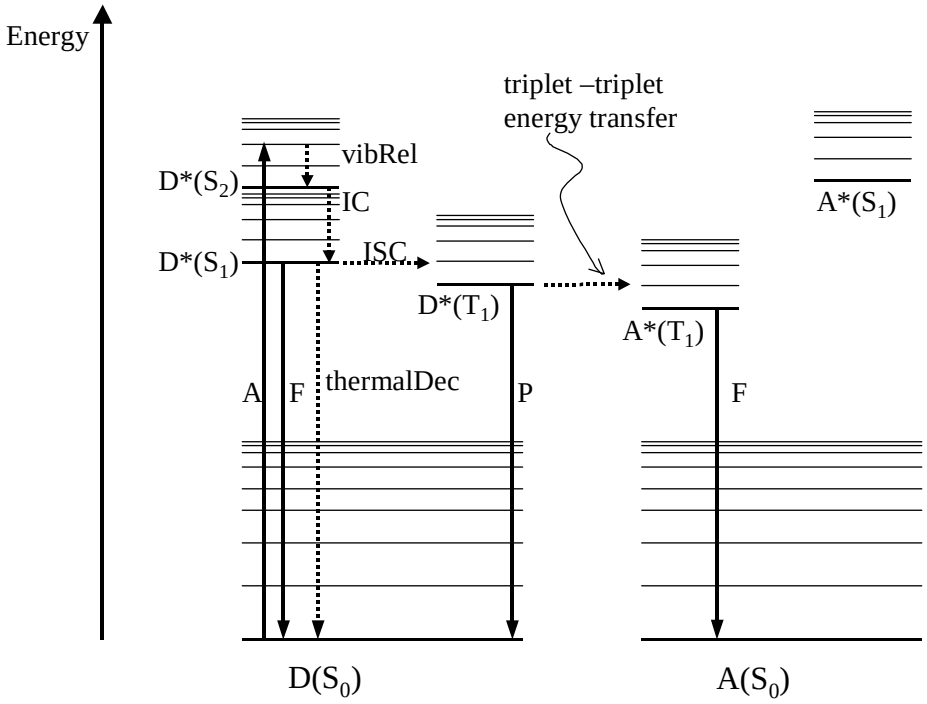

Figure 1: Jablonski diagram for a molecule D. A triplet-triplet energy transfer with a molecule A is also shown. A= radiant energy absorption; F=fluorescence; P=phosphorescence; vibRel=vibrational relaxation; thermalDec=thermal decay or non radiative transition, IC=internal conversion; ISC=intersystem crossing. Solid arrows represent radiative transitions whereas dash arrows non-radiative ones. The star denotes an excited state.

Once an excited vibronic state of a molecule is populated (e.g. absorption of radiant energy has occurred), there are two main deactivation pathways: photophysical or photochemical ones. The Jablonski diagram (shown in figure 1) provides a useful summary of the possible photophysical processes. These latter can be further divided

into radiative and non-radiative processes. Let us suppose that after absorption of a photon, a given molecule is in its S_n excited vibronic state. A fast vibrational relaxation (non radiative transition) occurs after the electronic transition, leading to the lowest vibrational level of the electronic excited state S_n. Generally, the energy difference between electronic states S_n and S_{n-1} is such that their vibrational levels partially overlap and a fast deactivation process called internal conversion (IC) is active. It consists of a non-radiative transition between electronic states with the same spin multiplicity. Internal conversion is usually very efficient (ps time scale) so that the first excited state S_1 can be regarded as the most relevant state from which photochemical and radiative processes take place, after light absorption (Kasha's rule). It is noteworthy that internal conversion between S_1 and S_0 is less efficient due to the higher separation in energy of these two states. Once in its first excited state S_1, a molecule can undergo either a radiative deactivation process to the ground state, called fluorescence (lifetime from 10^{-12} to 10^{-6} s), or non-radiative processes such as thermal deactivation to the ground state or intersystem crossing (ISC) to a triplet state. The latter is generally slower than IC and, consequently, a triplet state is generally longer-lived (10^{-11} to 10^{-6} s for $S_1 \rightarrow T_1$ and 10^{-7} to 10 s for $T_1 \rightarrow S_0$) than a singlet state. This is the reason why nearly all bimolecular photochemical reactions occur from the lowest triplet state (T_1). Finally, a radiative transition between states of different spin multiplicity (e.g. $T_1 \rightarrow S_0$) is called phosphorescence. Photophysical deactivation pathways are usually very efficient and this is why colorants do not fade as fast as it would be expected solely on the basis of their high absorption coefficients and of the average intensity of the daylight irradiation [Neevel].

So far only unimolecular deactivation processes have been considered. In fact, a photophysical non-radiative energy transfer between two molecules can also occur. The excited molecule (called donor, D*) transfers its energy to an acceptor molecule (A) in its ground state so that the former is deactivated (D) and the latter is excited (A*). This process might be regarded as a photosensitization of the acceptor or as a quenching of the donor depending on perspective. This process can be described as follows:

$$D \xrightarrow{h\nu} D^* \tag{1}$$

$$D^* + A \rightarrow D + A^* \tag{2}$$

Triplet-triplet energy transfer (figure 1) is an important type of photosensitization and it will be described in more detail later.

Besides photophysical deactivation pathways there are also photochemical processes. For a photochemical pathway to be significant, it has to compete with other deactivation processes of the excited state. For this reason, photochemical reactions take place from the lowest excited singlet or triplet states, which have sufficiently long lifetimes. This class of reactions can be divided into two subgroups: primary photochemical processes and secondary (or dark) reactions. Examples of photochemical reactions comprise radical formation (e.g. homolytic bond scission leading to depolymerization of cellulose or to the breakdown of the conjugated system of dyes), intra- or intermolecular electron transfer, photoaddition (e.g. intermolecular hydrogen abstraction), photoionization, intramolecular decomposition.

The electronic transitions are usually classified in terms of the type of orbital involved. The most energetic transitions occur between bonding and antibonding sigma orbitals ($\sigma \rightarrow \sigma^*$). They are responsible for far ultraviolet absorption and usually imply bond cleavage. Another class of transitions consists of an excitation from a bonding π orbital to an antibonding π^* orbital. They are typical of unsaturated and aromatic compounds. The $\pi \rightarrow \pi^*$ transitions lie in the near ultraviolet or visible region of the spectrum, depending on the degree of conjugation and on the presence of chromophores. Another kind of transition (usually the least energetic) is between a non-bonding n orbital and an antibonding π^* orbital. This transition is typical of ketones and aromatic amines and are responsible for absorption of near UV and Visible light

Two examples of photochemical reactions involving electronically excited carbonyl groups are the homolytic scission in α position with respect to the carbonyl group and the intramolecular hydrogen abstraction (figure 2). In both cases reactive radical species are formed.

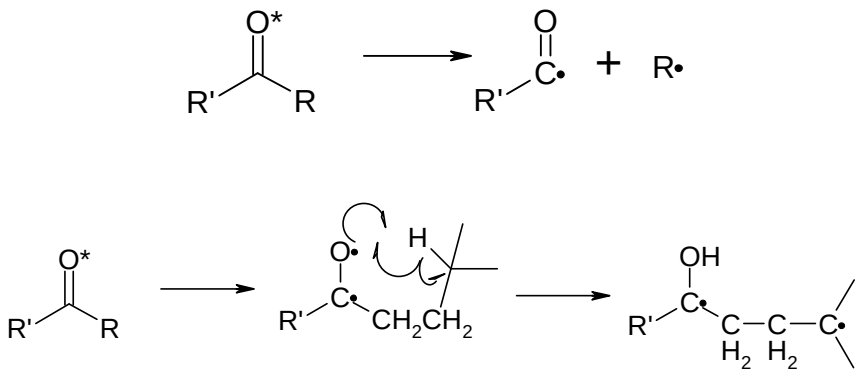

Figure 2: homolytic scission in α position (above) and intramolecular hydrogen abstraction (below) from an excited carbonyl group.

Photo-induced degradation is a step of primary importance in the process of aging of materials: suffice it to think of a piece of low-grade paper or of a felt pen drawing left in the sun. Paper will quickly yellow whereas the colors of the drawing will rapidly fade.

In this work I will be primarily concerned with the discoloration and fading of synthetic organic dyes on paper. In particular, I will consider an early synthetic dye called *Crystal Violet*, which have been used for making purple inks since the last decades of the XIX century.

For a compound to be used as a dye, it has to fulfil two basic requirements: it has to be colored (i.e. absorb visible light) and its molar extinction coefficient has to be high enough for the color to be intense. Therefore, because of their strong light absorption properties, dyes are exposed to photophysical and photochemical processes (direct fading). Moreover, as it has already been noted previously, in some cases it is also possible that the energy absorbed by a molecule (called sensitizer) is transferred to dye molecules. A mechanism of dye fading of this type is called indirect fading or sensitized fading. When this mechanism is working the sensitizer can absorb light of lower energy than the dye, and transfer energy to the dye, which would not otherwise be activated. A particularly interesting case of sensitized activation is the triplet-triplet energy transfer. In this case the donor molecule is in its excited triplet state T_1 whereas the acceptor is in its singlet state S_0. After the energy transfer, the donor is deactivated to its S_0 state and the acceptor is excited to its T_1 state as summarized by the following equation:

$$D^*(T_1)+A(S_0)\rightarrow D(S_0)+A^*(T_1) \qquad (3)$$

This mechanism is particularly important because it allows in some cases to populate triplet states not reachable by an efficient ISC. To this respect, ketones are efficient sensitizers. As it has already been underlined, due to its longer lifetime a triplet state is more likely involved in photochemical reactions than a singlet state: hence the importance of the role of sensitizers in photo-induced degradation of materials.

A different and very important example of energy transfer is represented by the photosensitized excitation of oxygen from its triplet ground state to its excited singlet state:

$$D^*(T_1)+{}^3O_2\rightarrow D(S_0)+{}^1O_2 \qquad (4)$$

Singlet oxygen is a very reactive species which is quickly involved in further degradation reactions. Its typical reactivity is very specific and involve three main classes of reactions: 1,4-cycloaddition, 1,2-cycloaddition and ene reaction (figure 3).

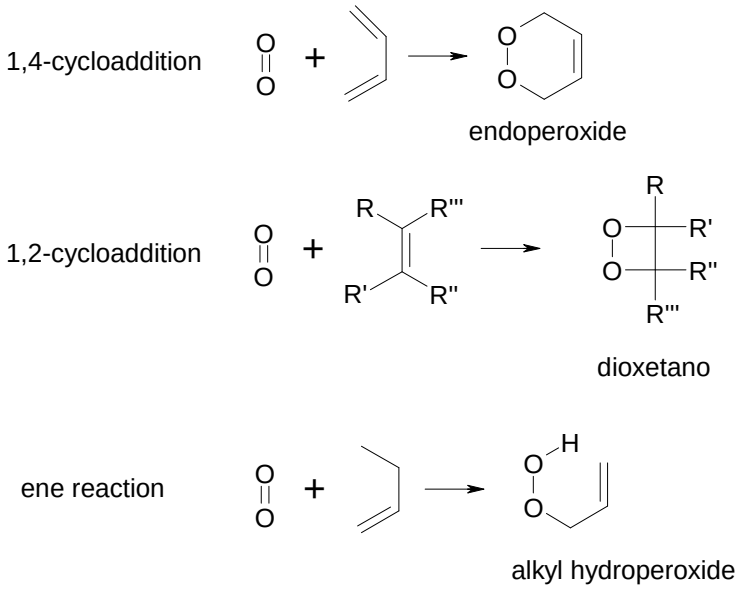

Figure 3: typical reactivity of singlet oxygen.

Ground state triplet oxygen can also be involved in another common mechanism, whereby a radical (produced for example by a photoinduced hydrogen abstraction or a photoinduced bond cleavage) reacts with triplet oxygen yielding highly reactive peroxy radicals (see reactions 5, 6 and 7). Peroxy radicals are easily involved in a chain of radical reactions that end up in an overall oxidation of the starting molecule.

$$^3S^* + RH \longrightarrow HS^{\bullet} + R^{\bullet} \quad (5)$$

$$R^{\bullet} + {}^3O_2 \longrightarrow ROO^{\bullet} \quad (6)$$

$$HS^{\bullet} + {}^3O_2 \longrightarrow {}^1S + HOO^{\bullet} \quad (7)$$

An oxidation reaction involving sensitized oxygen is called photosensitized oxidation.

Other efficient degradation catalysts are constituted by transition metal ions such as iron or copper [Proost et al.]. A well-known example is the Fenton reaction:

$$Fe^{2+} + H_2O_2 \rightarrow Fe^{3+} + HO^{\bullet} + HO^{-} \quad (8)$$

through which hydroxyl radicals are formed. In the presence of reducing agents, the Fe^{3+} ion is reduced back to Fe^{2+} and the Fenton reaction can continue:

$$Fe^{3+} + H_2O + h\nu \rightarrow Fe^{2+} + H^{+} + HO^{\bullet} \text{ or} \quad (9)$$

$$Fe^{3+} + ROOH \rightarrow Fe^{2+} + H^{+} + ROO^{\bullet} \quad (10)$$

In addition to the Fenton reaction, in the presence of Fe^{2+} and oxygen, the formation of superoxide radicals can take place (reaction 11). Successively, superoxide radicals can be further reduced to peroxide radicals (or peroxides) as shown in reaction 12.

$$Fe^{2+} + O_2 \longrightarrow Fe^{3+} + O_2^{\bullet} \quad (11)$$

$$Fe^{3+} + O_2^{\bullet} + RH \longrightarrow HOO^{\bullet} + R^{\bullet} + Fe^{2+} \quad (12)$$

Peroxides are powerful degradation agents because of their oxidizing power and of their ability to act as photoinduced (near UV) radical initiators.

Besides oxygen, other reactive gases involved in degradation reactions are related to some common pollutants. In this work, the effect of NO_2 and O_3 on the early synthetic dye crystal violet will be investigated. Besides oxygen, some common pollutants act as reactive gases involved in degradation reactions. In this work I will take into account the effect of NO_2 and O_3 on the early synthetic dye crystal violet.

Moreover, when studying the reactivity of a material as part of a composite object, such as for example an ink on paper, one should take into account the physical and chemical behaviours of all the components, as they might (and often do) play a role in the degradation on the material at issue. Indeed, many studies suggest that the photodegradation mechanism of triarylmethane dyes may consist of photooxidation of non-protein substrates such as cellulose, and of photoreduction on protein ones, such as silk and wool. This work will be concerned exclusively with cellulosic substrates.

Besides pointing out the types of reactions involved in degradation mechanisms, the question as to how (and for how long) reagents are brought into contact is also of fundamental importance. In this regard, the physical state of materials plays a role. For instance, amorphous domains of cellulose are less tightly packed than crystalline ones and therefore they are more easily reached by degradation agents such as water or oxygen. Indeed, materials that are swollen in the presence of water (e.g. cellulose) are more exposed to degradation at high values of relative humidity (RH). Moreover, high concentrations of dyes and pigments favour the formation of aggregates which often show a higher light fastness than monomolecular layers or small clusters. This increased fastness of large particles to surface degradation mechanisms such as photo-induced fading is due to the lower surface to volume ratio. The smaller the surface, the lower the exposure to degradation agents (e.g. light, oxygen, moisture). Large particles would also

dissipate the energy from (reactive) excited states easier than small particles, resulting in a shorter lifetime of these states [Gordon et el.].

Finally, we must take into account the type of exposure to photochemical action, which is the resultant of three factors: irradiance, duration of exposure and spectral power distribution of the light source [Cuttle]. Photoinduced degradation depends on exposure and, according to the reciprocity principle, the effects of an exposure of, say, 10 W m^{-2} for 10 hours or of 20 W m^{-2} for 5 hours are the same [Saunders et al.] [Feller 1994]. This means that, all other parameters being the same, the effects of light exposure only depend on the total number of photons (of a certain frequency) striking the sample and not on the way they are delivered. In fact, some deviations from the principle are observed, mainly at high light intensities; for instance, some photochemical processes depend on the square root of light intensity. Also, one must take into account the radiant heating effect of the light on the exposed surface, which is increasing with the light intensity. This can produce for example a progressive decrease of the moisture content of the sample. Accordingly, materials exposed to discontinuous lighting conditions during natural aging (cycles of light and dark or variations in the light intensity) experience variations in temperature and relative humidity which lead to different behaviours compared to those produced by a continuous light flux. Nevertheless, the reciprocity principle has important applications both on the designing of accelerated aging tests and on the control of luminous flux in museum lighting through illuminance or exposure limitation or a balance of the two procedures.

As far as the spectral power distribution is concerned, what matters is the absorbance of the material, and the probability of a given photochemical reaction, on varying the wavelenght. A useful model in this regard is the *action spectrum*, which is a plot of the efficiency of an irradiation in producing a degradation effect (such as the yellowing of paper) through one or more photochemical reactions, versus the wavelength and the light intensity. Action spectra of many materials showed that there is no truly safe region from the UV through the visible to the IR portion on the electromagnetic spectrum. While the UV and IR regions of the spectrum do not make any useful contribution to the visual experience (except for some luminescent materials), and consequently, in theory, they may well be completely eliminated, exposure to visible light can not be avoided, unless an object is never exhibited.

Effects of common pollutants. Ozone and nitrogen dioxide

Although photo-induced degradation is the principal degradation agent for many materials (e.g. triarylmethane dyes among others), the presence in the atmosphere of urban areas of pollutants such as ozone (O_3) and nitrogen dioxide (NO_2) often poses serious problems of conservation of (museum) objects. Indeed, in the presence of these reactive gases, corrosion of metals, yellowing of paper and discoloration or fading of dyes have indeed already been observed in many instances [Druzik] [Whitmore et al. 1989].

With particular regard to triarylmethane dyes, the ability of O_3 to act as a strong oxidant, react with unsaturated carbon-carbon bonds and give electrophilic attack (for instance at the nitrogen atom) also in the absence of light, is of particular interest. Indeed, other works have already revealed the formation of oxidation products of triarylmethane dyes on exposure to O_3. The following scheme (figure 4) shows examples of the reaction pathways reported in literature for triarylmethane dyes and ozone [Reife et al.] [Grosjean et al. 1989]:

A. oxidative cleavage of unsatured carbon-carbon bonds

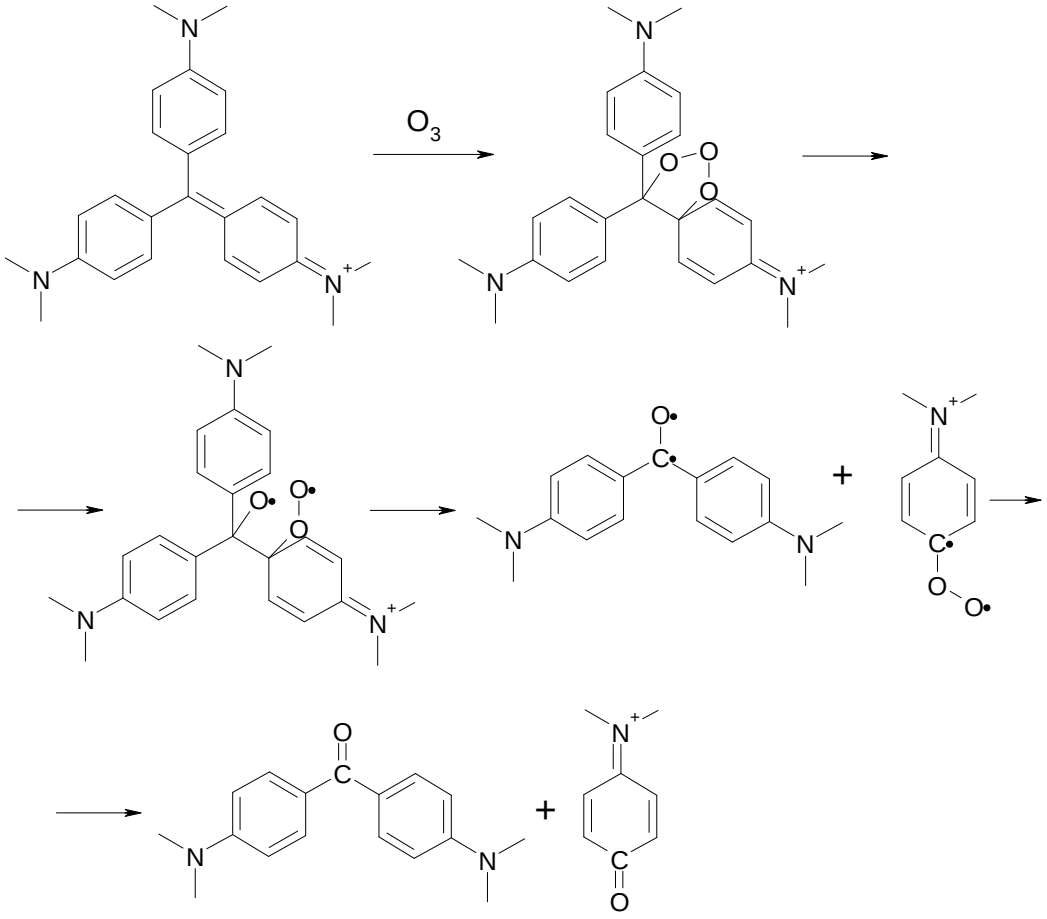

B. electrophilic attack to nitrogen atoms

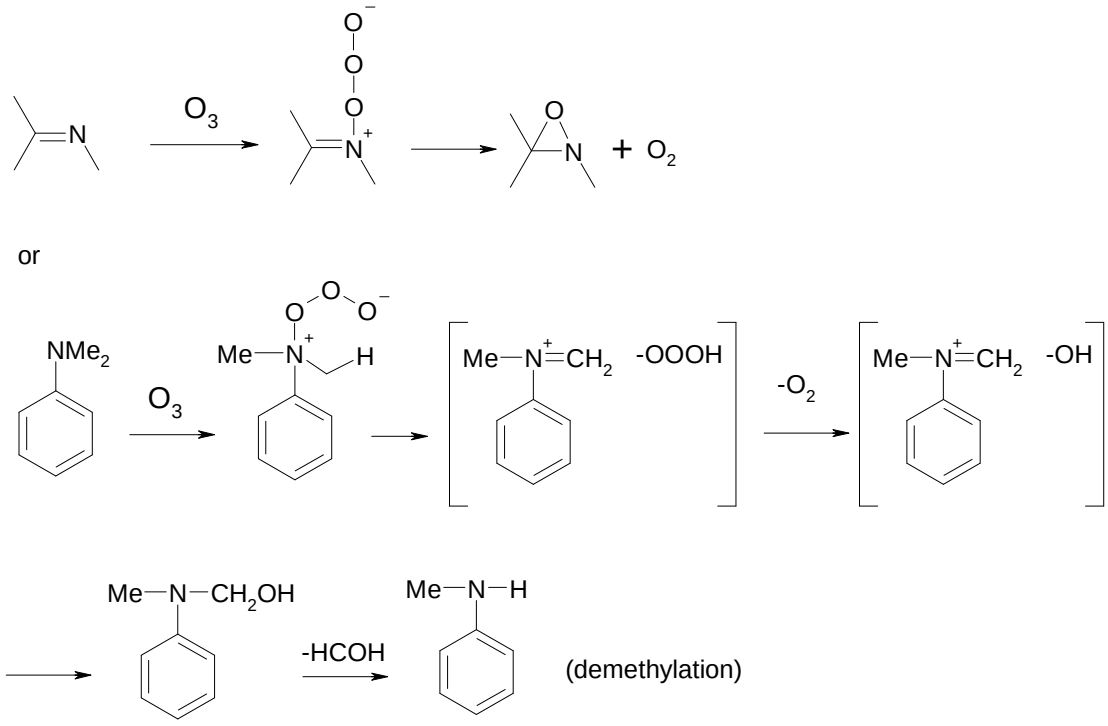

Figure 4: Some reaction pathways for triarylmethane dyes and ozone.

A different mechanism (with ionic intermediates rather than radicals) for oxidative cleavage of unsatured carbon-carbon bonds (pathway A in figure 4) is also reported [Reife et al.], but reaction products are consistent with what shown in figure 4.
Significantly, leuco bases or reduced form of triarylmethane dyes (e.g. pararosaniline base) were demonstrated to be less sensitive to ozone than triarylmethane dyes, since they lack the highly reactive unsatured C=C bond at the central carbon atom [Grosjean et al. 1989].

NO_2 is a mild oxidant, particularly for unsatured organic compounds, and can account for the formation of yellow colored nitro (-NO_2) and nitroso (-ONO_2) groups. Moreover, it gives nitrates and acidic species such as nitric and nitrous acids on the surface of materials. Figure 5 provides examples of the possible reactions between NO_2 and some of the functional groups present in triarylmethane dyes [Giamalva et al.].

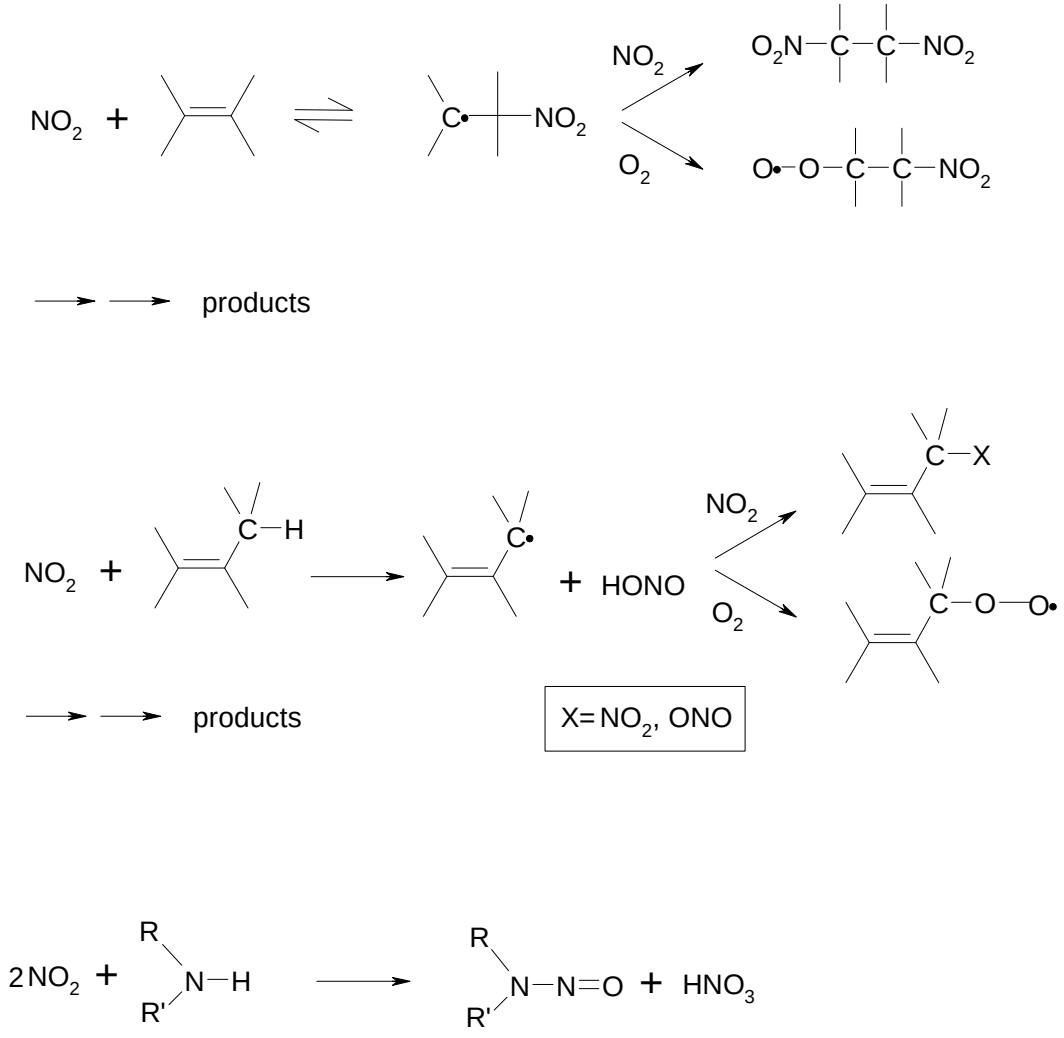

Figure 5: examples of the possible reactions between NO_2 and some of the functional groups present in triarylmethane dyes.

The formation of nitric acid from NO_2 and moisture present on the surface of materials is particularly dangerous, because of the double nature (acidic and oxidant) of this compound. In particular, it was demonstrated that triarylmethane dyes are very fugitive to nitric acid yielding organic nitrate esters (at the central carbon atom) or oxidation products such as derivatives of benzophenone [Grosjean et al. 1992].

CHAPTER THREE
WRITING MATERIALS

INTRODUCTION

This chapter will deal with the paper and parchment photo- and thermal- degradation processes, studied via NMR-MOUSE relaxometry. The NMR-MOUSE technique allows, in principle, to distinguish between aged and unaged samples by measuring differences in the nuclear spin relaxation properties. The analysis will be applied here to cellulose paper, to lignin paper and to some historical samples of paper (XV century) and parchment in different states of conservation. In order to provide a brief understanding of the following part, a short description of the chemistry of paper and parchment and their main degradation processes is given here.

1) Paper

Paper is a material of vegetable origin, constituted mainly of cellulose and water. To make a sheet of paper it is necessary to grind cellulose-based materials (i.e. cotton or linen rags, wood or straw) with water and NaOH or $Ca(OH)_2$: this is the so called refining process during which cellulose fibers swell up and separate. Raw materials for ancient paper production were composed exclusively of cotton or linen rags so that pure and durable cellulose paper was obtained. From around the middle of the XIX century, wood was introduced as a cheaper and more easily available ingredient for paper making. The pulp obtained during the refining process of wood contained cellulose, hemicelluloses and lignin and gave only paper of low quality and durability. The reason is that non cellulosic residuals introduced with wood prevent fibers felting and are responsible for a series of chemical reactions which speed up paper degradation, as it will be discussed later in this chapter.

Before the mechanization of paper production took place, the pulp obtained from the refining process was applied on a loom constituted by a rectangular rigid frame on which a net was mounted: this operation allowed water to drip away and fibers to come nearer till inter-fiber bounds create (i.e. hydrogen bonds). The tight chemical and physical interconnection of cellulose fibers is called felting: it gives cohesion to the sheet and it is at the base of paper formation. After the mechanization of the production,

more efficient procedures were developed for papermaking. Nevertheless, the basic stages of paper formation were the same.

Besides the principal operations discussed so far, many others entered the production process: they all had the final aim of improving aesthetic or mechanical features of paper. For example, the pulp could be treated with whitener chemicals (chlorine and its derivatives) or enriched with $CaCO_3$ powder in order to increase whiteness or give opacity and consistency to the sheet. Moreover the surface of the sheet was often protected by a film of glue (made of gelatine, starch or colophony) that conferred impermeability and avoided ink spreading. This protective film is called sizing.

At a microscopic level, paper is composed of amorphous cellulose domains incorporating a small amount of tightly bound water, and amorphous cellulose domains where water is absorbed in a looser and more dispersed way [Capitani et al. 2002]. A small amount of volatile water can also be adsorbed to cellulose fibers. Other secondary components that might be found in paper are lignin and hemicelluloses. Moreover, traces of metallic ions (Fe^{3+}, Cu^{2+}, Mn^{2+}) can be introduced with inks, raw materials or factory machinery.

In a well-preserved paper the amount of water is about 9% w/w and the amorphous over crystalline cellulose ratio is about 50%-50%. Chemical reactions on cellulose start usually from the amorphous domains, whose disordered and consequently less densely packed structure is more permeable and easily attacked than crystalline domains.

1.1) Cellulose, hemicelluloses and lignin [Campanella et al.]

Cellulose is a polymer obtained from the condensation of β-glucose units. The chemical bond formed, called β(1→4) glycosidic, forms a linkage between the units, in which an oxygen atom binds carbon atoms C_1 and C_4 of two units of glucose (figure 1).

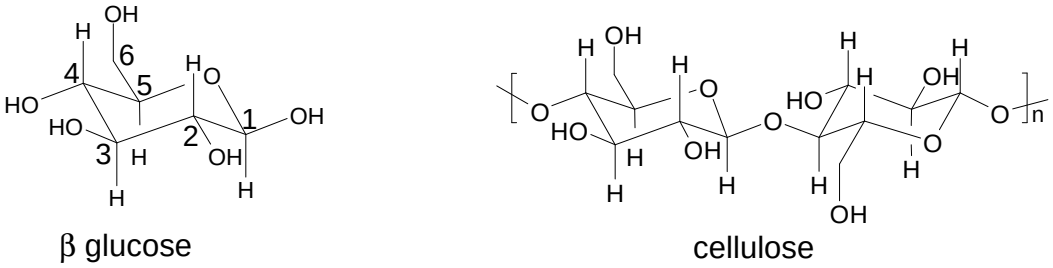

Figure 1: monomer unit of β -glucose and β(1→4) glycosidic bond in cellulose.

The β(1→4) glycosidic bond confers a linear structure to cellulose polymers, thus maximizing intra-molecular hydrogen bonds. Moreover, each cellulose macromolecule

interacts through hydrogen bonds with the others macromolecules, thus forming fibrous structures called microfibrils. In turn, microfibrils arrange themselves into macro-fibrils together with emicellulose, pectine, and other proteins.

The average length of macro-fibrils varies according to the vegetal species: from few millimeters in conifers or up to 20 or 60 mm in cotton. Microfibrils are constituted of both amorphous and crystalline domains. The former give elasticity to the fibers.

Hemicelluloses are polysaccharides resulting from the co-polymerization of different saccharide units (figure 2 shows the most common). Hemicellulose chains are shorter and more branched than cellulose chains and this characteristic is responsible for their amorphous and highly hydrophilic structure. Consequently, hemicelluloses are more easily swollen than cellulose in water and more reactive. Finally, hemicelluloses form hydrogen bonds with cellulose, thus weakening the network of inter-fiber interactions (mainly hydrogen bonds) of cellulose.

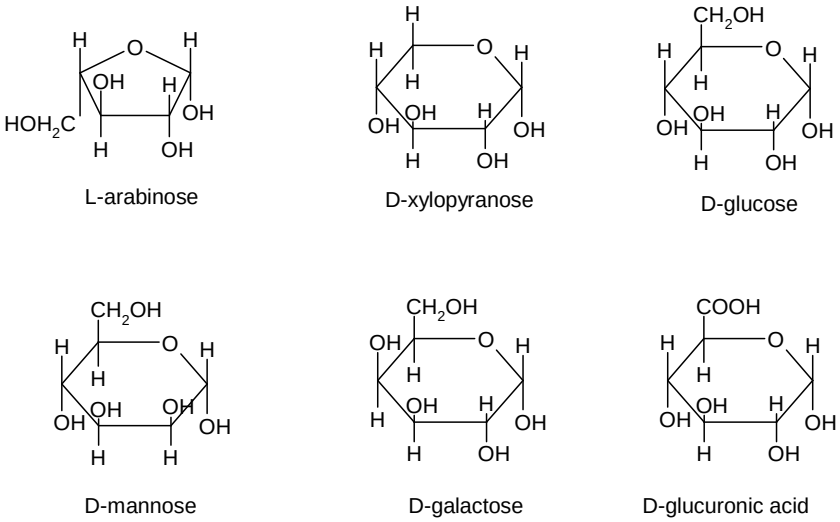

Figure 2: most common monomer units of hemicelluloses.

Lignin is a fundamental component of wood and consists of a 3-D amorphous polymer whose monomer units are unsaturated alcohols related to phenylpropene (shown in figure 3).

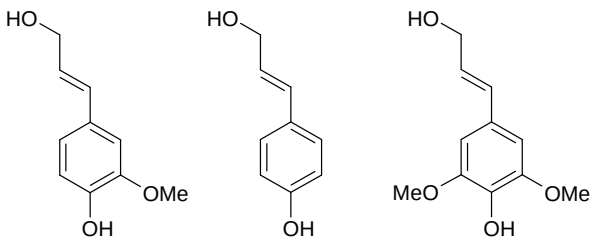

Figure 3 monomer units of lignin.

These monomer units are randomly linked in lignin, through C-O-C (such as in ethers, acetals, esters) or C-C bonds to give a rigid, hydrophobic structure which does not allow for a network of hydrogen bonds.

1.2) Degradation of paper

The main chemical reactions responsible for cellulose degradation are oxidation and hydrolysis. Hydrolysis (acid or base catalyzed) involves the scission of glycosidic bonds and leads to the depolymerization of cellulose. Depolymerization is in turn associated to loss of tensile strength and increased brittleness of paper.

Oxidation involves the aldehydic end-group of the polymer and secondary and primary hydroxyl groups yielding ketones, aldehydes and carboxylic acids. The oxidized cellulose obtained is called oxycellulose. Oxidation of cellulose brings about the following consequences:

- the formation of acidic functional groups which catalyze hydrolysis;
- destabilization of the network of hydrogen bonds due to carbonyl group formation from hydroxyl groups. As a consequence, cellulose fibers are destructured;
- onset of light absorption in the blue region of the visible, due to the presence of α,β-unsaturated carbonyl groups and consequent yellowing of paper. Moreover, these groups can easily form radicals, which are involved in further degradation reactions of cellulose.

Pristine cellulose does not absorb visible light but can absorb radiation in the UV range below 350nm, leading to the formation of radical species and to depolymerization (photolysis). In the presence of oxidized cellulose, the absorption extends into the visible range and may therefore induce further photo-reaction mechanisms (e.g. in the presence of ketones).

Metallic ions (even in traces) such as Fe(III) may accelerate oxidation of cellulose by catalyzing the generation of reactive oxygen species in a series of redox reactions such as the Fenton reaction.

Cellulose is insoluble in the large majority of solvents but it is swollen by polar solvents which can destroy inter-fiber hydrogen bonds. This process starts preferentially in the amorphous domains of the polymer. Once swollen, cellulose is more easily attacked by degradation agents.

Hemicelluloses undergo the same reactions as cellulose, but they are more easily swollen in water and are more reactive.

Due to its numerous different monomers, lignin shows a number of chemical reactions. Aromatic rings can react via aromatic electrophilic substitution. This is the reaction exploited in industrial processing of wood pulp, which produces soluble compounds of lignin, easily separated from cellulose pulp. Moreover, light exposure or bases can transform phenolic groups of lignin into radicals or anions, which in turn yield quinoid structures (figure 4). These latter are often efficient light absorbers and can undergo further oxidation.

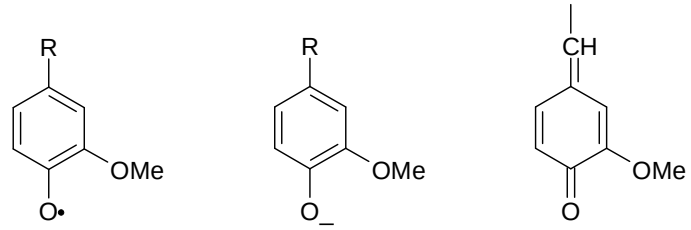

Figure 4: examples of radicals (left) and anions (middle) of lignin that are precursors of quinoid structures such as the one shown to the right.

2) Parchment

Parchment is a material of animal origin constituted mainly of collagen. The raw material for parchment production is animal skins (sheep, goat, calf…). After being washed in cold water, the skin has to be soaked in water and lime in order to remove hair and grease. Subsequently, the skin is first scraped with special curved knives to complete hair removal and to take epidermis away and then it is rinsed in water to clear it from the lime. After these treatments, the skin is stretched with a frame and left to dry. To improve smoothness and whiteness, scraping operation can be repeated in various phases and parchment surface can be rubbed with chalk and pumice.

At a microscopic level, animal skin is mainly constituted of flexible layers of randomly interwoven collagen fibers and of water molecules. It is assumed that water is dispersed in the material in three different forms [Florian], [Larsen]:

- *bound water*: this is water chemically bound to collagen that is irreversibly lost only when collagen is denatured. It constitutes 2% of the dry collagen weight .
- *associated or multilayer water*: this is water weakly bound via hydrogen bonds to surfaces of the fibrous molecules as water layers and located between fibers in pores less than 30÷50 μm in diameter; it changes with relative humidity (RH)

variation and constitutes about 8% of the dry collagen weight at room temperature at 50% RH.

- *free water:* this is water not bound to collagen but located into large pores or capillaries over 30÷50 μm in diameter. It takes part to many chemical reactions, is readily available for microorganism growth and easily evaporates.

In parchment, collagen fibers are more or less aligned due to skin stretching during the drying in frame.

2.1) Collagen

The structure of the protein called collagen is characterized by a high amount of amino acids such as glycine (1/3 of the total aminoacids is glycine), proline and 4-hydroxyproline and by the presence of 5-hydroxylysine and low amounts of sulphur-containing amino acids (cysteine and methionine). Figure 5 shows examples of the most common amino acids of collagen.

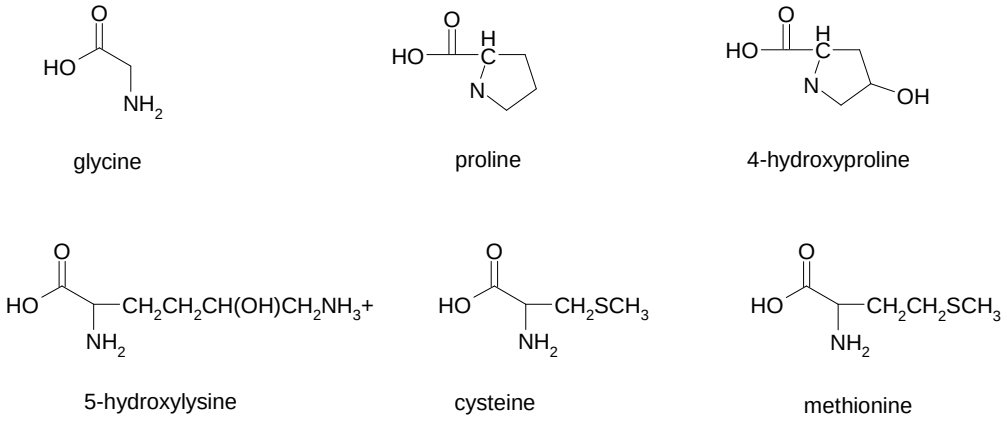

Figure 5: The most abundant amino acids of collagen.

The characteristic sequence of amino acid residues of collagen gives the polypeptide chains of this protein a left-handed helix shape in which each glycine residue is located at the interior of the helix. Left-handed helices interact with each other to form triple helices (or coiled coils), called tropocollagen helices, which are held together by a network of intermolecular hydrogen bonds. In turn, tropocollagen helices form super-coils that are referred to as collagen microfibrils.

Crystalline domains confer to collagen a tight packed structure which is therefore not easily accessed by degrading agents.

2.2) Degradation of collagen

Protein materials undergo degradation through a number of chemical reactions. Hydrolysis (acid or alkali catalyzed) of peptidic bonds bring about a depolymerization of collagen associated to a loss of tensile strength and potentially to an increase in the number of acidic groups. The presence of a higher than normal amount of free water[1] in parchment may also lead to the weakening or breakdown of the hydrogen bonds network which is responsible for the conformation of collagen aggregates. This is in turn associated to collagen denaturation and swelling.

As it was the case for cellulose, photo-induced degradation of parchment causes the formation of organic radicals via homolytic cleavage of chemical bonds of collagen. Again, this is associated to depolymerization and loss of tensile strength. Moreover, the radicals formed are almost always highly reactive species that are involved in further reactions. Some of the possible reaction routes are hydrogen abstraction (with consequent radical propagation), cross-linking with radicals centered on neighbouring collagen molecules (associated to increased fragility of parchment), peroxide or hydroxyl radical formation in the presence of oxygen and water. Peroxides are themselves capable of radical initiation.

Finally, heat is particularly dangerous to protein materials: it causes protein denaturation, i.e. the loss of their quaternary structures. As for collagen, heat is able to disrupt fibril structures and even unravel the triple helices. As a consequence, after denaturation the structure of collagen is less ordered, more permeable to degradation agents and characterized by a lower tensile strength.

3) NMR-MOUSE analysis of paper and parchment

All degradation mechanisms described so far are responsible for a variation of the interactions between water molecules and its environment, i.e cellulose in paper or collagen in parchment. Depolymerization is generally associated to a less densely packed structure of polymeric materials (and consequently a more water permeable one) whereas oxidation and hydrolysis lead to a change in the chemical composition. In particular, in the case of paper and parchment, oxidation and hydrolysis are associated to the formation of polar functional groups (carbonyl, carboxyl, hydroxyl or amino groups).

[1] Although this work is concerned with degradation of chemical or physical type, among the causes of degradation of paper and parchment there is also an attack of biological type.

Nuclear spin relaxation times depend on the physico-chemical nature of a given sample; in particular, nuclear spin relaxation times depend on the specific local magnetic interactions and on the molecular motions characterizing the environment of each spin-bearing nucleus. Consequently, analyzing different samples or samples in different states of conservation, different nuclear spin relaxation times are expected [Blümich et al.2010]. Therefore relaxation times, in particular of protons, are potential markers of the state of conservation of a material. For sensitivity reasons it is easier to detect the NMR signal from hydrogen nuclei, which are particularly abundant in organic materials. Moreover, it is usually more informative to analyze the NMR signals from water hydrogen nuclei (protons), rather than the hydrogen of the solid cellulose, lignin or collagen matrices. The reason is that the solid-like relaxation times (the transverse relaxation time T_2) of hydrogen nuclei are almost independent on the material considered, and therefore are not able to provide specific information. On the other hand the signal intensity from water protons is usually rather low and this is normally a drawback for the sensitivity of the measurements.

Upon degradation of paper, the ratio of crystalline over amorphous cellulose decreases and a number of new polar functional groups is formed; consequently the environment of water molecules changes and so do water-cellulose interactions. Each environment experienced by water molecules gives rise to specific nuclear relaxation times of protons. For this reason, the variation of nuclear relaxation times can be associated to a variation of the interactions between water molecules and cellulose, i.e. to a variation in the microstructure of the material.

As for pure cellulose paper, the decay of transverse magnetization is characterized by a bimodal distribution of relaxation times. The faster relaxation time ($T_{2,F}$) is attributed to cellulose protons whereas the slower one ($T_{2,S}$) is attributed to water protons [Capitani et al.1996], [Blümich et al. 2003].

It has been suggested that transverse relaxation time (T_2) of water in cellulose decreases in old degraded paper but also after accelerated aging (thermal and photo-induced), whereas, as expected, transverse relaxation time of cellulose (T_2) is not affected by aging [Casieri et al.], [Viola et al.], [Blümich et al. 2003]. The behavior of T_2 for water can be explained as follows: the T_2 value for water in paper corresponds to the weighted average of the relaxation times of water tightly bound to cellulose (with T_2 of the order of magnitude of micro seconds) and of free water (T_2 =3÷5 s for distilled water). Therefore, the decrease of T_2 value after accelerated aging can be explained with

a decrease of the ratio of free water over bound water. This effect can be due to an increase of the number of bound water molecules or to the transformation of cellulose into oxycellulose, i.e. a compound with a higher affinity with water.
As for parchment, no previous studies are reported so far concerning the analysis of water relaxation times after normal or accelerated aging.

EXPERIMENTAL

1) Sample preparation

1.1) Lignin paper

Samples of lignin paper were exposed at room temperature to UV-VIS radiation from a 300W Xe lamp, with the IR portion filtered out using a 10cm distilled water filter. The exposure time was 1,5 h for each paper side. Thermal aging was obtained using an atmosphere oven set at 100 °C for 24h.

Nuclear transverse relaxation times (T_2) were measured for all samples before and after aging.

1.2) Samples of historical paper (XV century)

The samples were kindly provided by Prof. C. Federici and were stored inside an envelope in a drawer. Nuclear transverse relaxation times (T_2) of two historical samples of paper (XV century) in different state of conservation (good or bad) were measured. Inverse Laplace transform (ILT) of the Hahn echo decay was calculated with the UPEN algorithm[2].

1.3) Parchment

The relaxation times T_2 and T_1 of several parchment samples have been measured. The parchment listed in table 1 are either modern samples of different origin (sheep, goat) or old samples dated from the XVIII century. The samples were kindly provided by Prof. C. Federici (private collection) and were kept dry and in the dark, with no further special protection.

Samples of modern sheep and goat parchment were exposed to UV-Vis radiation from a 300W Xe lamp for 1,5 h/side or thermally aged at 100 °C for 24h. Unaged

[2] Software developed by the Magnetic Resonance in Porous Media (MRPM) research group, Departments of Physics and DICMA, University of Bologna, Italy.

samples were also analyzed as a reference. Inverse Laplace transform (ILT) of the Hahn echo decay was calculated with the UPEN algorithm.

Modern sheep parchment	Modern goat parchment	Parchment XVIII century (P2)
Modern sheep parchment, thermally aged	Modern goat parchment, thermally aged	Parchment XVIII century (P3)
Modern sheep parchment, exposed to UV-Vis	Modern goat parchment, exposed to UV-Vis	Parchment XVIII century (P4)

Table 1:The nine parchment samples investigated.

2) NMR-MOUSE analysis

NMR-MOUSE analysis was performed with a relaxometer Bruker Minispec Profiler connected to a MOUSE probe with a sensitivity depth of about 1 mm. The operating radiofrequency of this probe is around 15 MHz. The instrument was controlled with the minispec software for windows (Bruker).

Nuclear transverse relaxation time (T_2) was measured using the Hahn echo pulse sequence. CPMG pulse sequence, although faster, has been discarded because of the dependence of the measured values on the experimental parameters (i.e. the dephasing time) for this kind of samples. The Hahn echo pulse sequence is the following:

$$-[t-(\pi/2)_x-\tau(n)-(\pi)_x- \text{ echo-}]_n-$$

where $(\pi/2)_x$ and $(\pi)_x$ represent radiofrequency pulses along the x axis (of the rotating system) causing a rotation of the magnetization in the yz plane of 90° and 180° respectively, $\tau(n)$ is the dephasing time (a function of the number n of the repeated sequences) and t is the time required for the equilibrium to be restored after each Hahn echo is measured (recycle delay).

Nuclear longitudinal relaxation time (T_1) was measured using the Hahn echo-detected Inversion Recovery sequence:

$$-[t-(\pi)_x-\tau(n)-(\pi/2)_x- \tau'-(\pi)_x- \text{ echo-}]_n-$$

where $(\pi)_x$ and $(\pi/2)_x$ represent radiofrequency pulses along the x axis (of the rotating system) causing a rotation of the magnetization in the yz plane of 180° and 90° respectively, $\tau(n)$ is the time during which the longitudinal magnetization is left to recover its equilibrium value, τ' is a dephasing time and t is the time required for the equilibrium to be restored after each echo is measured (recycle delay).

All the measurements were performed at room temperature and the experimental parameters were the following:

Hahn echo pulse sequence							
	Number of scans	Recycle delay/s	Gain/ dB	First echo time/ms	Last echo time/ms	Increment factor	
paper	1024	0.8	109	0.03	1.3	---	
parchment	1024	0.5	105	0.03	1.5	1.05	
Hahn echo-detected Inversion Recovery sequence							
	Number of scans	Recycle delay/s	Gain/ dB	First recovery delay/ms	Last recovery delay/ms	Increment factor	Echo time/ ms
Paper	1024	1	110	0.5	1160	1.4	0.04
parchment	1024	1	110	0.5	1650	1.4	0.04

RESULTS AND DISCUSSION

1) NMR-MOUSE analysis of lignin paper

The decay of the transverse magnetization of cellulose paper is characterized by a bimodal distribution of T_2 relaxation times: the faster relaxation time, $T_{2,F}$, was attributed to cellulose protons whereas the slower one, $T_{2,S}$, was attributed to water protons. The analysis was extended here to lignin paper. Examples of Hahn echo decays for lignin paper before and after thermal and photo-induced aging are shown in figure 6. Data were fitted with the following bi-exponential function:

$$I = W_F e^{\left(-\frac{t}{T_{2,F}}\right)} + W_S e^{\left(-\frac{t}{T_{2,S}}\right)} \quad (1)$$

where I is the Hahn echo intensity, t is time and W_F and W_S are weighting factors representing the amount of transverse magnetization due to protons of cellulose and water respectively. The best-fit parameters $T_{2,F}$, $T_{2,S}$ and percent W_F and W_S are shown in table 2.

In agreement with what observed for cellulose paper, the slow component of transverse relaxation time of lignin paper decreased after both thermal and photo-induced aging (see table 2). Moreover, the relative amount of protons of cellulose slightly increased after accelerated aging (from 73% before aging to 78% after photo-induced or thermal aging). This is probably due to the irreversible loss of water that was proved to be associated to photo-induced and thermal aging [Confortin].

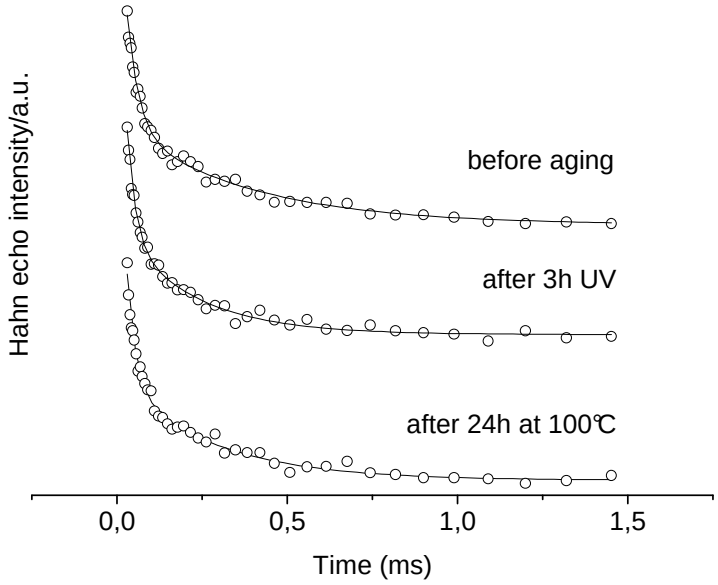

Figure 6: Experimental Hahn echo decays (circles) and fitting curves (solid line) for lignin paper before and after thermal and photo-induced aging.

	$T_{2,F}$/μs	% W_F	$T_{2,S}$/μs	% W_S
Before aging	33±3	73%	370±50	27%
After 3h UV-Vis	26±3	77%	280±40	23%
After 24h at 100°C	24±3	78%	220±20	22%

Table 2: best-fit parameters $T_{2,F}$, $T_{2,S}$ and percent W_F and W_S of lignin paper.

2) NMR-MOUSE analysis of samples of historical paper (XV century)

Hahn echo decays for two historical samples of paper in good and bad conservation state are shown in figure 7. Data were fitted with the bi-exponential function (1). The best-fit parameters $T_{2,F}$ and $T_{2,S}$ and percent W_F and W_S are shown in table 3.

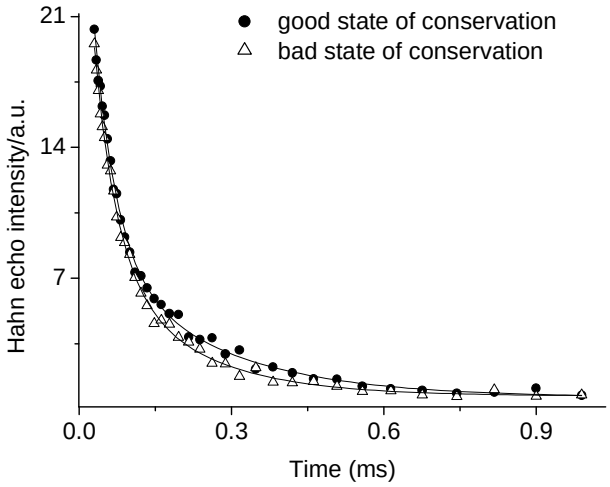

Figure 7: Hahn echo decays and fitting curves of two samples of paper from the XV century.

State of conservation	$T_{2,F}$/μs	% W_F	$T_{2,S}$/μs	% W_S
good	44±4	75%	230±40	25%
bad	44±5	72%	180±30	28%

Table 3: best-fit parameters $T_{2,F}$, $T_{2,S}$ and percent W_F and W_S of two samples of paper from the XV century.

In agreement with previous results, the more degraded sample showed the lower value of $T_{2,S}$ whereas $T_{2,F}$ did not vary with the state of conservation. The trend of percent W_F and W_S was not the one expected since the degraded sample showed a lower $\%W_F$.

Since in this case the values of $T_{2,S}$ of the 2 samples were not as much separated as for the samples of lignin paper (before and after aging), a second type of analysis was performed on experimental data. The decay of Hahn echo was analyzed with inverse Laplace transform (ILT). This mathematical operator allows to obtain a distribution of transverse relaxation times instead of a discrete number of relaxation times as it is the case of multi-exponential fitting. In this way, a more realistic description of local chemical-physical environments for different nuclei is obtained. ILT results are showed in figure 8. Significantly, the distribution of transverse relaxation times for both samples consisted of two bands, centered at T_2 values of the order of magnitude of 10^1 (cellulose protons) and 10^2 μs (water protons) respectively. This is in agreement with the best-fit parameters previously obtained. Moreover, in this case a shift of the band corresponding

to water protons toward shorter relaxation times is clearly visible for the sample in bad conservation state.

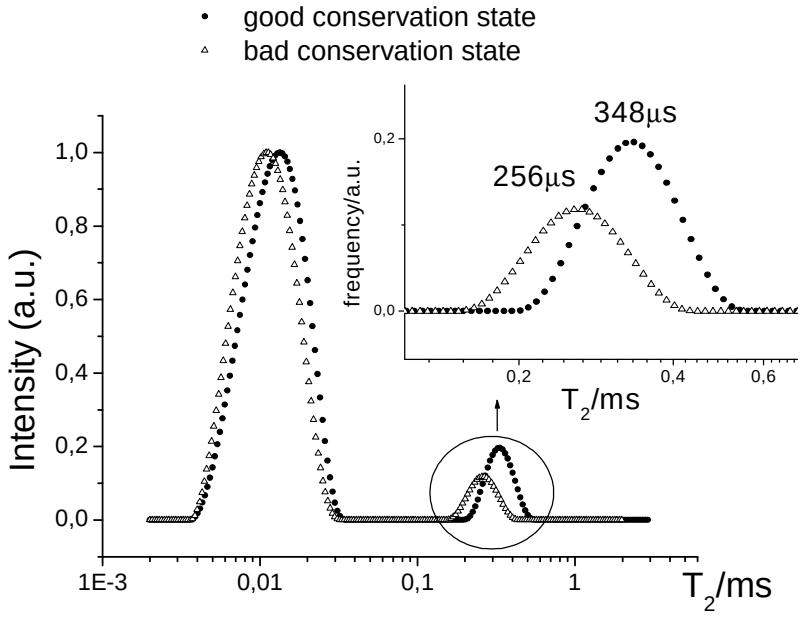

Figure 8: Plot of the ILTs of the Hahn echo decays of XV century paper in two different state of conservation. The inset shows an expanded part of the plot, regarding the slow T_2 components.

It is therefore possible to conclude that :

1. The results of NMR-MOUSE analysis of artificially aged paper are valid also for naturally aged paper. That is, two main types of protons were detected in historical paper: cellulose protons, whose T_2 relaxation time (≈10 µs) is poorly affected by aging, and water protons, whose T_2 relaxation time varies from about 350 µs for the sample of well preserved paper to about 250 µs for the sample in bad state of conservation.
2. The slow component of the echo decay $T_{2,S}$ is confirmed to be a useful marker of the state of conservation of paper.

3) NMR-MOUSE analysis of parchment

In this section, the NMR-MOUSE analysis of the 9 parchment samples, listed in table 1, (3 from the XVIII century and 6 from the XX century) is presented. As described in the experimental section, modern sheep and goat parchments were analyzed both before and after accelerated aging. As it is the case for paper, the amount of water and its distribution among the three sites described above affect physical properties of parchment. For instance, variations in relative humidity can lead to severe

parchment deformation due to collagen fibers rearrangement. NMR-MOUSE analysis on parchment had thus the aim of verifying if the three types of water could be distinguished and, if so, to reveal any correlation between the nuclear spin relaxation times of protons and the state of conservation of parchment.

As a first analysis, Hahn echo decays of all the samples of parchment were fitted with a tri-exponential function in order to verify whether the 3 types of water were distinguishable with NMR-MOUSE. The result was not satisfactory because of the large errors on the best fit parameters, which did not allow to separate three different contributions to the decay. As a further attempt to improve the results, still using multiexponential description of the experimental data, a logarithmic plot have been examined as follows:

1. the echo decay intensities have been normalized to the initial value and the logarithm has been calculated: $I_{calc}=\log[I_{exp}(t)/I_{exp}(t_0)]$ where $I_{exp}(t)$ is the experimental Hahn echo intensity at time t;
2. a graph I_{calc} versus t has been constructed and the obtained data set has been divided into the following three time intervals: 0.03 to 0.08 ms, 0.12 to 0.49 ms and 0.5 to 1.18 ms [3];
3. data belonging to each group have been fitted with the linear function $I_{calc}=-tau*t+c$.

An example of the logarithmic plot and the corresponding fit of the data is shown in figure 9.

Hahn echo decay data for all samples, processed according to the method described, showed three linear regions characterized by three different relaxation times (tau1, tau2, tau3). The values of tau1, tau2 and tau3 (with the exception of sample P2), listed in table 4, can be compatible with the expected relaxation times of bound, associated and free water respectively. However, the free water fraction is not detected with good precision because of the experimental conditions used for the data acquisition: the relaxation delay chosen (the time interval between successive acquisition) is too short for free water, and the observed decay (about 1.5 ms) is too short for decay times T_2 of several milliseconds.

[3] These intervals were chosen by visual inspection of the plots. They correspond to regions of linearity of the data.

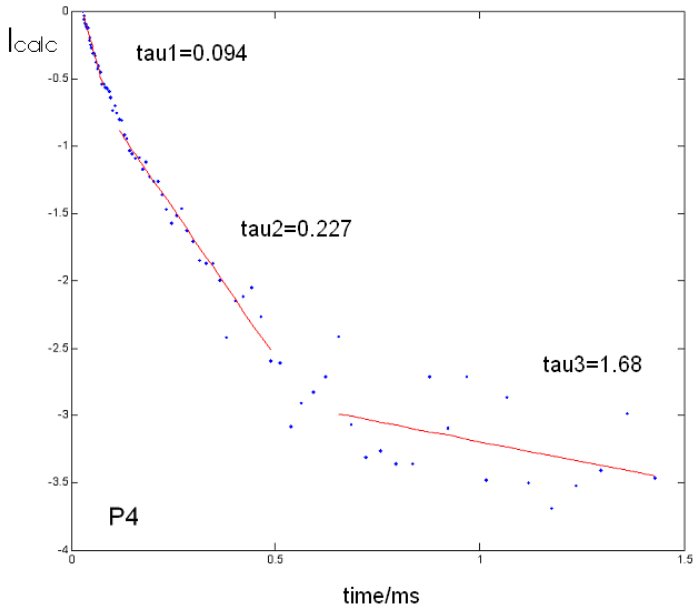

Figure 9: plot of I_{calc} versus t and of the three fitting curves for parchment sample P4.

sample	tau1/ms	tau2/ms	tau3/ms
Modern sheep parchment	0.09	0.25	1.52
Modern sheep parchment, thermally aged	0.10	0.38	0.69
Modern sheep parchment, exposed to UV-Vis	0.10	0.35	0.76
Modern goat parchment	0.09	0.27	1.11
Modern goat parchment, thermally aged	0.10	0.31	0.76
Modern goat parchment, exposed to UV-Vis	0.10	0.34	0.95
Parchment XVIII cent.(P2)	0.08	0.22	10.5
Parchment XVIII cent. (P3)	0.08	0.22	1.37
Parchment XVIII cent. (P4)	0.09	0.23	1.68

Table 4: Best fit coefficients tau1, tau2 and tau3 for the Hahn echo decay data of parchment samples.

Therefore it was decided to use a simplified data analysis, applying the same biexponential fitting function used in the case of paper samples. This is equivalent to neglecting the small contribution from free water. The values of $T_{2,F}$ and $T_{2,S}$ obtained for each sample of parchment are shown in figure 10.

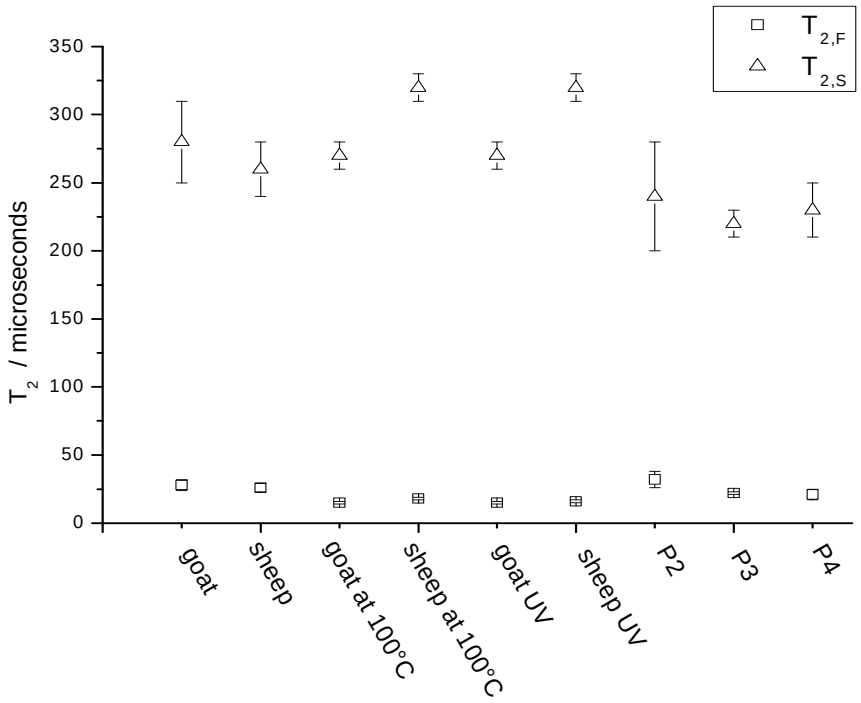

Figure 10: $T_{2,F}$ and $T_{2,S}$ values obtained from the bi-exponential fitting of Hahn echo decays of parchment samples.

In agreement with what observed for paper samples, a very short transverse relaxation time, typical of solids, and a longer transverse relaxation time were obtained.

Let us consider the longer relaxation time, which has so far demonstrated to be dependent on the conservation state of paper. The values of $T_{2,S}$ for modern parchment samples before and after accelerated aging did not follow the same trend observed for paper. As for goat parchment, there was no measurable effect of either thermal or photo-induced aging on T_2 relaxation times. On the contrary, sheep parchment samples showed a slight increase rather than a decrease of $T_{2,S}$ upon aging. As for the historical samples (XVIII century), all samples P2, P3 and P4 showed a slightly shorter value of $T_{2,S}$ with respect to modern samples.

The fact that the dependence of $T_{2,S}$ on accelerated aging of parchment was not as marked as for paper is consistent with the well known information that parchment is a more durable material than paper. More ancient samples or samples in worse conservation state would therefore be required in order to appreciate a significant effect on nuclear transverse relaxation times of parchment.

Inverse Laplace transforms (ILT) of Hahn echo decay data were calculated and an example of the result obtained for modern sheep parchment is shown in figure 11. The

positions of the maxima and the ratio of band 1 area (A_1) over band 2 area (A_2) are reported in table 5.

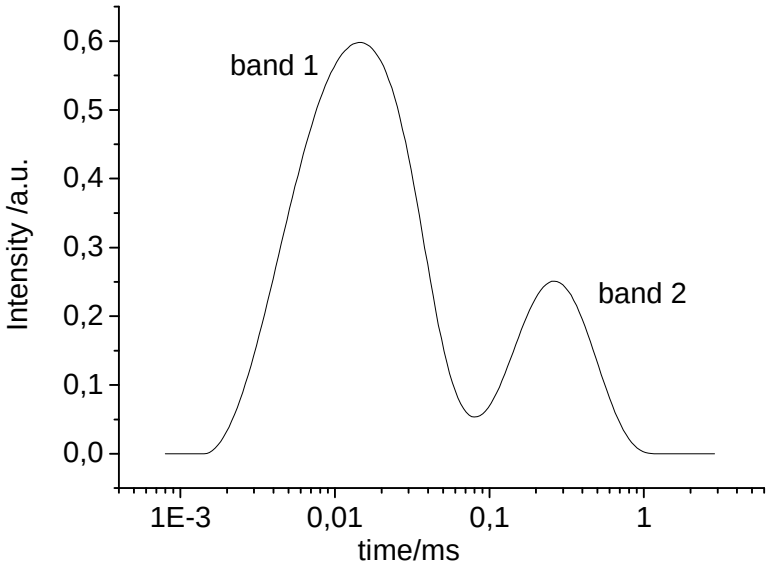

Figure 11: ILT of the Hahn echo decay of modern sheep parchment.

sample	**$T_{2,1}$/μs**	**$T_{2,2}$/μs**	**A_1: A_2**
Modern sheep parchment	20±20	270±50	1:4
Modern sheep parchment, thermally aged	10±10	320±50	1:7
Modern sheep parchment, exposed to UV-Vis	10±10	310±50	1:7
Modern goat parchment	20±20	250±50	1:5
Modern goat parchment, thermally aged	10±10	270±50	1:5
Modern goat parchment, exposed to UV-Vis	10±10	260±50	1:5
Parchment XVIII cent.(P2)	20±20	200±50	1:2
Parchment XVIII cent. (P3)	20±20	210±50	1:3
Parchment XVIII cent. (P4)	10±10	210±20	1:6

Table 5: ILT results for parchment samples. A_1 and A_2 are integrated band areas.

The distribution of transverse relaxation times for all samples consisted of two bands centered around values of 10 μs ($T_{2,F}$) and 10^2 μs ($T_{2,S}$), in agreement with the result of the bi-exponential fitting just described.

The following attributions for transverse relaxation times $T_{2,F}$ and $T_{2,S}$ are proposed:

- $T_{2,F}$, whose value is indicative of a solid phase, is due to bound water;

- $T_{2,S}$ is due to associated water.

Moreover, the order of magnitude of the experimental A_1/A_2 ratio is consistent with the associated over bound water ratio reported in literature (about 4 in parchment at room temperature and 50% RH). The values of $T_{2,F}$ and $T_{2,S}$ obtained for each sample of parchment via ILT are reported in figure 12. The trend of data points is consistent with what obtained with the biexponential fittings (see figure 10), i.e. a slight decrease in $T_{2,S}$ was associated to the historical samples.

Nevertheless, the uncertainty of the measurements was still high, due to the width of the T_2 distributions. Consequently, based on these measurements, it was not possible to draw definitive conclusions on the ranges of expected T_2 for modern parchment and parchment from the XVIII century. However, as it has already been noted, with older or more degraded parchment the T_2 variations might be sufficiently large to allow a clear identification of the effects of aging.

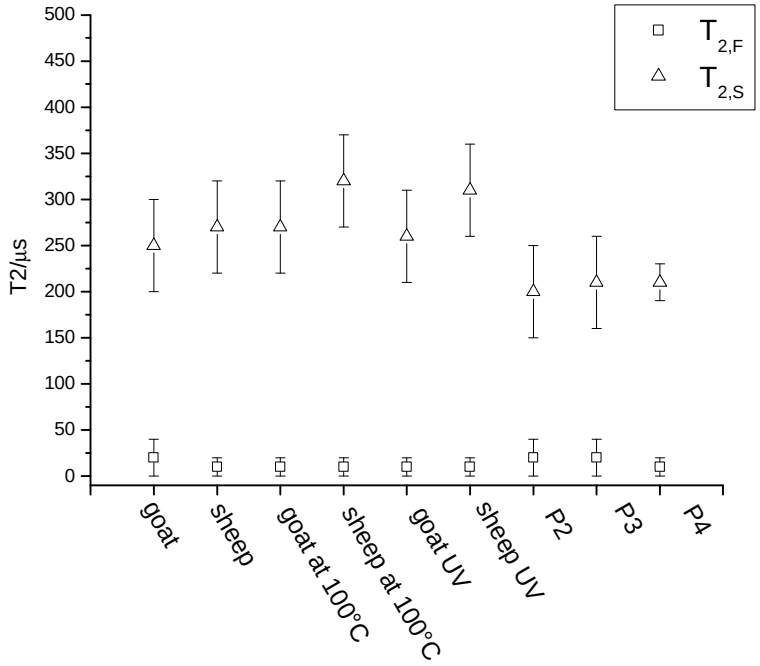

Figure 12: $T_{2,F}$ and $T_{2,S}$ values obtained from the ILT of Hahn echo decays of parchment samples.

Spin-lattice (or longitudinal) relaxation times T_1 of all parchment samples were measured using inversion recovery (IR); data were best-fitted with a bi-exponential function. Fast longitudinal relaxation time $T_{1,F}$ and slow longitudinal relaxation time $T_{1,S}$ for all samples have been obtained and are shown in figure 13, whereas table 6 summarizes the best fit parameters. W_F and W_S are weighting factors representing the amount of longitudinal magnetization decaying according to the time constants $T_{1,F}$ and

$T_{1,S}$ respectively in the fitting function. A tentative assignment of these two T_1 components (fast and slow) can be proposed, considering the following points:

1) the solid-like protons of the protein matrix and of the strongly bound water should not be contributing to the observed signal because the echo detection was obtained using a relatively long interpulse delay (τ=100μs). At this delay, the echo intensity from solid protons is vanishingly small.
2) The associated water and free water may have T_1 relaxation times comparable with those observed in our measurements.

Consequently, the short T_1 can be assigned to the associated water and the long T_1 to the free water. The relative amount of these two fractions was strongly different between samples, and this could be due to different contents of the easily exchangeable free water.

Longitudinal relaxation time showed a dependence upon sample age: modern parchments (XX century) gave the highest $T_{1,F}$ and $T_{1,S}$ values which were in the range from 53 to 46 ms and from 7 to 11 ms respectively. XVIII century parchments showed values of $T_{1,F}$ and $T_{1,S}$ comprised in the range from 14 to 28 ms and from 1.3 to 2.3 ms respectively.

On the contrary, it seemed that accelerated aging does not sensibly affect longitudinal relaxation times. Again, this can be referred to the higher durability of parchment compared to paper, which depends on the higher resistance to photolysis and depolymerization.

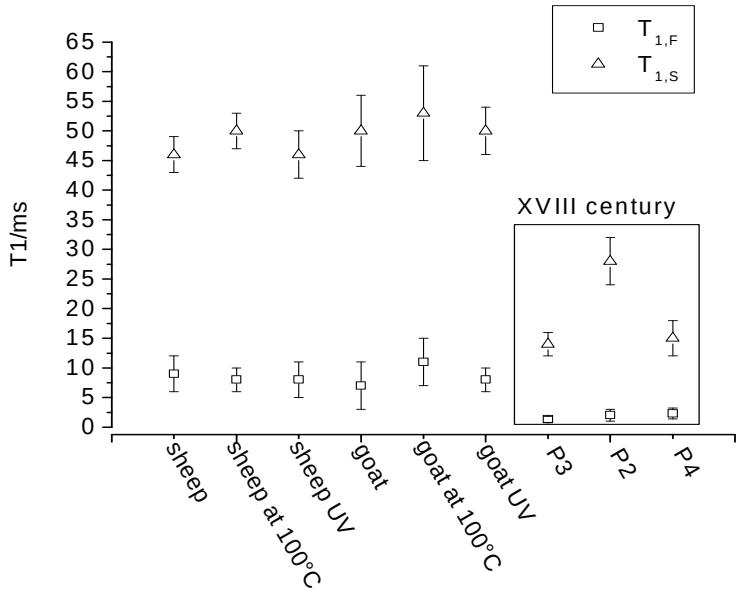

Figure 13: $T_{1,F}$ and $T_{1,S}$ values obtained from the biexponential fitting of Inversion Recovery data of parchment samples.

sample	**$T_{1,F}$/ms**	**$T_{1,S}$/ms**	**W_F:W_S**
Modern sheep parchment	9±3	46±3	1 : 5
Modern sheep parchment, thermally aged	8±2	50±3	1 : 3.3
Modern sheep parchment, exposed to UV-Vis	8±3	46±4	1 : 3.7
Modern goat parchment	7±4	50±6	1 : 3.7
Modern goat parchment, thermally aged	11±4	53±8	1 : 1.9
Modern goat parchment, exposed to UV-Vis	8±2	50±4	1 : 2.7
Parchment XVIII century (P3)	1.3±0.5	14±2	1 : 1.9
Parchment XVIII century (P2)	2±1	28±4	1 : 2.4
Parchment XVIII century (P4)	2.3±0.9	15±3	1 : 1.4

Table 6: best fit parameters for the biexponential fittings of Inversion Recovery data of all parchment samples.

The inverse Laplace transform (ILT) of Inversion Recovery data for all samples was calculated and an example of the obtained result is shown in figure 14.

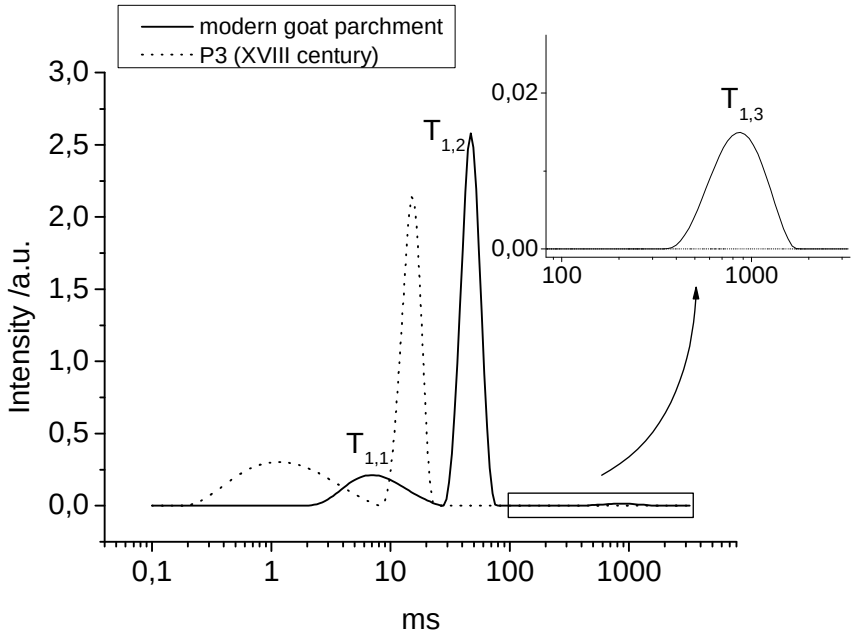

Figure 14: ILT of Inversion Recovery data of modern goat parchment (solid line) and of a sample of parchment from the XVIII century (dotted line)**.**

With the only exception of sheep parchment, inverse Laplace transforms of Inversion Recovery data of all modern parchment samples were characterized by the presence of 3 bands located into the following time intervals: 6÷10 ms, 40÷50 ms and 500÷1000 ms. The positions of the maximum of frequency of each band were called $T_{1,1}$, $T_{1,2}$ and $T_{1,3}$ respectively. On the contrary, parchment samples from the XVIII century did not show the band at higher relaxation times, but were instead characterized by 2 bands located into the following time intervals: 0.78÷2 ms and 15÷30 ms. $T_{1,1}$, $T_{1,2}$ and $T_{1,3}$ values and the relative areas of the bands are reported in table 7[4] whereas a plot of $T_{1,1}$, $T_{1,2}$ and $T_{1,3}$ values for each sample is shown in figure 15. The trend of $T_{1,1}$ and $T_{1,2}$ values was consistent with the result of bi-exponential fittings of Inversion Recovery data shown in figure 13. Nevertheless, the separation between modern samples and XVIII century samples was not as straightforward as before (figure 13). The relative areas of the bands are instead very different from the weight (W_F or W_S) of each time constant ($T_{2,F}$ and $T_{2,S}$) obtained previously. In particular, the A_2/A_1 ratio is much larger than the W_F/W_S ratio.

[4] Errors were not reported for the samples whose ILT bands were too superimposed for calculating a reliable error.

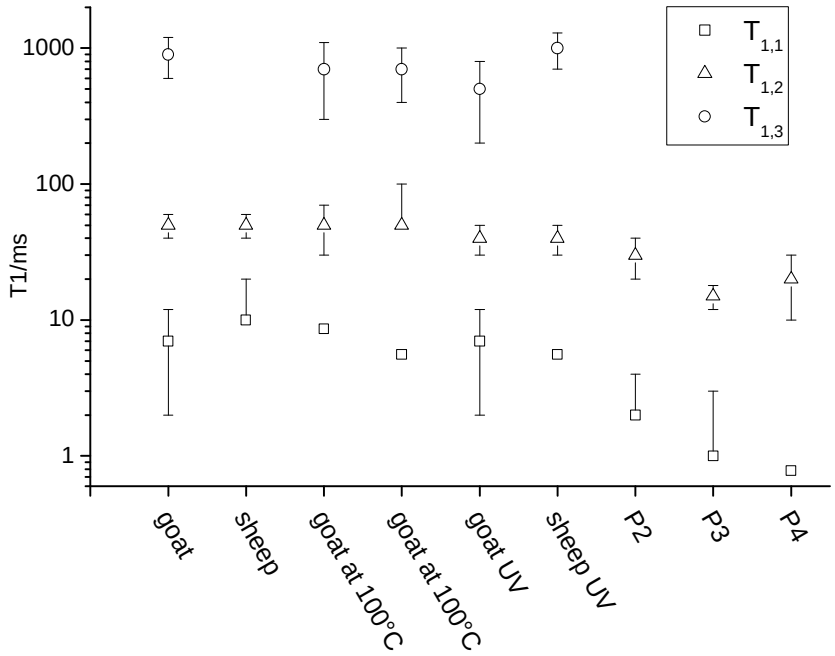

Figure 15: $T_{1,1}$, $T_{1,2}$ and $T_{1,3}$ values obtained from the ILT of Inversion Recovery data of parchment samples.

Sample	$T_{1,1}$/ms	$T_{1,2}$/ms	$T_{1,3}$/ms	A_1:A_2:A_3
Modern sheep parchment	10±10	50±10	---	1:18
Modern sheep parchment, thermally aged	5.6	50±50	700±300	1:12
Modern sheep parchment, exposed to UV-Vis	5.6	40±10	1000±300	1:14:0.80
Modern goat parchment	7±5	50±10	900±300	1:23:4
Modern goat parchment, thermally aged	8.6	50±20	700±400	1:4:2
Modern goat parchment, exposed to UV-Vis	7±5	40±10	500±300	1:19:13
Parchment XVIII cent. (P3)	1±2	15±3	---	1:14
Parchment XVIII cent. (P2)	2±2	30±10	---	1:34
Parchment XVIII cent. (P4)	0.78	20±10	---	1:19

Table 7: ILT results for parchment samples. A1, A2 and A3 are integrated band areas

CONCLUSION

Nuclear Magnetic Resonance spectroscopy (NMR) has proved to be potentially useful in the field of conservation science. The NMR relaxometry, using the NMR-MOUSE instrument, is a completely non-destructive and portable technique that provides information linked to the bulk microstructure of materials: nuclear relaxation times of water protons depend on water molecule environment and provides information on the distribution of water in a given material. This information is linked to the state of conservation: for instance, degradation of polymeric materials (i.e. paper, parchment) is often associated to an increase in the (less densely packed) amorphous phase or a change in distribution of water molecules inside the material. The possibility to detect a change in the chemical or physical microstructure of an object without sampling is particularly useful when dealing with works of art.

In this work, with NMR-MOUSE it was possible:

- to identify physico-chemical parameters, namely the transverse relaxation times of water protons in cellulose, correlated to the state of conservation of paper. In more details, the transverse relaxation time T_2 of water is observed to decrease, compared to pristine samples, after accelerated aging or in old degraded papers.
- to distinguish between water in two different locations in parchment (bound to collagen or condensed into micropores less than 30÷50 μm in diameter between collagen fibers) on the basis of transverse relaxation time;
- to distinguish modern parchment from XVIII century parchment on the base of longitudinal relaxation time;

Despite the promising results, much work is still to be done in order to improve the reliability of the NMR relaxometry for the assessment of degradation status of writing materials composed of cellulose (paper) or proteins (parchment).

CHAPTER FOUR
PIGMENTS AND DYES

Pigments and dyes have always been used for their colors and also for their supposed magic properties. In most cases, pigments and dyes were difficult to find or to produce and they had to be imported from distant countries or skilled craftsmen (or even alchemists) and chemists were to prepare them. Interestingly, the names used to qualify colorants often reflected their geographical origin or the symbolic values attributed to them, rather than describing their chemical nature. For instance, the semi-precious stone lapis lazuli was called ultramarine blue because it came from “beyond the seas” (it was mainly imported from Afghanistan) and another blue pigment obtained from a plant was called Indigo because it originally came from India. In other cases, the names referred to the hue of the colorant and different trade names were sometimes given to the same colorant in different countries. It is the case of the term ‘mountain green’ to refer to malachite green or of one of the first synthetic dyes, known with names such as fuchsine or magenta. Thus the names of dyes and pigments are often fantastical or ambiguous and information on their chemical nature would be fundamental both for identification and conservation purposes.

In this work, a number of known and unknown pigments or dyes deposited on inorganic substrates (lakes) were analyzed with Electron Paramagnetic Resonance (EPR) with the aim of comparing their spectral features. Moreover, some linseed oil paints (and pure linseed oil, as a reference) were deposited on glass slides and analyzed with NMR-MOUSE during drying, in order to study the effect of the pigments on oil polymerization.

1) EPR study of pigments and dyes

EPR analysis was performed with an X-band (9-10 GHz) Bruker ER200 spectrometer for continuous wave EPR spectra and an X-band (9-10 GHz) Bruker Elexsys580 spectrometer for both continuous wave and pulsed EPR spectra. The low temperature spectra have been recorded using a nitrogen flow temperature control system Bruker BVT2000.

EPR is sensitive to radicals and paramagnetic species, i.e. species with one or more unpaired electrons. Pigments are themselves very often based on paramagnetic

transition metal ions and consequently EPR is in principle a powerful micro-invasive technique for pigment identification. Moreover, this technique can also give information on the coordination geometry of paramagnetic centers. Finally, its sensitivity is very high and for this reason also impurities or defects in the crystalline lattice can be detected. For instance, samples of marble coming from different quarries have been distinguished with EPR [Attanasio et al.] on the basis of the different coordination geometry of the Mn(II) impurities.

Consequently, it has been decided to verify if EPR was effective also for identifying pigments. The objective was to evaluate the possibility of using EPR as an efficient tool for qualitative analyses. For this reason, the EPR spectra of small amounts of pigments (about 10mg) were recorded without any pre-treatment of the samples.

Interestingly, all the pigments analyzed showed an EPR signal, at least due to the ubiquitous metal cations Fe(III) and Mn(II) which can be present in low concentration as impurities. Moreover, even from a simple visual analysis it is evident that almost all of them give rise to characteristic spectral features.

As an example, it is possible to distinguish very easily between three kinds of blue pigments, i.e. Ultramarine blue, Cobalt blue and Prussian blue (figure 1).

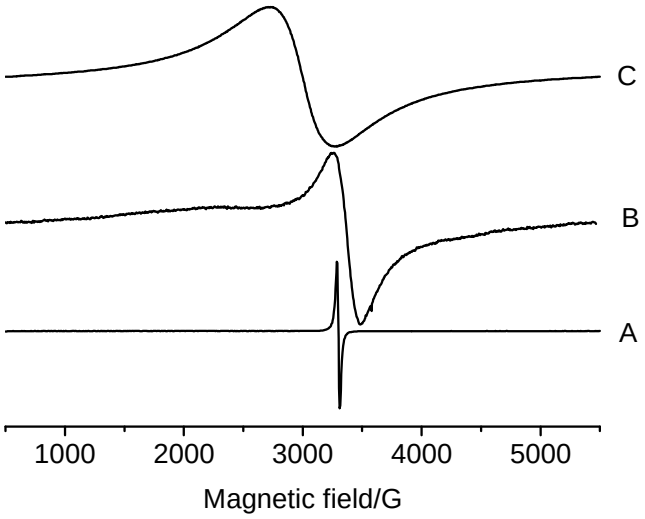

Figure 1: EPR spectra of blue pigments at room temperature. A. Ultramarine blue (from Kremer), B. light Cobalt blue (from Kremer) and C. Prussian blue (from Maimeri).

Without analyzing in details the EPR spectral features of the three blue pigments, it is sufficient to describe the different spectra as arising from paramagnetic sulfur clusters (Ultramarine, see below), from Co(II) ions (Cobalt blue) and from Fe(III) ions (Prussian blue).

Another interesting case comes from the comparison of three types of ultramarine pigments (from Kremer): Ultramarine red, Ultramarine blue and Ultramarine violet. The Ultramarine pigments are composed of sodium aluminum silicates including sulfur atoms. The color is due to several paramagnetic clusters of sulfur ($S^{2-\cdot}$, $S^{3-\cdot}$ and $S^{4-\cdot}$) which are present with different amounts in the pigments [Arieli et al.], [Clark et al. 1978], [Clark et al. 1983] . It is clearly seen in figure 2 that all the paramagnetic sulfur clusters show different spectra. In this case, the spectra were recorded at 120 K and the differences among the three pigments are pronounced.

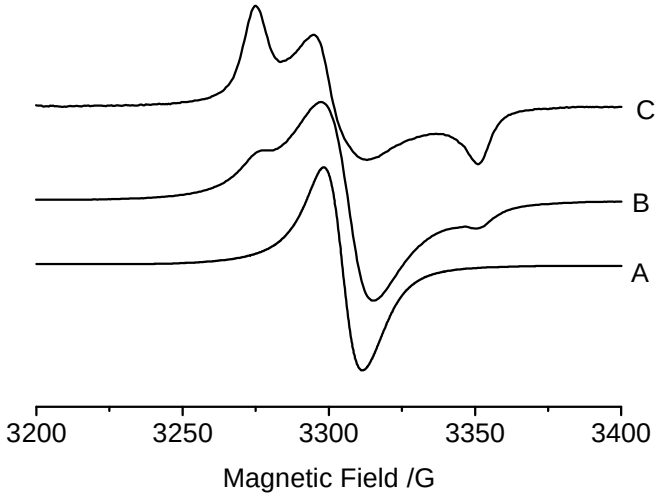

Figure 2: EPR spectra of three Ultramarine pigments (from Kremer) at 120K. A. Ultramarine blue, B. Ultramarine violet, C. Ultramarine red.

The EPR spectra of ultramarine pigments can be interpreted as arising from paramagnetic species (sulfur clusters) with different properties of local symmetry. They can be fitted assuming the presence of two main species, having rhombic and almost isotropic (spherical) symmetries, revealed by the g tensor components [Arieli et al.]. In the case of ultramarine red, the rhombic g-tensor shows three distinct values, whereas in ultramarine blue the g-tensor is almost isotropic, showing a single component. The ultramarine violet results as a superimposition of the two components.

Also cadmium sulphide (CdS) showed an evident EPR signal, with a g=2.004 (3290 G) (figure 3). This signal is likely attributable to a lattice defect. In fact, undoped single crystals of CdS have been examined and different EPR lines were found, attributable to lattice vacancies [Brailsford et al.]. The distribution and nature of these defects are likely to change in pigment samples from different sources, so that in principle EPR could be used as a tool to assess the origin of a CdS pigment.

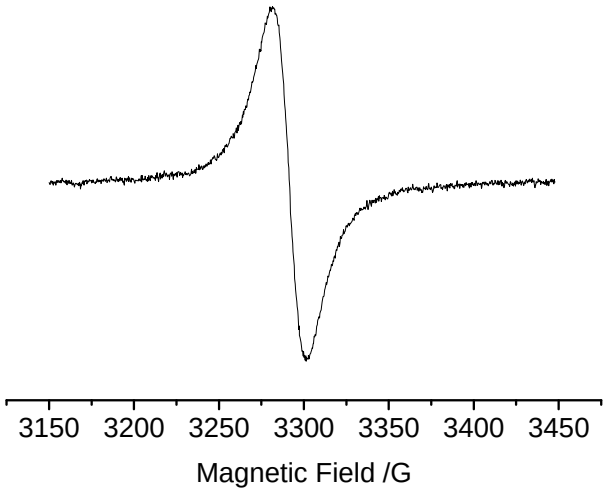

Figure 3: EPR spectrum of a CdS pigment (from Maimeri).

Several red/yellow or brown ochres have been examined: all the ochres exhibited the typical EPR profile of Fe(III) (an example is shown in figure 4): a broad signal around g=2.0 and (sometimes) a sharp signal around g=4.3 (around 1500 G). The broad signal is related to Fe(III) in an octahedral coordination, whereas the sharp signal is due to Fe(III) in a distorted site. A signal of Mn(II), occurring as an impurity, is present sometimes in the pigments. In this case, the Fe(III) profile is similar but not equal in all the cases, and by an accurate analysis of EPR Fe(III) spectra or of the lines associated to the impurities, it should be possible to distinguish the different ochre pigments.

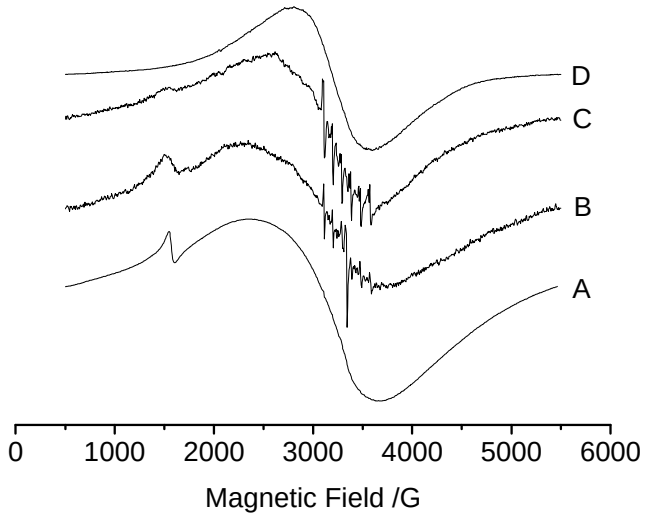

Figure 4: EPR spectra of three yellow-brown ochres. A. ‘ocra francese’ (French ochre, from Kremer), B. ‘ocra dorata’ (golden ochre, from Kremer), C ‘terra di Siena’ (Sienna from Dolci), D. ‘terra ombra bruciata Cipro’ (Cipro burnt umber from Dolci).

As an example of lake (organic dye deposited on an insoluble substrate in order to make a pigment), the EPR spectrum of Alizarin Crimson (1,2-dihydroxyanthraquinone)

in shown in figure 5. The signal is dominated by Fe(III) present as vicariant ion in the inorganic substrate (broad features), and a sharp anisotropic signal around g=2 (3340 G) which might be due either to a lattice defect or to trapped organic radicals (e.g. oxidized alizarin).

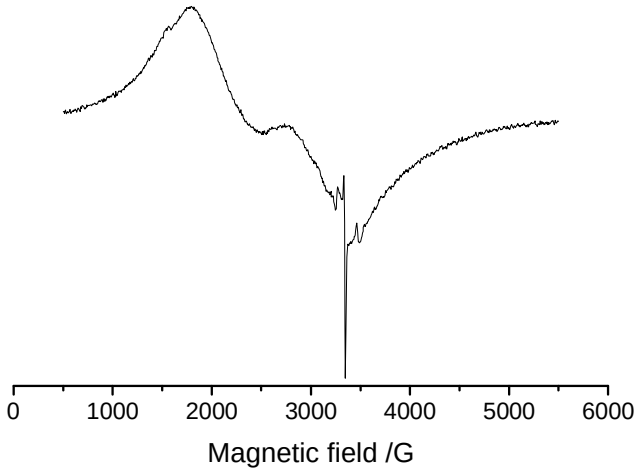

Figure 5: EPR spectrum of Alizarin Crimson lake (from Kremer).

Also the EPR spectra of several green pigments look very different (figure 6). Chromium-based pigments show broad lines, but marked differences can be observed according to the different coordination of Cr(III) in the lattice (figure 6b and 6d). In some organic-based green lakes (bought from Renner, figure 6a and 6c) a typical six-line pattern due to Mn(II) overlapping a broad signal maybe due to Fe(III) can be observed, due to metal impurities in the inorganic substrate. Small signals due to Cu(II) and, at g=2.002, a line from organic radicals are also visible.

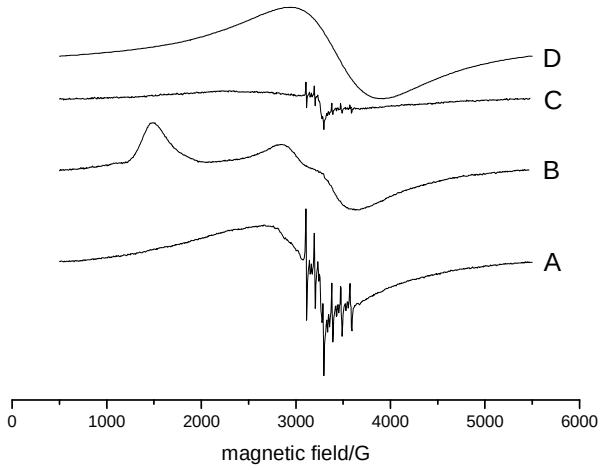

Figure 6: EPR spectra of green pigments and lakes. A. ‘verde simil cromo’ (chrome green–like lake, from Renner), B. ‘verde cromo’ Cr_2O_3 (chrome green, from Kremer), C. ‘verde 4 FR 37’ (green lake labeled ‘4 FR 37’, from Renner) and D. ‘verge Guignet’ $Cr_2O_3*H_2O$ (Guignet green, from Kremer).

As the last example, in figure 7 the EPR spectra of two zinc white pigments (Zinc Oxide) from different brands are shown. The common feature of the spectra is the broad unresolved band attributed to iron impurities. The single narrow line at the centre of the spectrum, visible only in one of the samples, is due to surface defects of ZnO crystalline, which are dependent on the preparation method and the microscopic morphology of the material [Halliburton et al.], [Ischenko et al.]. This line could therefore be used as a marker for the identification of white ZnO pigments of different provenance or produced by different methods.

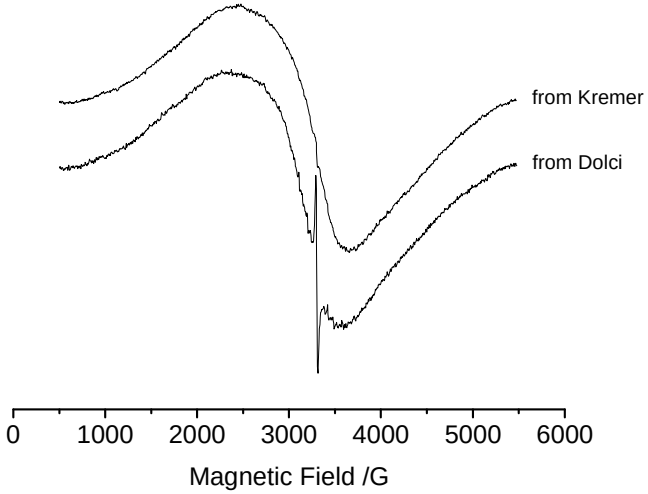

Figure 7: EPR spectra of zinc white pigments.

As a general conclusion of the examples of EPR analysis on several pure pigments, it can be said that EPR spectroscopy is potentially an useful technique for the identification of different pigments and for provenance studies. Of course the best results would be obtained in combination with other analytical and spectroscopic techniques. The small EPR signatures of impurities or of crystalline defects may allow also for the analysis of different production methods, helping in the historical and technological analysis of the work of art.

2) NMR-MOUSE analysis of linseed oil and linseed oil paints

2.1) Introduction

Linseed oil is composed mainly of unsatured triacylglycerols with mixtures of fatty acids; triacylglicerols of linseed oil are esters of linolenic acid (≈50%), linoleic acid (≈10-20%) and oleic acid (≈10-20%) with glycerol (figure 8). It is classified as drying

oil since it contains more than 65% of unsatured fatty acids and forms a solid film on exposure to air and light.

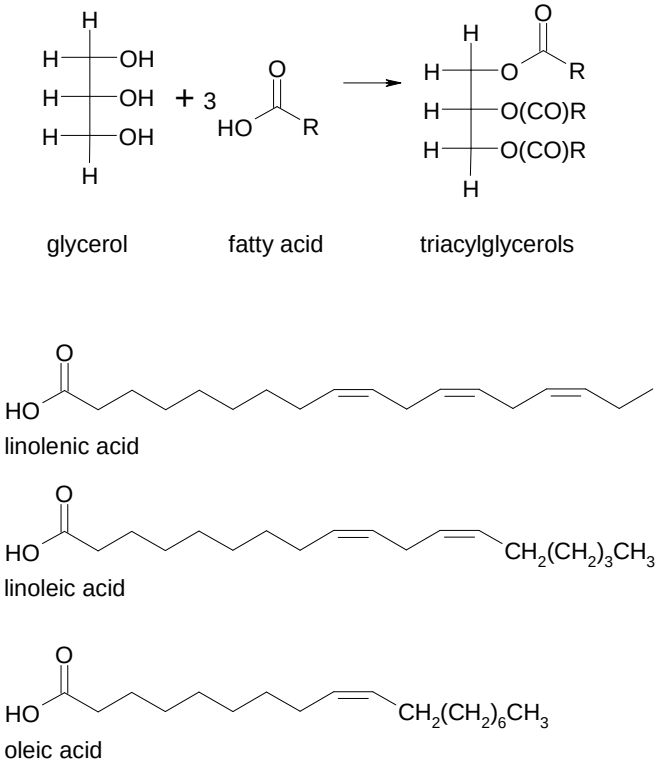

Figure 8: esterification of glycerol with fatty acids yields triacylglycerols (above). The characteristic unsatured fatty acids of linseed oil are linolenic acid, linoleic acid and oleic acid (below).

The curing (or drying) of linseed oil consists of a series of radical chain reactions initiated by light, heat or transition metals such as Cu, Co, Mn, Fe. [Campanella et al.], [van den Berg]. During initiation, organic radicals of unsatured fatty acids and triacylglycerols are formed. If peroxides are present, they might initiate radical chain reactions as well. Examples of initiation reactions are the following:

$$RH \xrightarrow{h\nu} R^{\bullet} + H^{\bullet} \quad (1)$$

or

$$RH + M^{n} \longrightarrow R^{\bullet} + H^{+} + M^{n-1} \quad (2)$$

or

$$ROOH + M^{n-1} \longrightarrow RO^{\bullet} + OH^{-} + M^{n} \quad (3)$$

where M^{n} and M^{n-1} are two different oxidation states for the same metal ion.

These radicals react with oxygen during the so-called propagation of the chain through the so-called autoxidation[1] process, which yields peroxyl radicals and peroxides. Finally, during the termination of the chain, peroxyl radicals recombine to give cross-linking of fatty acids or triacylglycerols. Moreover, alkyl and alkoxyl radicals formed during reactions (1), (2) or (3) during the termination of the chain can cross-link forming ethers or carbon-carbon bonds. Since triacylglycerols and fatty acids of linseed oil have more than one unsatured carbon-carbon bond, at the end of the chain an extensive 3D cross-linking and a consequent increase of the average molecular weight is obtained. As a result, a dried film is formed, although still a flexible one and with an open structure, permeable to solvents. In figure 9 the main steps of the drying process are shown.

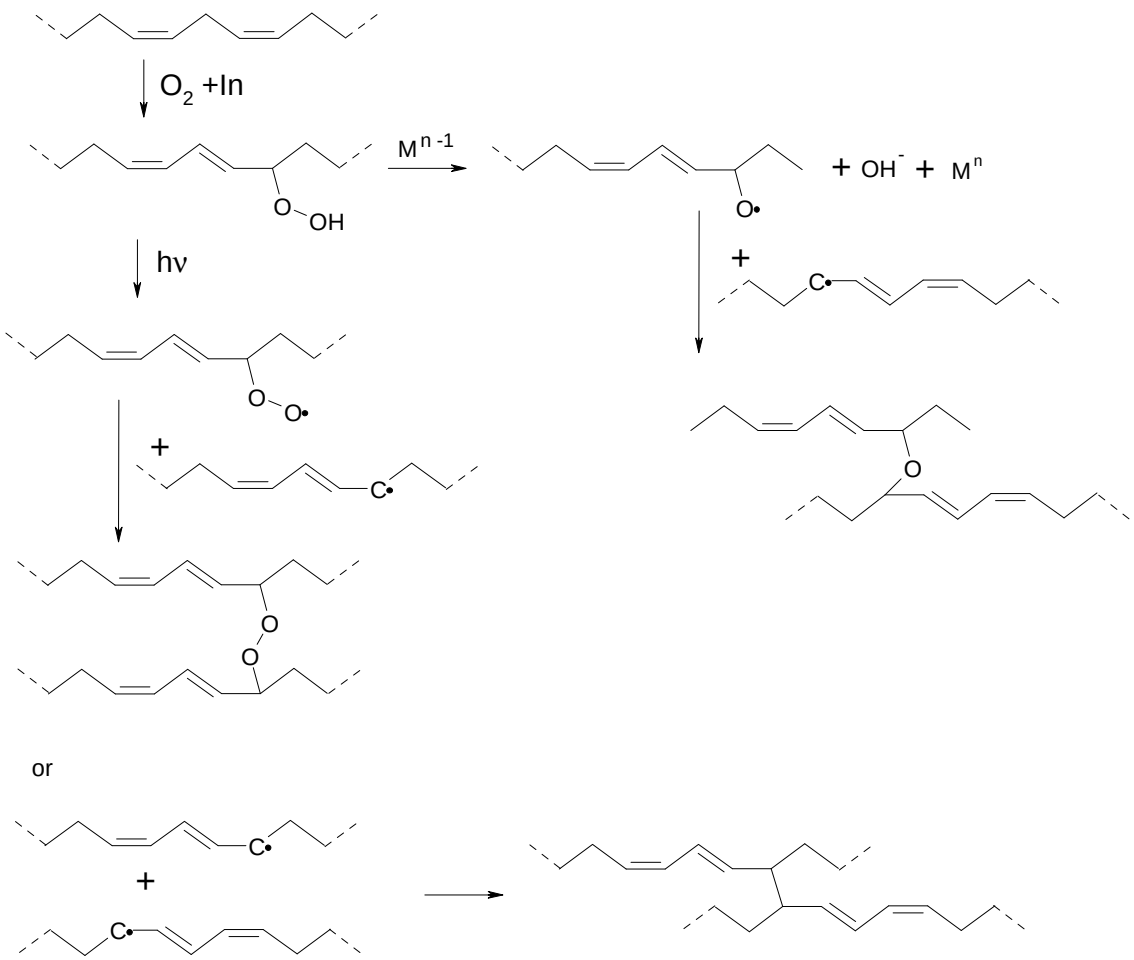

Figure 9: schematic representation of the initiation, propagation and termination of the drying of linseed oil.

[1] Due to the participation of oxygen, the reaction is more properly defined as an oxidation process.

The radical species present during the drying process may also undergo other reactions than cross-linking and form volatile low molecular weight species, such as aldehydes, ketones, alcohols, acids and hydrocarbons.

After the flexible oil film is formed, the uptake of oxygen continues and is responsible for the formation of acidic oxidation products. Moreover, other acidic species (carboxylic acid groups and free fatty acids) may be produced from the hydrolysis of the triglyceride ester bonds. In the presence of metal ions (such as those of pigments), all these acidic groups are involved in the formation of various coordination sites, which strengthen the cross-linked network of the film (lithification stage). What is eventually obtained is a mature aged oil paint [van den Berg].

Because of its good quality as a drying oil, linseed oil has been widely used in oil painting. For this reason it was decided to study with NMR-MOUSE the curing of this oil in the presence and absence of pigments.

Pure linseed oil and six linseed oil paints (Amsterdam oil color) were spread on seven microscope slides. Nuclear relaxation times were measured with NMR-MOUSE for all samples before and during oil drying, over a period of 30 weeks. The pulse sequences used to measure longitudinal (T_1) and transverse (T_2) relaxation times were Inversion Recovery (IR) and Carr Purcell Meiboom Gill (CPMG) respectively. Contrary to what observed for paper samples, in this case the results of the CPMG pulse sequence did not depend on the experimental parameters chosen and therefore this sequence was preferred to the more time-consuming Hahn echo pulse sequence. The CPMG pulse sequence is the following:

$$(\pi/2)_x\text{-}[\text{-}\tau\text{-}(\pi)_{ax}\text{-}\tau\text{-echo-}]_n\text{-}$$

where a is equal to ±1, $(\pi/2)_x$ and $(\pi)_{ax}$ represent radiofrequency pulses along the x (or –x if a=-1) axis (of the rotating system) causing a rotation of the magnetization in the yz plane of 90° and 180° respectively, τ is the dephasing time and n is the number of repetitions.

All the measurements were performed at room temperature and the experimental parameters are given in table 1.

CPMG pulse sequence							
	Number of scans	Recycle delay/s	Gain/ dB	First echo time/ms	Number of echoes		
Liquid oil[1]	32	0.5	102	0.8	3000		
Dry oil	128	1	110	0.03	1000		
Hahn echo-detected Inversion Recovery sequence							
	Number of scans	Recycle delay/s	Gain/ dB	First recovery delay/ms	Last recovery delay/ms	Increment factor	Echo time/ ms
Liquid oil[1]	32	3	105	1	1850	1.4	0.04
Dry oil	64	1	105	0.5	1160	1.2	0.04

Table 1: experimental parameters characterizing the pulse sequences used for measuring T_1 and T_2 of linseed oil and linseed oil paints. [1]within the first ten days.

2.2) Results and discussion

The dependence of longitudinal (T_1) and transverse (T_2) nuclear relaxation times on drying time of linseed oil and the influence of pigments on drying time was studied.

As for transverse relaxation time, Hahn echo decay of protons in pure linseed oil appeared to be mono-exponential within about the first 10 days of drying whereas afterwards it became at least bi-exponential (figure 10 and table 2). This can be rationalized in terms of degree of oil polymerization. When oil is still un-polymerized, protons of oil in liquid phase show a single relaxation time, in a low resolution experiment. On the contrary, with the onset of the polymerization, at least two types of protons can be identified: it is reasonable to assign the two components to the protons belonging to polymerized oil, which give rise to a fast relaxation time $T_{2,F}$, and to the protons belonging to liquid (or not completely polymerized) oil, which give rise to a slow relaxation time $T_{2,S}$.

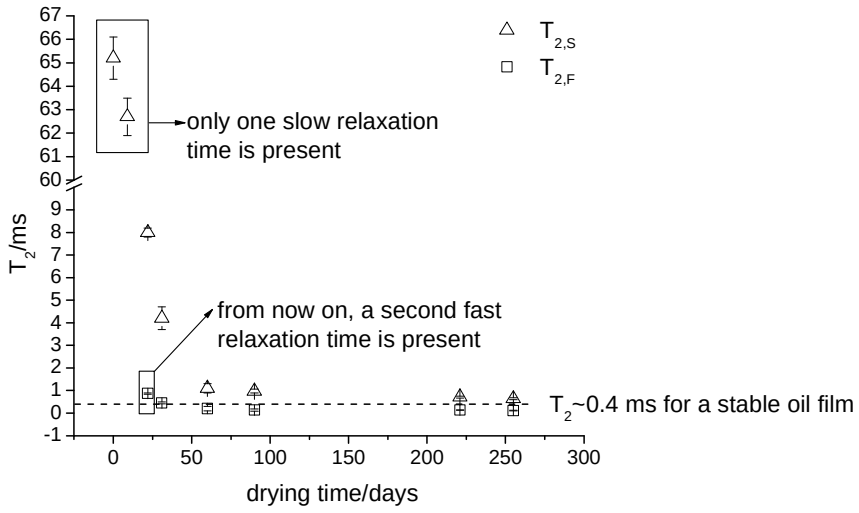

Figure 10. dependence of the transverse relaxation time on drying time for pure linseed oil.

Drying time/days	$T_{2,S}$/ms	$T_{2,F}$/ms	T_1/ms
0	65.2±0.9	--	120±4
9	62.7±0.8	--	127±9
22	8.0±0.2	0.87±0.03	48±3
31	4.2±0.5	0.45±0.04	52±3
60	1.1±0.2	0.2±0.1	59±3
90	0.98±0.08	0.13±0.05	66±7
221	0.71±0.04	0.13±0.01	56±2
255	0.64±0.04	0.11±0.01	67±4

Table 2: transverse and longitudinal relaxation times of pure linseed oil over drying time.

The Inversion Recovery of longitudinal magnetization of linseed oil was satisfactorily fitted with a mono-exponential function regardless of drying time (table 3). In figure 11 a plot of T_1 versus drying time is shown. Longitudinal relaxation time was equal to about 120-130 ms during the first 10 days of drying, whereas afterwards it sharply decreased and remained in a range from 48 to 67 ms during the rest of the drying time. The decrease in longitudinal relaxation time is likely due to the progressive increase in viscosity of the oil during polymerization. The presence of a single relaxation time rather than two, as it was instead the case of the transverse relaxation time, is probably due to an efficient exchange of the magnetization between protons of the polymerized domains of oil (solid phase) and the liquid ones. Therefore, the longitudinal relaxation time can not be used to distinguish between different phases (as it was instead the case of the transverse relaxation time), but it can still be considered an indicator of the progress of the polymerization, since it depends on the viscosity of the oil.

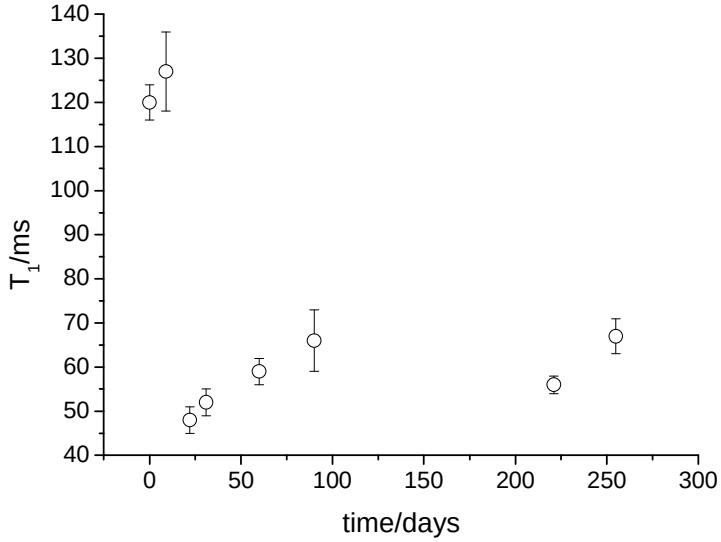

Figure 11. dependence of the longitudinal relaxation time on drying time for linseed oil.

Given the widespread diffusion of linseed oil in painting, it was decided to analyze with NMR-MOUSE six different pigments and lakes in linseed oil (cadmium yellow, cobalt blue, chromium green, Prussian blue, cadmium red and alizarin crimson) in order to evaluate the influence of pigments on drying time of oil. The chemical formulas for the pigments studied are shown in table 3.

Pigment	**Chemical formula**
cadmium yellow (cadmium sulphide)	CdS
cobalt blue (cobalt(II) oxide)	CoO
chromium green (chromium sesquioxide)	Cr_2O_3
Prussian blue (iron (III) ferrocyanide)	$Fe_4[Fe(CN)_6]_3$
cadmium red (cadmium sulphoselenide and sulphide)	Cd(S,Se) and CdS
alizarin crimson (1,2-dihydroxyanthraquinone on alumina)	$C_{14}H_8O_4$

Table 3: chemical composition of the pigments studied.

In figure 12, T_2 values (reported in table 4) corresponding to the six paint layers dried for 4 weeks (circles) and 30 weeks (triangles) are compared. All paints but Prussian blue and alizarin crimson showed a decrease in the value of T_2 after 30 weeks, as it was also the case for pure linseed oil.

With respect to the values of $T_{2,F}$ and $T_{2,S}$ of pure linseed oil dried for 4 weeks (0.45±0.04 ms and 4.2±0.5 ms respectively), either freshly deposited or four-week-old Prussian blue and alizarin crimson paints showed lower T_2 values. A possible explanation of this finding would be that the pigments contained in these paints are able to accelerate oil polymerization or that they contain paramagnetic species that can accelerate the relaxation process. Indeed, as it has already been said, iron ions (in this case coming from Prussian blue) are known for being efficient initiators of linseed oil curing.

On the other hand, $T_{2,F}$ and $T_{2,S}$ values for four-week-old cadmium red are extremely high: it is therefore possible to hypothesize that cadmium red pigment slows down oil polymerization.

As for $T_{2,F}$ and $T_{2,S}$ values of 30-week-old paints, cobalt blue is the only exception, with a very high relaxation time with respect to pure oil ($T_{2,F}$=0.13±0.01 ms and $T_{2,S}$=0.71±0.04 ms for pure oil). Although cobalt can act as a polymerization catalyst, it is possible that it produces a polymer with a smaller average molecular weight, which would cause a higher local mobility of hydrogen atoms, and hence the longer T_2 values.

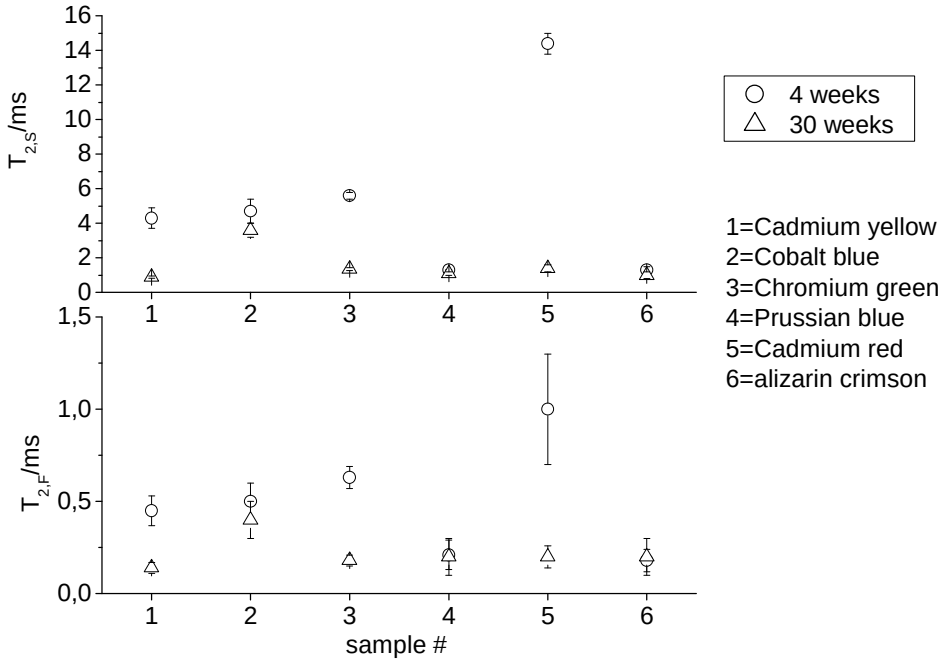

Figure 12. $T_{2,F}$ and $T_{2,S}$ values for six paints after drying times of one month (circles) and seven months (triangles).

oil paint	4-week drying time			30-week drying time		
	$T_{2.S}$/ms	$T_{2.F}$/ms	T_1/ms	$T_{2.S}$/ms	$T_{2.F}$/ms	T_1/ms
cadmium yellow	4.3±0.6	0.45±0.08	50±4	0.89±0.06	0.14±0.03	47±7
cobalt blue	4.7±0.7	0.5±0.1	45±4	3.6±0.4	0.4±0.1	41±3
chromium green	5.6±0.2	0.63±0.06	38±2	1.35±0.09	0.18±0.03	35±2
Prussian blue	1.30±0.02	0.21±0.08	40±5	1.1±0.1	0.2±0.1	34±4
cadmium red	14.4±0.6	1.0±0.3	45±2	1.4±0.2	0.20±0.06	44±2
alizarin crimson	1.3±0.2	0.18±0.06	46±3	1.0±0.2	0.2±0.1	39±4

Table 4: transverse and longitudinal relaxation times of six paint layers dried for 4 weeks and 30 weeks.

In figure 13, T_1 values of six paint layers dried for 4 weeks (circles) and 30 weeks (triangles) are compared. Either after 4 weeks or 30 weeks, all samples showed a shorter longitudinal relaxation time compared to that of pure linseed oil, except for the cadmium yellow paint, where the difference with pure linseed oil is very small. Moreover, all samples showed a decrease in T_1 after 30 weeks of drying, although the errors associated to each measure were quite large, making it difficult to distinguish with certainty between samples dried for 4 weeks and 30 weeks.

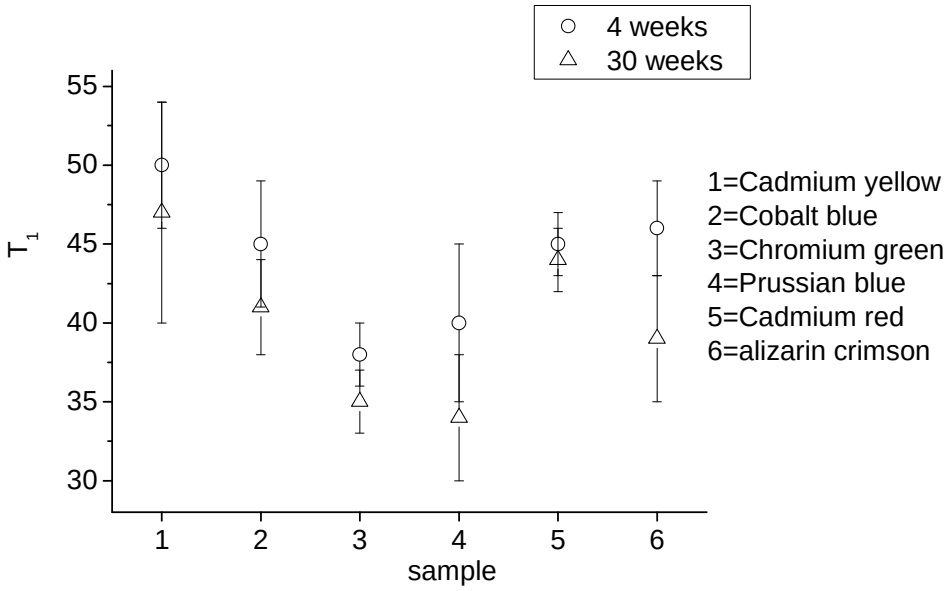

Figure 13. T_1 values corresponding to six paint layers dried for 4 weeks (circles) and 30 weeks (triangles).

NMR-MOUSE has thus pointed out a correlation between nuclear relaxation times and the degree of polymerization of samples of linseed oil and linseed oil paints. This correlation could be used to study the interaction between linseed oil and pigments in paint layers or to work out an evaluation method for the state of conservation of oil

paintings. Indeed, the effects of different pigments (cadmium yellow, cobalt blue, chromium green, Prussian blue, cadmium red) and dyes (alizarin crimson) on the polymerization of linseed oil were studied and NMR-MOUSE did confirm the role that pigments play in the polymerization process.

CHAPTER FIVE
DYES IN AQUEOUS SOLUTION AND ON PAPER: DISCOLORATION AND FADING

INTRODUCTION

Triarylmethane dyes and crystal violet

Since the discovery of Mauve in 1856 by William Henry Perkin, scientific research on synthetic dyes developed immensely and great effort was put on the study of new synthetic routes to bright colored (and profitable) dyes. Among the first chemical classes of dyes to be produced and marketed, triarylmethane dyes held a prominent position because of their wide variety of hues and of their very high molar extinction coefficient ($\varepsilon \geq 10^5 M^{-1}cm^{-1}$), i.e. high coloring power. Indeed, triarylmethane dyes, with their superior properties and lower price than Mauve, were soon preferred and the production of Mauve ceased after some ten years.

The first triarylmethane dye was synthesized in 1859; it concerned of a fuchsia colored dye called Magenta (or Fuchsine) obtained by oxidizing crude aniline with tin(IV)chloride and whose chemical composition consists of two main compounds, pararosaniline and homorosaniline (figure 1, A and B respectively).

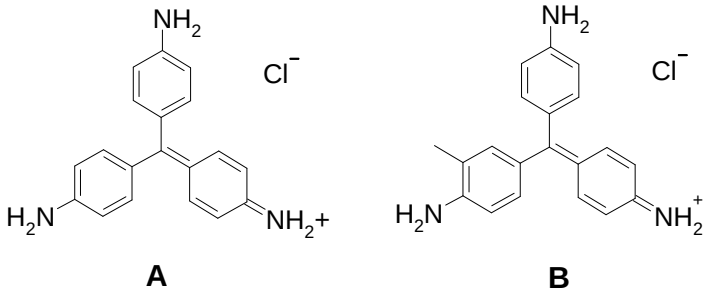

Figure 1: structures of pararosaniline (A) and homorosaniline (B).

Triarylmethane dyes are characterized the presence of three aromatic rings attached to a central carbon atom. The simplest triarylmethane dye is diamond green (DG) (figure 2 A), with two dimethylamino groups in para position with respect to the central carbon atom. In the presence of three para-dimethylamino groups, the dye obtained is called Crystal violet (figure 2 B).

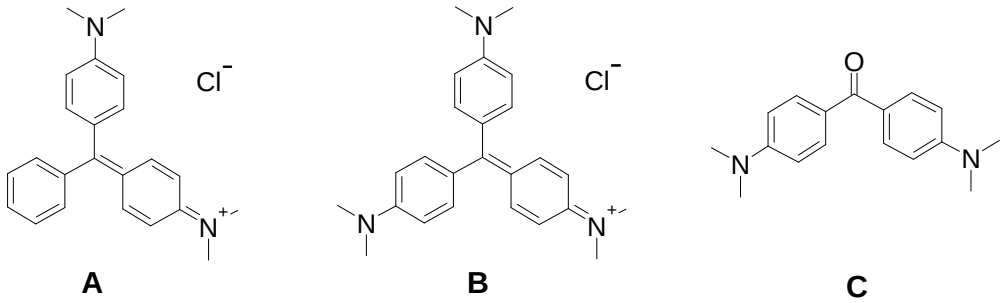

Figure 2 Structures of Diamond Green (A), Crystal Violet or hexamethyl pararosaniline (B) and Michler's ketone (C).

Triarylmethane dyes shown so far are characterized by a highly delocalized positive charge over the aromatic rings, on the central carbon atom and on the nitrogen atoms, as illustrated by some of the resonance forms of crystal violet in figure 3.

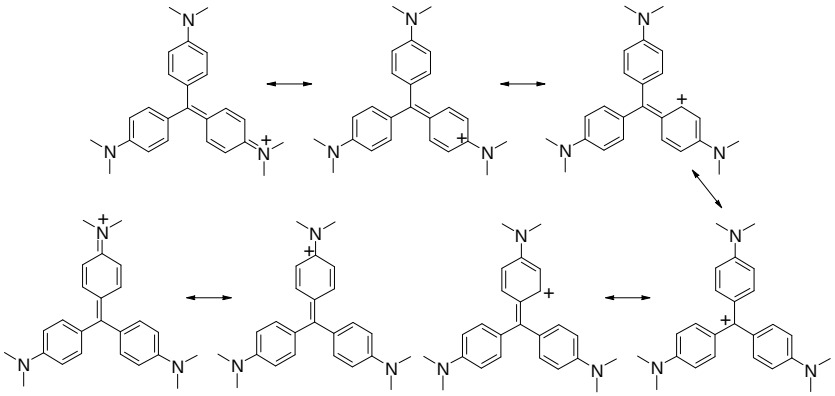

Figure 3: some of the resonance forms of crystal violet, showing the high delocalization of the positive charge over the molecule.

A highly efficient resonance is only possible in the presence of three coplanar aromatic rings (so that p orbitals on each carbon atom are parallel and can efficiently interact); in reality steric factors are also involved in the final conformation of triarylmethane dyes. In particular, the presence of six hydrogen atoms in ortho position with respect to the central carbon atom shapes the molecules of triarylmethane dyes into a three-blade propeller, with each aromatic ring twisted out of the plane.

Returning to the auxochrome-chromophore theory first proposed by Witt (see chapter one), the introduction in the ortho and ortho' positions of two aromatic rings of triphenylmethane (which is colorless) of an electron-withdrawing group (the chromophore according to the first theory by Witt) such as $=N^{+}(CH_3)_2$ and of an electron-donating group (the auxochrome according to the first theory by Witt) such as $-N(CH_3)_2$, is responsible for the green color of diamond green. The introduction of another dimethylamino group (ortho'' position) to get crystal violet produces a higher

delocalization of the positive charge (with respect to diamond green) and a different color is obtained (purple). Moreover, always according to the theory, the higher the electron-releasing power of the auxochrome, the larger the red shift (bathochromic shift) of the absorption spectrum of the dye. Indeed, in going from pararosaniline (no methyl groups attached to the nitrogen atoms) to crystal violet (six methyl groups) a red shift of the maximum of absorbance is observed.

Triarylmethane dyes are commonly synthesized through electrophilic aromatic substitutions of the S_E2 type. That is, en electrophile reacts with a nucleophilic aromatic compounds carrying an activating group such as amino (-NH_2, -NHR, -NR_2, -NHAr) or hydroxy (-OH) ones. Possible electrophiles are phosgene ($COCl_2$), formaldehyde (CH_2O), chloroform ($CHCl_3$), carbon tetrachloride (CCl_4), benzaldehyde (PhCHO) and benzophenone (Ph_2CO). Nevertheless, when electrophiles in an oxidation state different from IV are used (i.e. $CHCl_3$, CH_2O), triphenylmethane derivatives with one or two hydrogen atoms at the central carbon atoms are yielded. It is thus necessary to include an oxidation step in the synthetic route to triarylmethane dyes. The following scheme (figure 4) summarizes some of the possible synthetic routes to crystal violet, pararosaniline and diamond green. It is worth noting the presence of Michler's ketone among the possible reaction intermediates: this information is of particular interest because it demonstrates that Michler's ketone might have been present as an impurity of inks from the beginning. Since Michler's ketone can act as a sensitizer for the degradation of crystal violet, pieces of information on historical synthetic routes to crystal violets are of great importance for conservation scientists. Moreover, Michler's ketone is reported in literature as one of the possible degradation products of crystal violet [Duxbury].

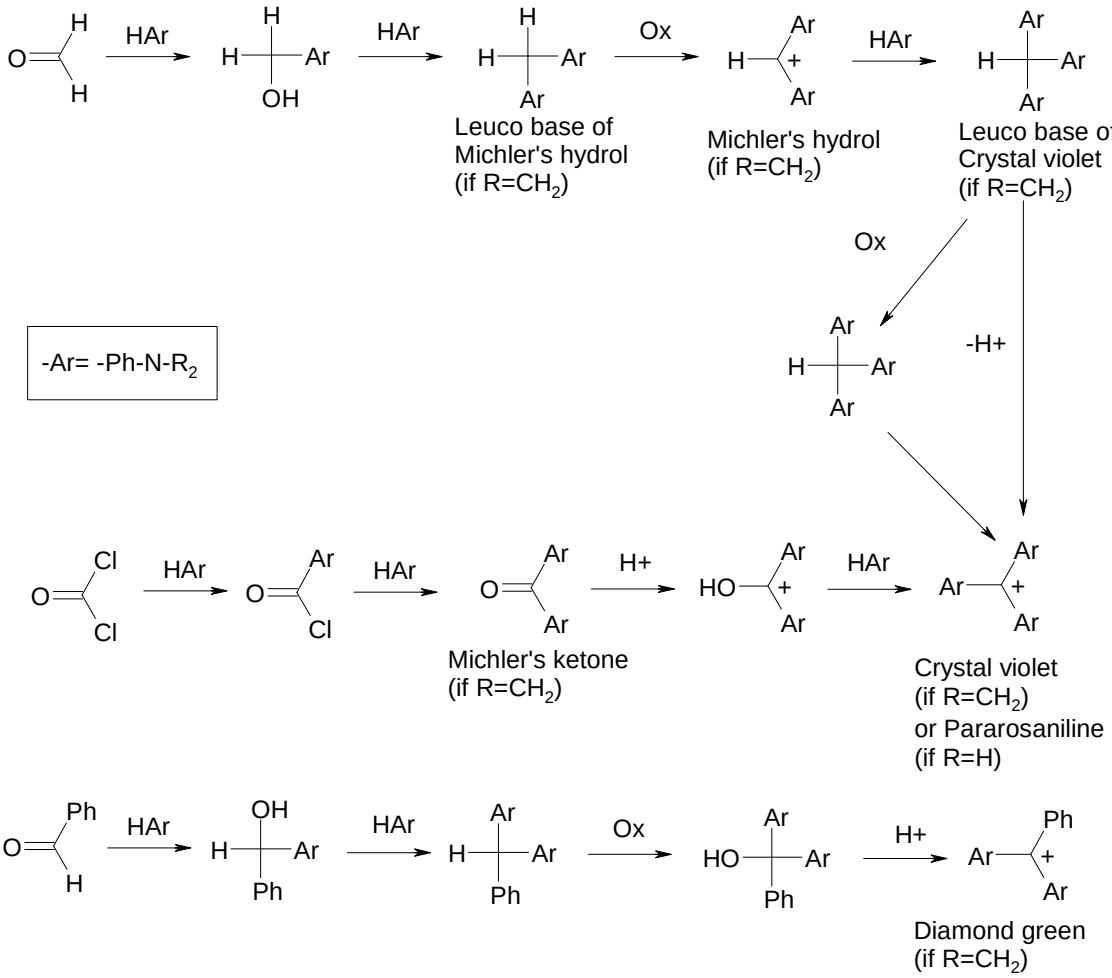

Figure 4: some of the possible synthetic routes to crystal violet, pararosaniline and diamond green.

Whether the counter ion is chlorine or a large polymeric anion (i.e. phosphomolybdates and phosphotungstates), water-soluble dyes or insoluble pigments are obtained.

Due to their high coloring power and relatively inexpensive production methods, synthetic dyes (initially known as aniline dyes) soon gained great popularity. In particular, Crystal violet (CV) or hexamethyl pararosaniline (figure 2B) with its deep purple hue has had (and in some cases still has) a widespread diffusion for dyeing fabrics and paper, as an ingredient of writing and drawing inks and, as a pigment, consisting of the copper ferrocyanide lake, in printing inks [Havlinova et al.]. Methyl Violet (MV), which consists of a mixture of tetra-, penta- and hexa- methylated pararosaniline (i.e. bi-demethylated crystal violet, mono-demethylated crystal violet and crystal violet itself) was first synthesized in 1861 by Charles Lauth and introduced onto the market in 1866. It is also known as Gentian Violet. In a report from the 1922 entitled ‘An Investigation of American Gentian Violets’ H. J. Conn wrote that ‘[…] at the present time the different manufacturers and dealers nearly all sell different mixtures

of these dyes under the name of gentian violet. This being the situation, the best use for the term gentian violet seems to be as a generic designation for any violet pararosanilin' [Conn]. Depending on the concentration of each methylated component, different shades of color may be obtained. If hexa-methylated pararosaniline prevails the color is bluer than if variously demethylated derivatives are present in larger amounts. In this regard, a special nomenclature was introduced to refer to the perceived degree of blue or red of the mixture, as explained by H. J. M. Creighton in 1919: 'The red or blue shades of the various alkyl substitution products of para-rosaniline are usually denoted by affixing to the name methyl violet the letters R, 2R, 3R, B, 2B, 3B, etc.'[Creighton]. Therefore, the 'number of Bs' (or Rs) indicates the perceived degree of blue (red) in the color of the dye. It should be noted that this is only a qualitative notation.

An efficient synthetic route to crystal violet was only developed between 1883 and 1884 by Kern and Caro, who reacted phosgene with N,N-dimethylaniline as shown in figure 5 [Reinhardt et al.].

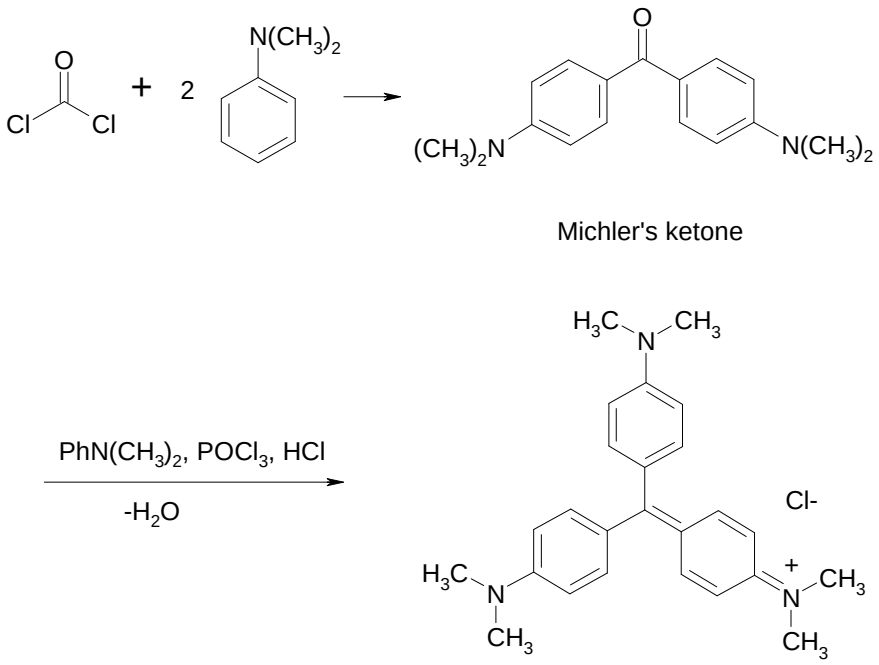

Figure 5: the first efficient synthetic route to Crystal Violet, developed between 1883 and 1884 by Kern and Caro.

Since the beginning of dye industry, the poor lightfastness of many synthetic dyes became apparent. Fading and discoloration of inks, leading to chromatic alterations of documents or drawings or even to a complete loss of readability, were soon observed.

In particular, among Van Gogh's signed works there is a group of drawings and letters produced in 1888 in Arles and all made with a purple ink which was

demonstrated to contain methyl violet, pararosaniline and other methylated derivatives of pararosaniline whose structures are not known yet. Significantly, a seemingly brownish drawing belonging to this group and entitled Montmajour (Arles, 1888. Van Gogh Museum) shows purple shades on the edges where the ink has been protected from light under the frame [Neevel et al.] (figure 6). In this case, traces of the original ink allowed us to draw conclusions about the original color of the drawing. But what if also other drawings, now completely brown colored, were in fact meant to be purple? What would this mean to art historians?

Figure 6: on the right, 'Montmajour' drawing (Van Gogh, Arles, 1888). On the left: inset showing purple strokes where the ink was protected from light under the frame. (image reproduced with the permission of the Van Gogh Museum, Amsterdam).

Traces of an ink made of methyl violet were also detected in another work by Van Gogh, a Menu drawn and written in Paris in 1886 (figure 7) [Vellekoop et al.]. Indeed, a reproduction of the Menu published in 1958 (figure 7, left) clearly shows the presence of a purple ink both in the written part and in the sketch along the side of the Menu [Van Gogh]. Some fifty years later (in 2001), the Menu looked completely different (figure 7, middle): the written part had faded away completely so that the Menu was no longer legible, except for some corrections made in pencil. The drawings along the side of the Menu met the same fate: suffice it to take a look to the inset in figure 7 (right). The same man who was walking arm in arm with a woman in the reproduction made in 1958 is now seemingly floating in air since no legs are visible.

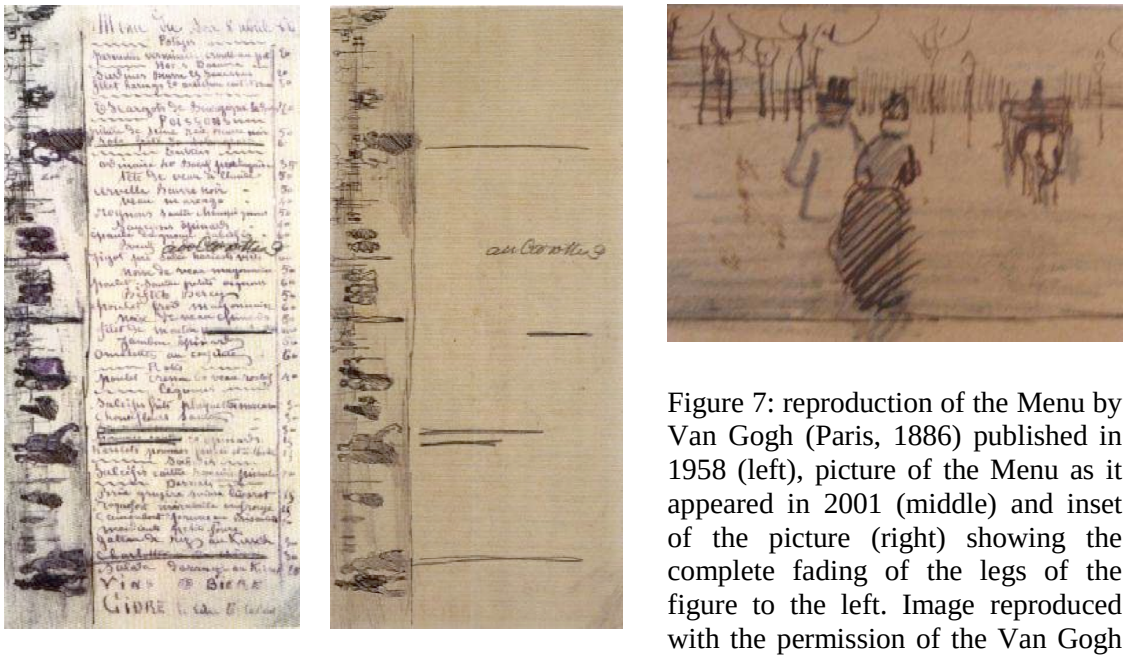

Figure 7: reproduction of the Menu by Van Gogh (Paris, 1886) published in 1958 (left), picture of the Menu as it appeared in 2001 (middle) and inset of the picture (right) showing the complete fading of the legs of the figure to the left. Image reproduced with the permission of the Van Gogh Museum, Amsterdam.

Therefore such topics as degradation mechanisms of synthetic dyes, and identification of synthetic dyes from their degradation products found in historical samples are gaining more and more importance in the field of cultural heritage study and conservation. For these reasons the Van Gogh museum and the Netherlands Institute for Cultural Heritage (ICN) became concerned on the discoloration of triarylmethane dyes such as methyl violet.

Crystal violet shows poor lightfastness, in particular on paper and on natural fibers such as cotton, silk and wool. Moreover, these substrates are not inert to light themselves, and the reactivity of the dye-substrate system is complicated by the degradation of the substrate when exposed to light and by such a phenomenon as phototendering, i.e. a change in chemical and/or physical properties of the fibers of the substrate caused by a sensitization effect of the dye. For this reason, so far many studies have dealt with the reactivity of the dye in solution (aqueous solution or solutions mimicking the substrates) in an attempt to simplify the complex reactivity of the dye-substrate system. Nevertheless, when dealing with a real object such as a drawing or a print, it is not possible to neglect the substrate reactivity [Gordon et el.] and a study of model systems for the dye on paper would be necessary [Abbott et al.]. The study of discoloration and fading of crystal violet in aqueous solution and on paper via chromatographic techniques (HPLC-PDA, LC-MS), optical and magnetic

spectroscopies (FORS, ATR-IR, EPR), micro-fading-meter will be dealt with in this part of my doctoral dissertation.

EXPERIMENTAL

1) Sample preparation

1.1) Identification of degradation products of Crystal Violet exposed to UV radiation.

To this purpose, the following samples were prepared:

1.a) aqueous solution of Diamond Green (sample from the ICN dye collection) $5x10^{-5}$ M. The solution was exposed to UV-Vis radiation for 10 minutes (300W Xenon lamp) and analyzed with LC-MS;

1.b) aqueous (water purified by a Simplicity system Millipore) solution of CV (Acros, pure, certified) $0.49*10^{-4}$M. A sample was taken before irradiation. Afterwards the solution was exposed to UV radiation (365 nm) from a Spectroline® Super High Intensity black light lamp (SB-100/F Spectronics Corporation, USA. power = 2 to 4 mW/cm^2) for 115 hours and samples were periodically analyzed with HPLC-PDA. A sample of the solution obtained after 150 was stored in the dark for one year and successively analyzed with LC-MS.

1.c) Aqueous solutions ($5x10^{-5}$ M) of reference samples of pararosaniline and ethyl violet were analyzed with HPLC-PDA and LC-MS.

1.d) Ethanol solutions of Michler's ketone (Acros, 98%) (concentrations ranging from 10^{-4} M to $1.8x10^{-2}$ M) were analyzed with HPLC-PDA

1.e) Aqueous solutions (20mg/l) of 10 historical (from the middle of the XX century) triarylmethane dyes from the ICN dye collection (table 1) were analyzed with HPLC-PDA. All the dyes chosen consisted of methyl violet.

Trade name	Brand	Collocation in the dye collection of the ICN
Methyl Violet 6B	farbenfabriken vorm. Friedr. Bayer & Co Elberfeld	4050
Methyl Violet 3B	farbenfabriken vorm. Friedr. Bayer & Co Elberfeld	4051
methyl violet N° 0, 4B	Anilin-Farben-Fabrik	4676
Methyl Violet 1B	Farbenfabriken vorm. Friedr. Bayer & Co Elberfeld	6316
Methyl Violet 2B	Farbenfabriken Fr. Bayer & Co	6320
Methyl Violet PV	imperial chemical industries limited, hexagonhouse, blackley, Manchester	6559
Methyl Violet 3B	Farbenfabriken Fr. Bayer & Co Elberfeld	7065
Methyl Violet 1R	Farbenfabriken Fr. Bayer & Co Elberfeld	7076
Methyl Violet 2B 200	imperial chemical industries limited, hexagonhouse, blackley, Manchester	7081
Methyl Violet 2BN 200	imperial chemical industries limited, hexagonhouse, blackley, Manchester	7093

Table 1: trade name, brand and identification number of the samples of methyl violet from the ICN collection analyzed in this work.

1.f) Crystal Violet was applied to Whatman paper discs (Cat No 1003 125) by soaking them for 10 minutes in an aqueous solution of CV (5×10^{-4}M) or in an ethanol solution of CV (5×10^{-4}M) and MK (1×10^{-3}M). Afterwards, the discs were left to dry horizontally. Samples were analyzed before and after different UV irradiation intervals (SB100/F Hg-lamp) with HPLC-PDA and FORS. Prior to HPLC-PDA analysis, the dye was extracted from each sample (1x0.5 cm strips of paper) with 200 µl methanol (Fluka, for HPLC, gradient grade, ≥99.8% (GC)) at 70 °C for 10 minutes. Samples of un-dyed paper were treated in the same way and used as a reference.

1.2) Degradation of Crystal violet in the presence of visible light alone.

Two sets of three kinds of paper (Whatman filter paper (Cat No 1003 125), lignin paper and printing paper) were soaked for 10 min in an aqueous solution of crystal violet $5.03*10^{-4}$ M or in an aqueous solution of crystal violet $5.03*10^{-4}$ M and gum arabic (20g/L) respectively. Once the samples got dry, a micro-invasive artificial aging of all dyed samples was performed via micro-fading-meter selecting only the visible portion of the light source and the color change ΔE was calculated.

1.3) Study of the degradation of Crystal violet on different paper substrates or in the presence of different ink additives or common gaseous pollutants.

3.a) Different kinds of paper (cotton linters paper, lignin paper and printing paper) were soaked in an aqueous solution of CV $5*10^{-4}$ M for 10 min and then left to dry. Dyed papers were aged in a Xenotest exposure device (Alpha High Energy by Atlas®. filtered Xenon-Arc-lamp (UV-Vis light present); 105 Klux, T 50°C, 40 % RH) and samples were periodically taken and analyzed with HPLC-PDA (in this case, the samples consisted of the methanol solutions extracted with methanol from dyed paper samples) and FORS. A second set of samples was prepared in the same way, but using an aqueous solution of CV and gum arabic (20g/L).

3.b) In order to study the effect of ink additives on the discoloration of crystal violet, an ink prepared[1] according to Sigmund Lehner (figure 8) [Lehner] was applied (with a brush or a fountain pen) on three kinds of paper (cotton linters paper, lignin paper and protein sized paper) in the presence or absence of additional Fe(III). Iron was added by soaking samples of undyed paper in an aqueous solution of $FeSO_4(H_2O)_6$ 10^{-3} M. Fe(III) was formed on the samples by spontaneous oxidation of Fe(II). All samples were aged by exposure to UV-Vis (Xenon lamp), to natural sun light or in oven at 100 °C for 24 hours.

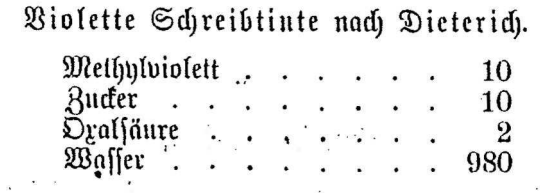
Violette Schreibtinte nach Dieterich.

Methylviolett	10
Zucker	10
Oxalsäure	2
Wasser	980

Figure 8: the recipe for this ink consists of methyl violet (a mixture of crystal violet and its mono- and bi-demethylated derivatives), sucrose, oxalic acid and water in a weight ratio of 10:10:2:980.

3.c) Both for cotton linters paper and lignin paper, two sets of reference samples (with or without additional Fe(III)) were prepared according to table 2. Samples of lignin paper were prepared following the same procedure, but no additional Fe(III) was used since it was already present in this kind of paper. Concentrations of all additives were the same as described in the recipe by Sigmund Lehner. All reference samples were exposed to natural sun light.

[1] by Judith Geerts, student of the University of Amsterdam.

sample number / additive	1	2	3	4	5	6	7	8
none	x				x			
oxalic acid		x		x		x		x
sucrose			x	x			x	x
	Paper without additional Fe(III)				Paper enriched with Fe(III)			

table 2: description of the two sets of reference samples of paper and additives studied.

3.d) Two sets of the same samples described in sections 3.b were exposed to common pollutants such as NO_2 and O_3 at a concentration of 5±0.25 ppm for two weeks at 25±2 °C and 50±5% relative humidity. All exposures to pollutants were carried out at the Image Permanence Institute (Rochester Institute of Technology), New York, by Daniel Burge and Nino Gordeladze.

1.4) EPR characterization of crystal violet, pararosaniline and diamond green radical cations.

4.a) A sample of pure cellulose paper (Whatman paper) was dyed with an aqueous solution of CV 10^{-4} M and exposed to UV radiation for 20 minutes. A reference sample of undyed Whatman paper was also exposed to UV radiation for 20 minutes. Both samples were analyzed with EPR spectroscopy.

4.b) Radical cations of crystal violet (CV), diamond green (DG) and pararosaniline (PR) were synthesised with [bis(trifluoroacetoxy)iodo]benzene (PIFA) in 1,1,1,3,3,3-hexafluoro-propan-2-ol/trifluoroacetic acid according to [Stanoeva et al.]. The concentrations of CV and PIFA were 0.1 M. The reaction mixture was carefully degassed and immediately analyzed with EPR.

4.c) Two samples of pure cellulose paper (Whatman paper) were dyed with an aqueous solution of CV 10^{-4} M and inserted into two quartz tubes. One of the tubes was sealed under vacuum, whereas the other was left open. The same was done for two samples of undyed paper. All of the samples were analyzed with EPR both before and after exposure to UV-Vis radiation.

1.5) Preliminary study of the color change of various colorants aged on paper.

The following colorants (table 3) were applied on cotton linters paper (by soaking the paper for 20 minutes in the solutions of colorants) and exposed to UV-Vis radiation from a 300W Xenon lamp (10h) or thermally-aged (24h at 100 °C). Unaged samples

were kept aside as reference. Colorimetric L*a*b* values were measured both before and after aging tests.

Colourant	Brand	Description
indigo	Zecchi	saturated alcoholic (MeOH) solution
indigo carmine	Riedel de Haën	aqueous solution $5x10^{-4}M$
cochineal carmine ink	Zecchi	used as such (conc. unknown)
copper logwood (synthetic route 1)	logwood by Zecchi	aqueous solution of equimolar amounts of logwood extract and $CuSO_4$
copper logwood (synthetic route 2)	logwood by Zecchi	aqueous solution of equimolar amounts of logwood extract and and $Cu(AcO)_2$
chromium logwood	logwood by Zecchi	aqueous solution of equimolar amounts of logwood extract and and $K_2Cr_2O_7$

Table 3: name, brand and description of the colorants used for the colorimetric study.

1.6) analysis of the ink from the 'Montmajour' drawing by Van Gogh (Van Gogh Museum)

A fiber of dyed paper was taken from a purple area of the 'Montmajour' drawing. The sample was treated with 50 µl of a solution of HCl:H_2O:Methanol (2:1:1 v/v/v) for 10 minutes at 100 °C. The solvent was then evaporated with nitrogen and the solid fraction was dissolved with 20 µl of dimethylformamide and centrifuged at 2000 rpm. The sample was finally analyzed with HPLC-PDA (injection: 10 ul). Both the extraction and the analysis were performed by Maarten van Bommel at the ICN.

2) HPLC-PDA analysis

HPLC analysis was performed with equipment from Waters Chromatography BV (Etten-Leur, The Netherlands). Mobile phase was delivered at a flow rate of 0.2 mL/min by a 616 LC pump, controlled by a 600S controller. An in-line degasser degassed all effluents used. Samples were injected by a 717 autosampler. Detection was performed with a 996 Photo Diode Array (PDA) detector equipped with a 10 mL detector cell, scanning from 200 to 700 nm at a scanning rate of 1 scan/sec. The equipment was controlled by a computer with Millennium 32 software, version 4.0, from Waters

Chromatography BV; the same system was used for data acquisition. Separation was performed on a luna C18 column (100mm x 2mm id) protected by a security C18 guard column, both supplied by Phenomenex (Torrance, CA, USA). The mobile phase consists of a gradient of water (HPLC grade 1, purified by a Simplicity system Millipore, Amsterdam, The Netherlands), methanol (gradient grade, Fluka, Zwijndrecht, The Netherlands) and 5% phosphoric acid in water (acs reagent, Sigma, Zwijndrecht, The Netherlands). The composition of the solvents and the gradient profile is given in table 4 Identification is based on both PDA spectra and retention time of the components which are compared with those of known reference materials.

Table 4. Gradient profile for the HPLC system.

Time/min	%A[1]	%B[2]	%C[3]
0	74	16	10
15	0	90	10
20	0	90	10
23	0	100	0
27	0	100	0
30	74	16	10
50	74	16	10

[1] A=10% methanol/water (v/v)
[2] B=100% methanol
[3] C=5% phosphoric acid (w/v)

3) LC-MS Q-TOF analysis

Chromatographic analysis was performed with UHPLC Agilent 1200 equipped with autosampler, degasser, thermostated column compartment (30 °C), micro flow cell (2 mL, 0.3 mm path) and diode array detector. Separation was performed on a Kinetex C18 column, 100x2.1 mm, 2.6 mm core shell, Phenomenex (Torrance, CA, USA). Mobile phase was delivered at a flow rate of 0.2 mL/min. The composition of the solvents and the gradient profile is given in table 5.

Time/min	%A A=100%methanol	%B B=0.1% TFA(aq)
0	30	70
14	70	30
24	70	30
28	30	70
38	30	70

Table 5: Gradient profile for the LC system.

Mass analysis was performed with Q-TOF Agilent 6520 (Santa Clara, CA, USA). The Electro-Spray Ionization mode used was positive; the capillary voltage 4000 V; the

pressure of the nebulizer gas was 35 psig; the flow rate of the drying gas was 11 L/min and its temperature 350 °C.

The equipment was controlled by a computer with MassHunter software.

All LC-MS analyses were performed in collaboration with Dr. Gabriella Favaro of the Department of Chemical Sciences of the University of Padua.

4) FORS and micro-fading analysis

FORS analysis was performed with a home-assembled equipment composed of a halogen lamp (AvaLight-Hal, AVantes), a reflection integrating sphere (ISP-50-8-REFL, AVantes) or a direct reflectance probe (for the analysis of the letters) and a spectrophotometer (AvaSpec-2048, AVantes). The equipment was controlled by AvaSoft 6.1 software. Reflectance spectra were collected in the range 380-800 nm, with an integration time of 200 ms and averaging 5 scans. Absorption spectra were calculated from reflectance spectra using Kubelka-Munk transform. Reflectance spectra for CV were recorded before and after exposure to UV radiation of a dyed disc of paper. Colorimetric L*a*b* values were calculated from reflectance spectra for a D65 illuminant and a 10° Standard Observer.

The micro-fading-meter used is a modified version (by J. G. Neevel) of the one described in [Whitmore et al.].

Colorimetric L*a*b* values were calculated using a software available online at www.brucelindbloom.com and selecting the D65 illuminator and the 10° Supplementary Standard Observer.

5) EPR analysis

EPR analysis was performed with equipment from Bruker. A spectrometer ER200 was used for recording continuum wave EPR spectra and a spectrometer Elexsys580 was used for recording both continuum wave and pulsed EPR spectra.

6) NMR-MOUSE analysis

NMR-MOUSE analysis was performed with a relaxometer Bruker Minispec Profiler connected to a MOUSE probe with a sensitivity depth of about 1 mm. The operating radiofrequency of this probe is around 15 MHz. The instrument was controlled with the minispec software for windows (Bruker).

7) ATR-IR analysis

Infrared spectra were recorded using Bruker Equinox55, with MCT detector and ATR Golden Gate (Specac) accessory.

RESULTS AND DISCUSSION

1) Identification of degradation products of Crystal Violet exposed to UV radiation

1.1) Dyes in solution

A color shift from purple to reddish was observed upon irradiation of an aqueous solution of Crystal Violet. The HPLC-PDA chromatograms for Crystal Violet in aqueous solution before and after prolonged irradiation (115 hours) are shown in figure 9. Before irradiation only two peaks are visible at around 21.1 min (relative area >98%) and 20.7 min (relative area <1%), due to Crystal Violet and mono-demethylated Crystal Violet respectively (as it will be demonstrated later).

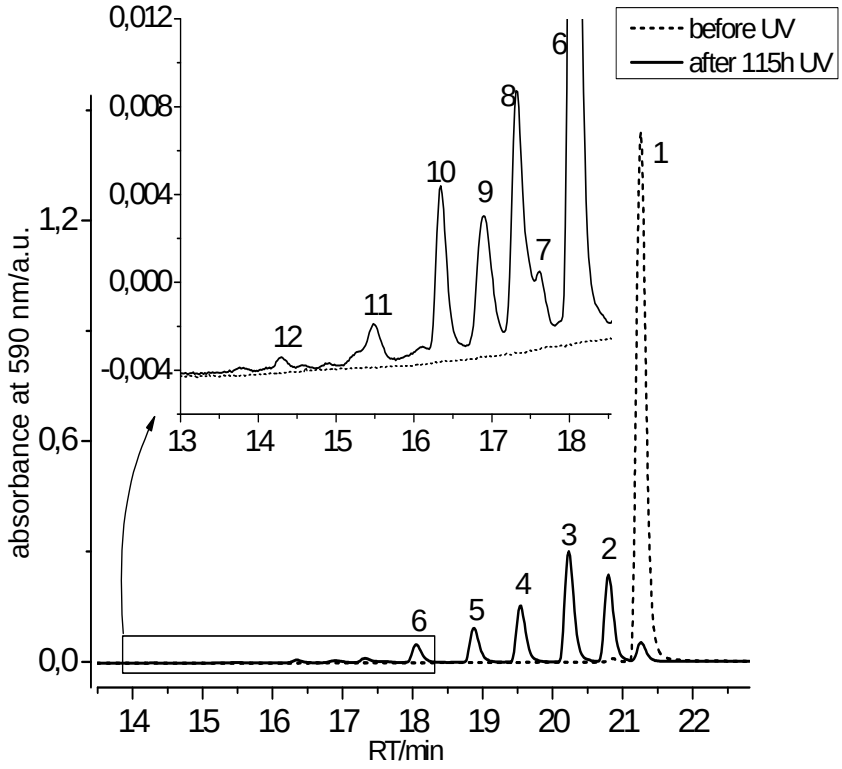

Figure 9: Chromatograms of CV(aq), before and straight after prolonged exposure to UV radiation.

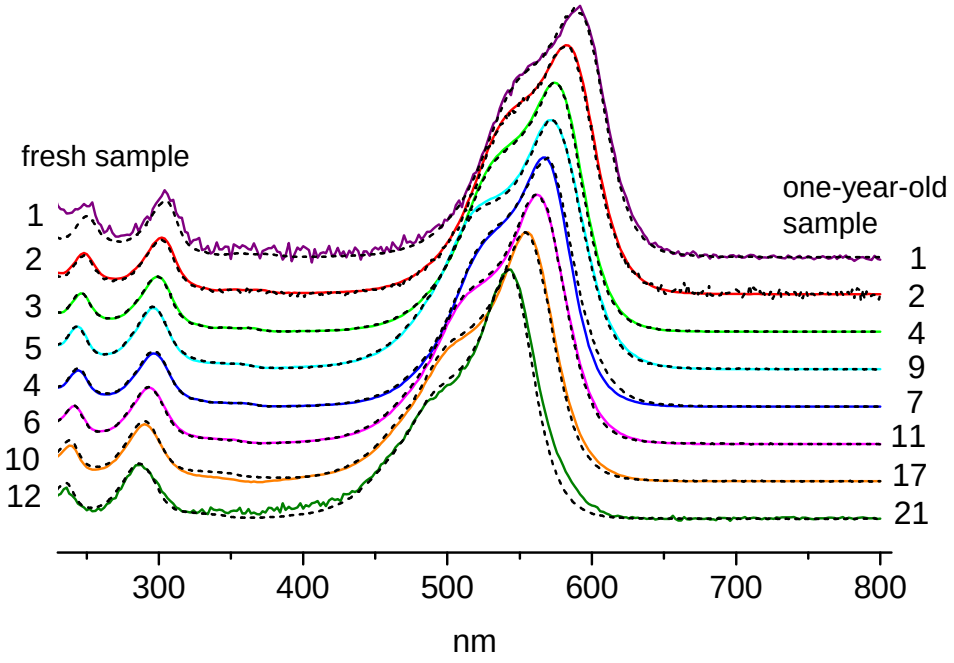

Figure 10: comparison between normalized absorption spectra corresponding to crystal violet and its demethylated derivatives, obtained with HPLC analysis of a freshly irradiated solution of crystal violet (dotted lines) and with LC-MS analysis of a sample of the same solution, after one year of storage (solid lines).

Upon irradiation, a decrease of the concentration of Crystal Violet and the formation of at least 11 degradation products were observed. Absorption spectra of chromatographic peaks number 1, 2, 3, 4, 5, 6, 10 and 12[2] are shown in figure 10. Table 6 reports the retention times and the maxima of absorptions obtained with HPLC-PDA for each chromatographic peak together with the identification proposed in this doctoral dissertation. The absorption spectra of the chromatographic peaks at issue are all very similar, except for a progressive blue shift of the maxima of absorption in going from peak 1 to peak 12. A comparison of the latter absorption spectra with those of reference samples enabled to identify peaks 1 and 12 as Crystal Violet and Pararosaniline, respectively. As for the other peaks in figure 9, an identification was not possible solely on the basis of their absorption spectra since no reference samples were available. Nevertheless, the blue shift in the maxima of absorption (in going from peak1 to peak 12) was hypothesized to be due to a step-wise demethylation of Crystal Violet, as suggested in literature.

[2] This numbering refers to the chromatogram of a freshly irradiated sample shown in figure 9.

Beside this series of crystal violet-like absorption spectra, a group of chromatographic peaks (number 7, 9 and 11 in the chromatogram shown in figure 9) with absorption spectra similar to the spectrum of diamond green was observed with HPLC-PDA for a freshly irradiated aqueous solution of crystal violet. Going from peak number 7 through 9 to 11, a progressive blue shift of the maximum of absorbance is visible (figure 11). There is no matching in retention time between species responsible for peaks 7, 9 and 11 and diamond green, though. Two identification hypothesis were proposed on the basis of the absorption spectra obtained. According to the first hypothesis, species responsible for peaks 7, 9 and 11 might be formed via deamination reactions of Crystal Violet. In other words, they might be identified as Diamond Green or its demethylation derivatives. Indeed Diamond Green has already been detected in faded samples of Crystal Violet by other authors [Nakamura et al.].

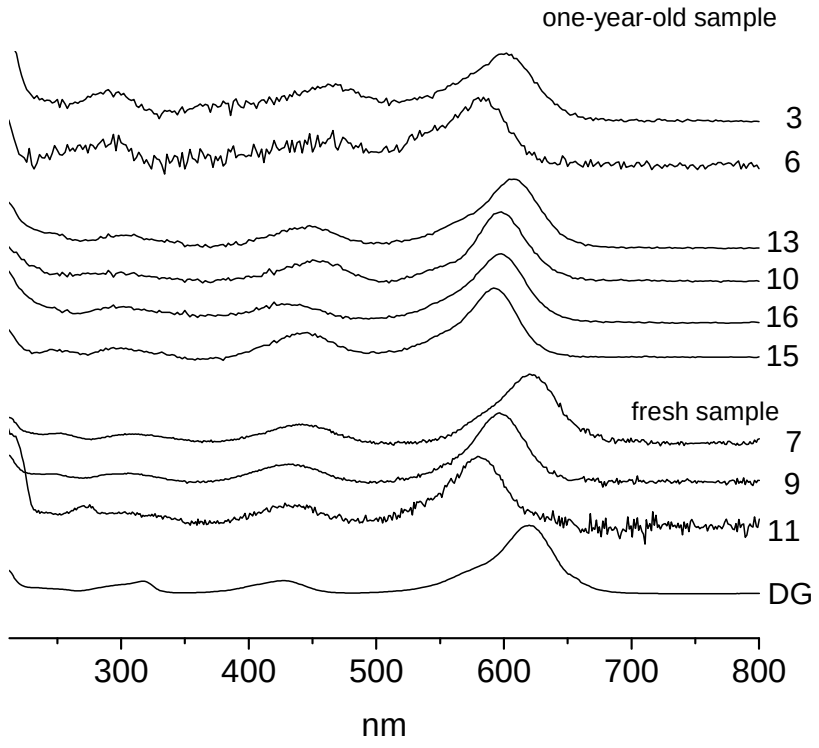

Figure 11: comparison between diamond green-like absorption spectra obtained with HPLC analysis of a freshly irradiated solution of crystal violet (peaks 7, 9 and 11 according to HPLC numbering system) and with LC-MS analysis of a one-year-old sample of the same irradiated solution of crystal violet (peaks 3, 6, 10, 13, 15 and 16).

Another hypothesis for the identification of peaks 7, 9 and 11 is reported in [Duxbury] and [Bangert et al.]: in these works it was reported that the absorption spectra of N-oxide derivatives of CV were very similar to the spectrum of diamond

green. The higher polarity for N-oxides would explain the lower retention times[3] obtained for peaks 7, 9 and 11 with respect to diamond green.

Finally, the absorption spectrum of peak 8 (figure 12) has not been identified yet but it is clearly due to the superimposition of at least two spectra as is suggested by the change in shape of the spectrum during irradiation.

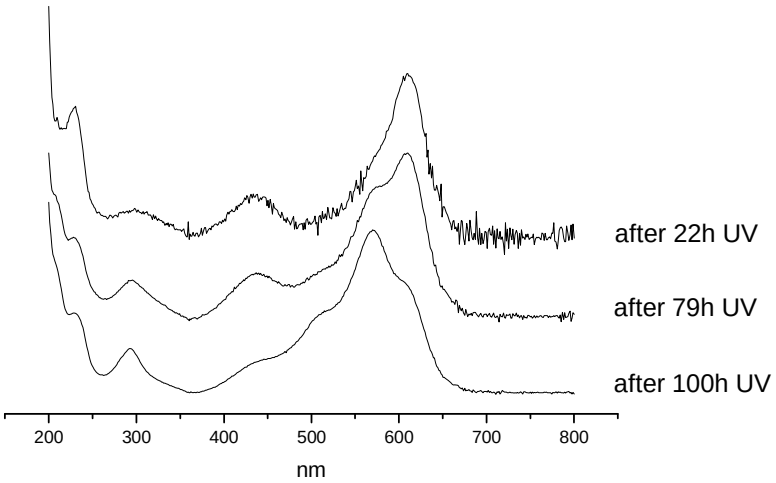

Figure 12: absorption spectra for peak 8 after different irradiation times.

Since it was not possible to identify all degradation products solely on the basis of HPLC-PDA analysis, additional LC-MS analysis was run on a sample of the same aqueous solution of crystal violet exposed to prolonged UV radiation which had been studied with HPLC-PDA [Huang et al.]. It is worth noting that it was possible to analyze the sample (labelled 'one-year-old sample' in this work) with LC-MS only one year after it was exposed to UV radiation. The chromatograms recorded at 590 nm and 300 nm are shown in figures 13 (high retention time range) and 14 (low retention time range)[4]. Retention times, maxima of absorption and m/z values for the most significant[5] peaks are reported in table 6, together with the identification proposed in this doctoral dissertation.

[3] The separation was performed via reversed-phase chromatography.

[4] It should be noted that two numbering methods are used for the chromatographic peaks described in this doctoral dissertation: one for the chromatogram of freshly irradiated CV(aq) obtained with HPLC-PDA (figure 4) and one for the chromatogram of one-year-old irradiated CV(aq) obtained with LC-MS (figures 5 and 6).

[5] The reason why some peaks were neglected is that they were too low in intensity, or it was not possible to obtain a good absorption spectrum or useful mass data.

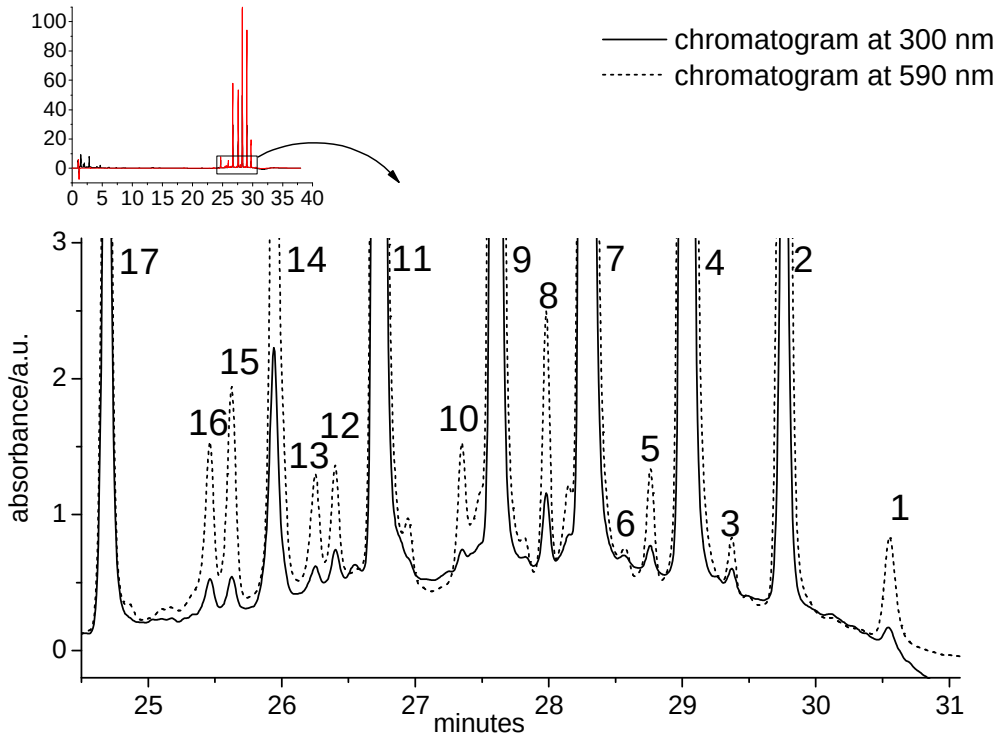

Figure 13: portion at high retention times of the chromatograms at 300 nm and 590 nm of an aqueous solution of crystal violet exposed to prolonged UV radiation one year before the LC-MS analysis was performed.

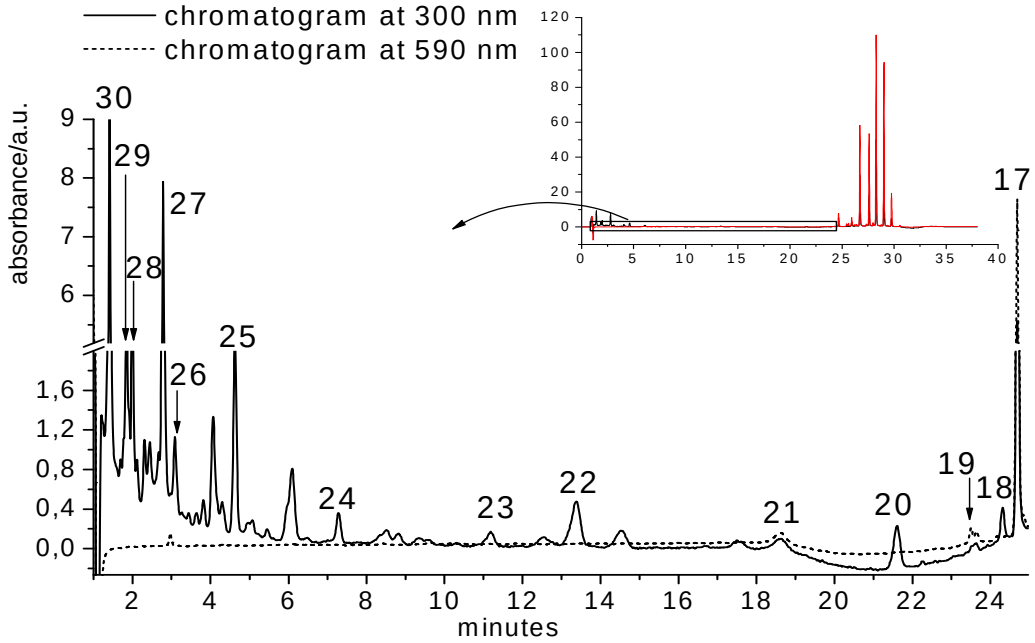

Figure 14: low retention time portion of the chromatograms at 300 nm and 590 nm of an aqueous solution of crystal violet exposed to prolonged UV radiation one year before LC-MS analysis.

Let us first consider colored species (chromatogram at 590 nm): a larger number of species was detected with LC-MS (at least 20) than with HPLC-PDA (at least 12), but it is not possible to say with certainty if the difference was due to the use of two different columns or to the aging of the sample (which had been stored for one year before it was analyzed with LC-MS) or both.

Peak numbering		RT/min		λ_{max}/nm		m/z	Identification
HPLC	LC-MS	HPLC	LC	HPLC	LC		
1	1	21.26	30.55	588	592	372.24332	CV
2	2	20.79	29.76	582	582	358.22794	Mono-demethylated CV
	3		29.37		602	Not determined (n.d.)	n.d. (DG-like absorption spectrum)
3	4	20.23	29.03	573	574	344.21202	Bi-demethylated CV
	5		28.76		238 596	360.20634	n.d. (CV-like absorption spectrum)
	6		28.57		≈ 582	n.d.	n.d. (DG-like absorption spectrum)
4	7	19.54	28.28	570	566	330.19678	Tri-demethylated CV
	8		27.98		582	346.19208	n.d. (CV-like absorption spectrum)
5	9	18.87	27.60	572	572	330.19650	Tri-dememthylated CV
	10		27.34		598	n.d.	n.d. (DG-like absorption spectrum)
6	11	18.05	26.72	562	562	316.18075	Tetra-demethylated CV
7		17.61		620			n.d. (DG-like absorption spectrum)
8		17.32		---			n.d.

Table 6: Comparison between the results of HPLC analysis of a freshly irradiated aqueous solution of crystal violet and of LC-MS analysis of the same sample, after one year of storage. Table continued on next page.

Peak numbering		RT/min		λ_{max}/nm		m/z	Identification
HPLC	LC-MS	HPLC	LC	HPLC	LC		
9		16.89		597			n.d. (DG-like absorption spectrum)
	12		26.40		≈582	332.17637 386.22252	Superimposition of at least two species
	13		26.25		608	358.19228	$C_{23}H_{24}N_3O$
	14		25.95		568	316.18143	n.d. (CV-like absorption spectrum)
	15		25.63		592	344.17654	$C_{22}H_{22}N_3O$
	16		25.46		598	358.19205	$C_{23}H_{24}N_3O$
10	17	16.34	24.69	554	554	302.16496	Penta-demethylated CV
11		15.48		579			n.d. (DG-like absorption spectrum)
	18		24.31		370; 244	255.14956	Mono-demethylated MK (protonated)
	19		23.51		565	318.16003	n.d. (CV-like absorption spectrum)
	20		21.61		360	copresence of many m/z values	n.d. (MK-like absorption spectrum)
12	21	14.29	18.61	543	544	288.14910	pararosaniline
			14.51		356	255.11252 main; 413.06851 277.09493	n.d. (MK-like absorption spectrum)
	22		13.38		362	241.13341	bi-demethylated MK (protonated)
	23		11.19		368	241.13345	bi-demethylated MK (protonated)
	24		7.28		264	n.d.	
	25		4.63		356	227.11749 main; 475.20934 secondary	tri-demethylated MK (protonated)

Table 6: Comparison between the results of HPLC analysis of a freshly irradiated aqueous solution of crystal violet and of LC-MS analysis of the same sample, after one year of storage. Table continued on next page.

Peak numbering		RT/min		λ_{max}/nm		m/z	Identification
HPLC	LC-MS	HPLC	LC	HPLC	LC		
	26		3.09		264	152.06991 200.20045	
	27		2.78		304	152.06941 215.12411 256.11848	
	28		1.99		342	n.d.	
	29		1.85		324	n.d.	
	30		1.41		222 main; 286 second.	n.d.	

Table 6: Comparison between the results of HPLC analysis of a freshly irradiated aqueous solution of crystal violet and of LC-MS analysis of the same sample, after one year of storage.

With the aim of finding a correlation between HPLC-PDA and LC-MS analyses, a comparison between absorption spectra of the peaks obtained with these two techniques was made. Moreover, whenever possible, spectroscopic data were combined with the results of mass analysis. In this way, a number of species was identified, as it will be described next.

The presence of a series of absorption spectra that are gradually blue shifted with respect to the absorption spectrum of crystal violet (figure 10), was confirmed also with LC-MS. As for the absorption spectra of the peaks belonging to this series, the results obtained with HPLC-PDA and LC-MS were reproducible, i.e. a good matching between absorption spectra was observed. The worst matching (although still a good one) was observed for peak number 12 (numbering system according to HPLC-PDA analysis) and peak number 21 (numbering system according to LC-MS analysis), but this was probably due to the low intensity of these peaks. It was thus possible to find a direct correlation between the chromatograms obtained with HPLC and LC-MS.

LC-MS analysis enabled to demonstrate that during irradiation with UV, crystal violet (peak 1 in figure 9) undergoes a series of demethylation reactions leading to mono-demethylated crystal violet (peak 2[6]), bi-demethylated crystal violet (peak 4), two isomers of tri-demethylated crystal violet (peaks 7 and 9), tetra-demethylated crystal

[6] From now on, LC-MS numbering system will be used, unless otherwise stated.

violet (peak 11), penta-demethylated crystal violet (peak 17) and hexa-demethylated crystal violet (peak 21) or pararosaniline (a red dye). Mass data were obtained for all of the above mentioned species and are consistent with the attribution proposed.

Also for the one-year-old sample, it was possible to detect chromatographic peaks (corresponding to absorption spectra number 3, 6, 13, 15 and 16 in figure 11) with absorption spectra similar to the one of diamond green. Nevertheless, none of these spectra was exactly the same as what obtained for a freshly irradiated sample of CV(aq) (figure 11, spectra 7, 9 and 11 according to HPLC numbering system). The difference with respect to the freshly irradiated sample might be due to the aging of the sample. The only analogy between diamond green-like spectra of the freshly irradiated sample and of the one-year-old sample is constituted of the absorption spectra corresponding to peak 9 (HPLC numbering) and peak 16 (LC-MS numbering) (figure 15, left). Nevertheless, these two spectra are not completely superimposed and it is difficult to say if they are due to the same species or not.

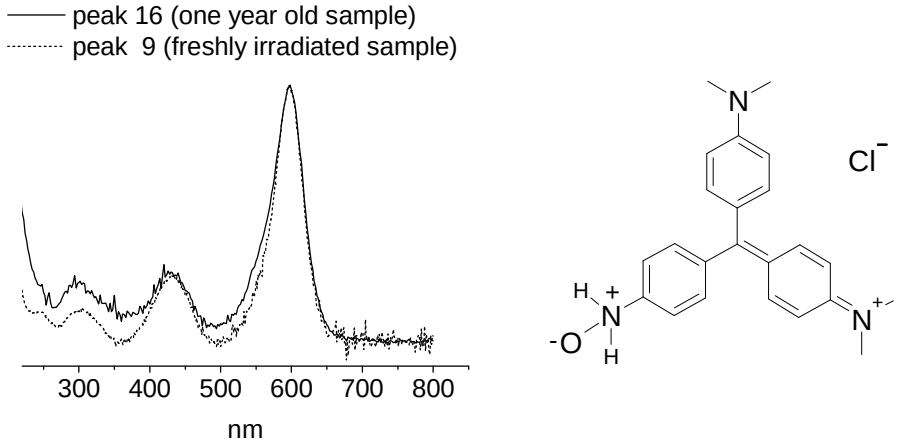

Figure 15: (left) comparison between peak 9 (HPLC numbering) and peak 16 in the chromatograms of a freshly irradiated sample of CV(aq) and of a one-year-old irradiated sample of CV(aq) respectively. (right) N-oxide of bi-demethylated crystal violet.

With the aim of shedding light on the nature of the species responsible for diamond green-like absorption spectra, a characterization of diamond green and its degradation products was planned. To this end, an aqueous solution of diamond green was exposed to UV-Vis radiation and analyzed with LC-MS. Chromatograms were registered at 300 nm and 590 nm (figure 16) in order to detect both colorless and colored species.

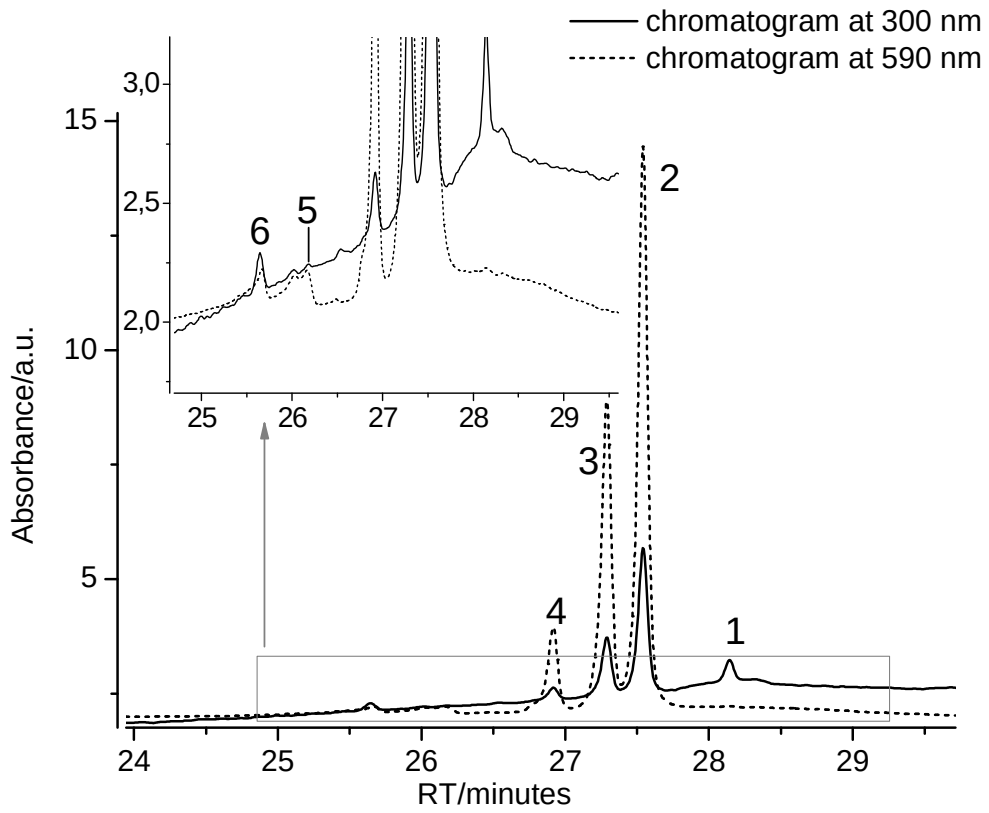

Figure 16: chromatograms recorded at 300 nm and 590 nm for an aqueous solution of diamond green exposed to UV-Vis radiation for 10 minutes.

On the whole, 6 peaks were detected with a diode array detector. Absorption spectra (figure 17), maxima of absorption, m/z values and retention times (RT) for the peaks are reported below, together with the identification proposed in this doctoral dissertation (table 7).

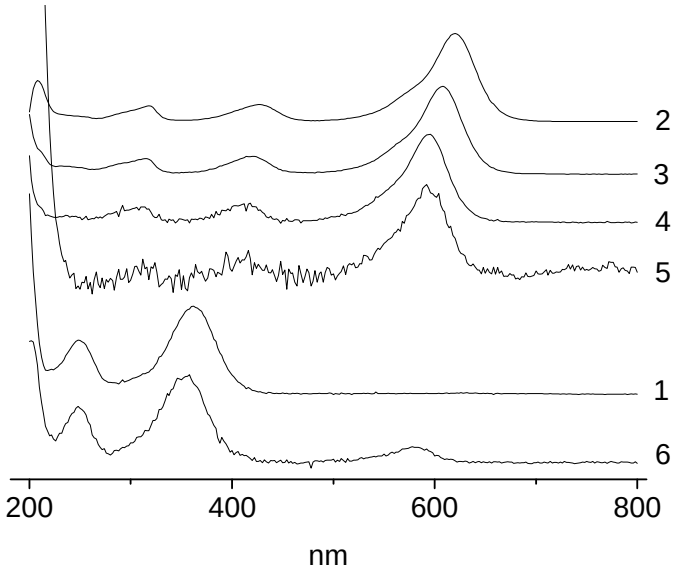

Figure 17: absorption spectra corresponding to peaks 1 to 6 in the chromatograms for an aqueous solution of diamond green exposed to UV-Vis radiation.

Peaks 2, 3 and 4 were identified as diamond green, mono-demethylated diamond green and bi-demethylated diamond green, respectively. Peak 5 showed an absorption spectrum very similar to the one of peak 4. According to the main m/z peak visible in the mass spectrum (not shown), peak 5 might be a different isomer of the bi-demethylated diamond green, although an unknown secondary peak is visible at m/z = 316.1811. Peak 1 showed a completely different absorption spectrum from peaks number 2 to 6, with a maximum of absorption in the UV range. The main m/z value (226.1231) visible in the mass spectrum of this peak is consistent with protonated 4-(dimethylamino)benzophenone, a ketone that can be formally obtained from the oxidation at the central carbon atom of one of the isomers of bi-demethylated diamond green.

Peak 6 showed an absorption spectrum similar to the one of peak 1, but with an additional (relative) maximum of absorption in the visible range (580 nm). It is not clear if this second maximum of absorption is due to the same species responsible for the band in the UV range. Mass spectrum of peak 6 showed a main peak (m/z=212.1074) and two secondary peaks. The main m/z value is consistent with protonated 4-(methylamino)benzophenone.

Thus, photo-induced degradation of diamond green has been demonstrated to consist, at least at a first stage, of reactions of demethylation of the nitrogen atom and oxidation at the central carbon atom.

Peak number	RT/min	λ_{max}/nm	m/z	Identification
1	28.14	362	main:226.1231; 473.2213; 554.3098	4-(dimethylamino)benzophenone
2	27.50	620	329.2002	Diamond green (DG)
3	27.28	608	315.1849	Mono-demethylated DG
4	26.90	596	301.1704	Bi-demethylated DG
5	26.16	around 592	301.1697	Bi-demethylated DG
6	25.66	358	main:212.1074 287.1549; 234.0894	4-(methylamino)benzophenone

Table 7: retention times, maxima of absorption, m/z values and identification of the six peaks in the chromatograms at 300 nm and 590 nm of an aqueous solution of diamond green exposed to UV-Vis radiation.

Returning to the irradiated solution of Crystal Violet, diamond green-like spectra detected both for the freshly irradiated sample and for the one-year-old sample, were different from the absorption spectra of the reference sample of diamond green irradiated with UV.

As for mass analysis, it is worth noting that m/z values obtained for peaks number 13 (m/z = 358.19228), 15 (m/z = 344.17654) and 16 (m/z = 358.19205) (figure 13) are not consistent with diamond green or its demethylation derivatives but are similar to the m/z values of some demethylated derivatives of crystal violet, i.e. peak 2 (m/z = 358.22794) and peak 4 (m/z = 344.21202) (table 6, LC-MS numbering system). In conclusion, no diamond green or demethylated derivatives of diamond green were detected among degradation products of crystal violet.

Despite the similarity of m/z value just described, the difference between the m/z value for peak number 2 and peak number 13 or 16 is of an order of magnitude higher than the accuracy of the mass analyzer (4 ppm) and the difference between the m/z value for peak number 4 and peak number 15 is of two orders of magnitude higher than the accuracy of the mass analyzer. This is to confirm that peaks number 13, 15 and 16 are due to species different from crystal violet and its demethylation derivatives that have been identified so far.

With the aim of shedding light on the nature of the species responsible for peaks number 13, 15 and 16[7] (figure 13), the isotopic distribution of the mass peaks was studied. The same was also done for those peaks corresponding to demethylated derivatives of crystal violet characterized by m/z values similar to the ones of the peaks in question, i.e. peak 2 and 4. The result was very satisfactory since isotopic distributions corresponding to the chromatographic peaks characterized by diamond green-like spectra were all consistent with the presence of an atom of oxygen. On the contrary, isotopic distributions corresponding to the chromatographic peaks characterized by crystal violet-like spectra were all consistent with molecular formula with no oxygen atoms. In particular, the following matchings were found. As for peaks 2 and 4, the isotopic distributions of the molecular ion were consistent with the molecular formulas $C_{24}H_{28}N_3$ (matching 98%) and $C_{23}H_{26}N_3$ (matching 97%) respectively, which is in agreement with the identification previously proposed (mono-demethylated crystal violet for peak 2 and bi-demethylated crystal violet for peak 4).

[7] Peaks three and six (figure 13) were too low in intensity to be included in the analysis.

As for peaks 13, 15 and 16, the isotopic distributions of the molecular ion were consistent with the molecular formulas $C_{23}H_{24}N_3O$ (matching 97%), $C_{22}H_{22}N_3O$ (matching 96%) and $C_{23}H_{24}N_3O$ (matching 99%) respectively.
In conclusion, the peaks in question (with absorption spectra similar to the one of diamond green) are likely due to oxidized derivatives of bi- and tri- demethylated crystal violet.

As for the position of the atom of oxygen, Bangert at al. noticed how absorption spectra of N-oxides of crystal violet or of its demethylated derivatives (figure 15, right) are similar to absorption spectra of diamond green or its demethylated derivatives. The reason most likely lies on the fact that both for diamond green (and its demethylated derivatives) and N-oxides of crystal violet (and of its demethylated derivatives), the resonance resonance forms are different from those of crystal violet (or its demethylated derivatives). Stable resonance forms can be obtained delocalizing the positive charge on nitrogen atoms and this is only possible if nitrogen atoms have a pair of non-bonding electrons available. While crystal violet has three resonance forms of this kind, diamond green and its N-oxides have only two. The different extent of conjugation is thought to be responsible for the difference between crystal violet-like spectra and diamond green-like spectra.
Therefore, it has been hypothesized that peaks number 13, 15 and 16 might be N-oxides of bi- and tri- demethylated crystal violet. As for peaks 3 and 6, they might be N-oxides of crystal violet or of its demethylated derivatives, in analogy with what found for peaks number 13, 15 and 16. Nevertheless, no mass data are available for these two low peaks.

Let us now go back to the chromatogram obtained with LC-MS at 590 nm for a one-year-old sample of the aqueous solution irradiated with UV (figures 13 and 14). We were describing the peaks detected with LC-MS. Besides crystal violet, the series of its demethylation products and its N-oxides derivatives just described, four other peaks were detected (number 5, 8, 12, 14 and 19), which show different absorption spectra with respect to the freshly irradiated sample (figure 18). Peak 19 is actually associated to an absorption spectrum that is similar to the one of tetra-demethylated crystal violet. Nevertheless, retention times of the species responsible for these two peaks are so different that different molecular structures must be invoked. Although it was possible to obtain m/z values for all of the peaks number 5, 8, 14, 12 and 19, for the moment no hypothesis for their structures is available.

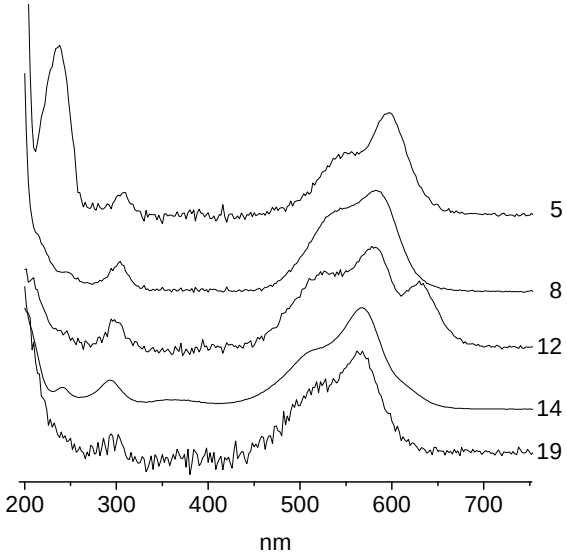

Figure 18: absorption spectra of peaks 5, 8, 12, 14 and 19 in the chromatogram of a one-year-old sample of irradiated CV(aq).

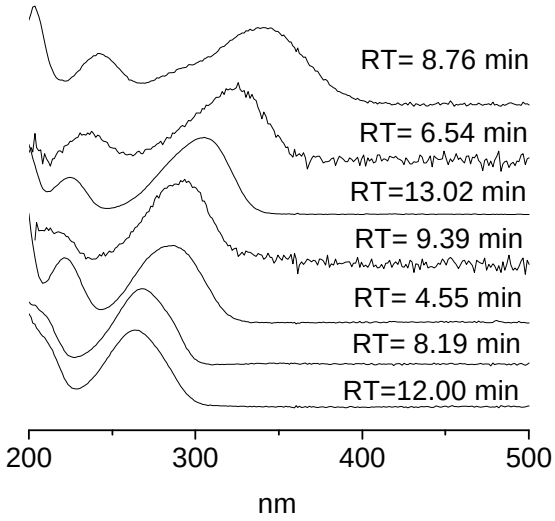

Figure 19: absorption spectra of colorless species detected in a freshly irradiated sample of CV(aq). Maximum of absorption lower than 350 nm.

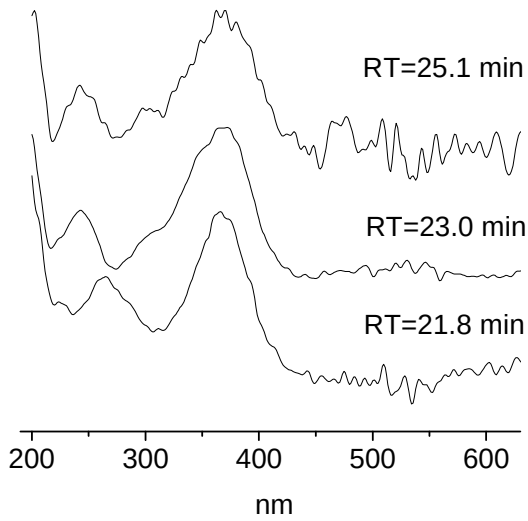

Figure 20 absorption spectra of colorless species detected in a freshly irradiated sample of CV(aq). Maximum of absorption higher than 350 nm.

All degradation products discussed so far are colored species; nevertheless crystal violet both in aqueous solution and on paper (as it will be discussed later in this chapter) discolored entirely after prolonged UV irradiation: colorless degradation products must therefore be formed. In an attempt to detect and identify colorless degradation products in a freshly irradiated (UV) sample of crystal violet (aq), the chromatogram recorded at 230 nm (not shown) was analyzed and the presence of many species with maximum of absorption in the UV range was revealed (figures 19 and 20). The position of their

maxima of absorption suggests the presence of ketones. Some of them, with a maximum of absorption at wavelength longer than 350 nm, might be aromatic ketones.

In particular, two of the peaks in the chromatogram at 230 nm have absorption spectra (figure 21) very similar to the ones associated to the secondary peaks detected in the chromatogram of a reference sample of Michler's ketone (figure 29). Although no mass data are available, the secondary peaks (or at least peaks number 2 and 3 in figure 29) detected in the reference sample of Michler's ketone are thought to be demethylated derivatives of Michler's ketone. Moreover, another peak in the chromatogram at 230 nm has an absorption spectrum similar to Michler's ketone itself, although the matching in retention time and the signal to noise ratio are worse than before (figure 22). According to spectral data, it is believed that such a reaction as the oxidation at the central carbon atom of crystal violet, or of its demethylated derivatives, is involved in the degradation mechanism of crystal violet.

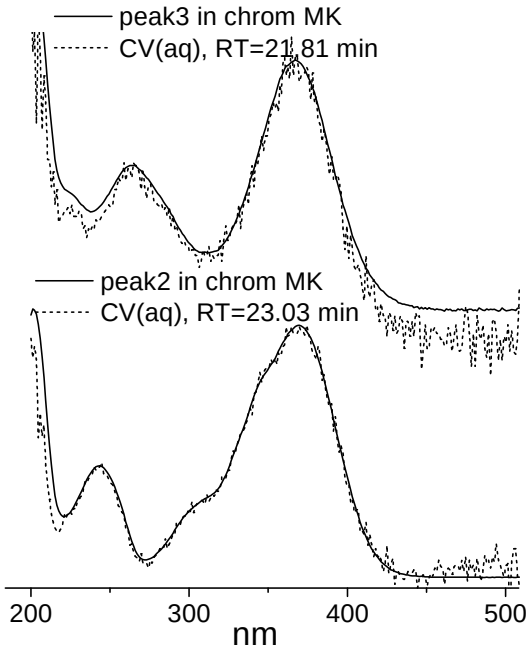

Figure 21: comparison between absorption spectra of colorless species detected in a freshly irradiated sample of CV(aq) and absorption spectra of what is believed to be demethylated derivatives of Michler's ketone (peaks 2 and 3 in figure 29).

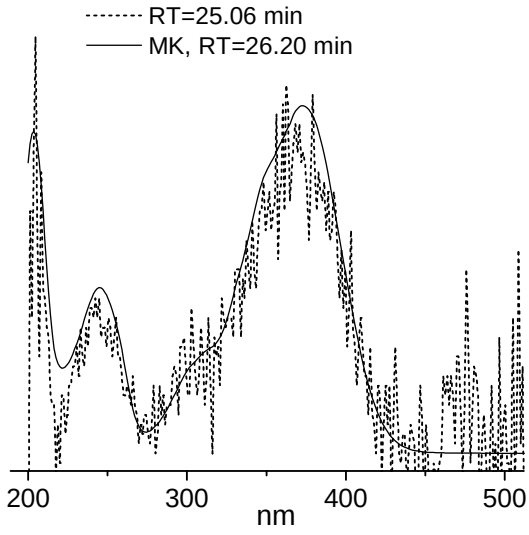

Figure 22: comparison between absorption spectra of a colorless species detected in a freshly irradiated sample of CV(aq) and of Michler's ketone.

LC-MS analysis of the one-year-old sample of irradiated crystal violet (aq) also revealed the presence of colorless species absorbing in the UV range. Indeed, in the chromatogram recorded at 300 nm (figures 13 and 14) many peaks are visible, which

were not present in the chromatogram of a blank analysis (not shown). In particular, a group of four peaks (number 18, 22, 23, 25 in figure 23) showed absorption spectra similar to the ones of a reference sample of Michler's ketone (spectra MK1 and MK2 in figure 23). Mass data for peaks number 18, 22, 23 and 25 are consistent with the presence of mono-, bi- and tri- demethylated Michler's ketone[8]. Nevertheless, Michler's ketone-like spectra detected in the one-year-old sample are different from those detected in the freshly irradiated sample. In particular, the matching between the experimental spectra and the spectra of a reference sample of Michler's ketone (obtained with HPLC-PDA) is better for the freshly irradiated sample (figures 21) than for the one-year-old sample (figure 23). In this regard, however, it can not be excluded that the differences are due to the use of two different instruments for the two analysis. Indeed, slightly different absorption spectra were obtained with HPLC-PDA and LC-MS for a reference sample of Michler's ketone. To conclude, it is believed that Michler's ketone or some of its demethylated derivatives were present, not only in the one-year-old sample, but also in the freshly irradiated one.

Besides peaks number 18, 22, 23 and 25, many others were detected in the chromatogram at 300 nm. Absorption spectra for some of them are shown in figure 24 and retention times, absorption maxima, and m/z values (when available) are reported in table 6. The reason why the rest of the peaks was neglected is that they were too low in intensity, or it was not possible to obtain a good absorption spectrum or useful mass data.

In the UV range, there is no correspondence between absorption spectra of the freshly irradiated sample and of the one-year-old sample. Only two spectra (number 26 in figure 24 and the spectrum at RT=12 min in figure 19) are the same. For the moment, no hypothesis can be offered for the identification of the species responsible for absorption spectra in figure 24.

[8] It is worth noting that Michler's ketone and its demethylated derivatives are neutral molecules and m/z values reported refer to their protonated derivatives.

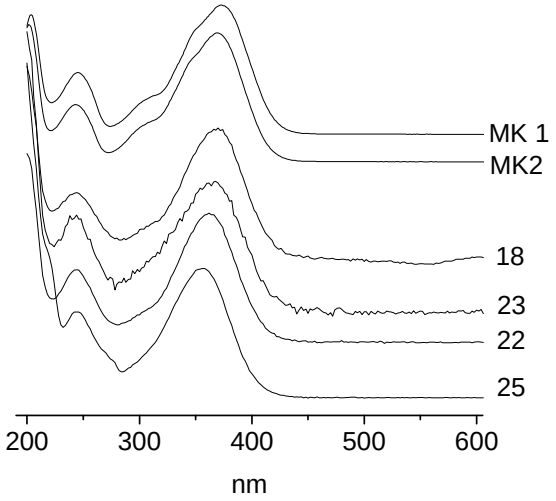

Figure 23: a group of four peaks (number 18, 22, 23, 25 in figure 14) in the chromatogram of a one-year-old sample of irradiated CV(aq) showed absorption spectra similar to the ones of a reference sample of Michler's ketone.

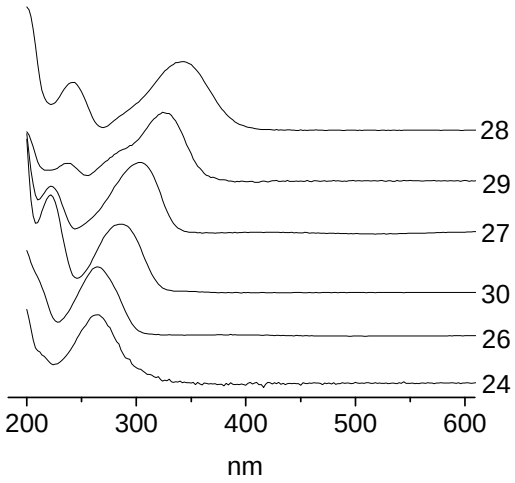

Figure 24: absorption spectra of colorless species detected in a one-year-old sample of irradiated CV(aq).

1.2) Crystal violet on cellulose paper.

1.2.1) HPLC-PDA analysis

Irradiation caused an evident fading of the color of dyed paper, from purple (before irradiation) to light blue after 340 hours of irradiation. A longer exposure caused the dye to fade almost entirely. A quantification of the color change, in terms of colorimetric L*a*b* values, is given later (table 10).

Chromatograms for dyed paper before and after 340 hours of irradiation are shown in figure 25 (HPLC numbering system will be used in this section). After 340 hours of irradiation, a significant decrease in CV concentration was observed and at least 10 other peaks increased in intensity, showing that degradation products were being formed.

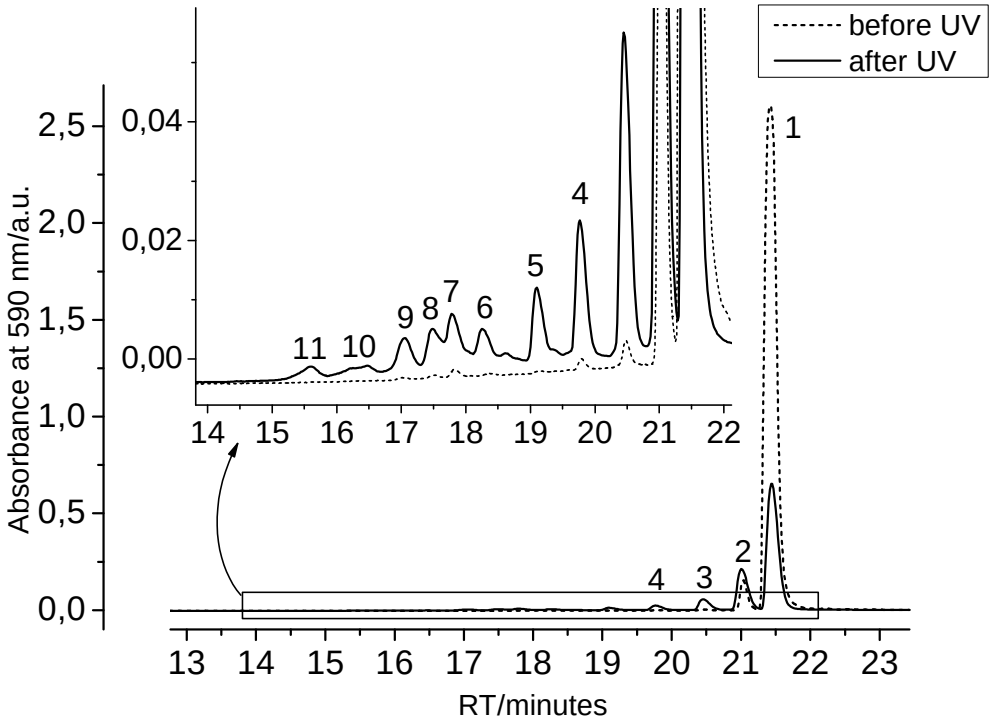

Figure 25: Chromatograms of CV extracted from paper before and after 340 hours of irradiation.

The identification of the peaks in the chromatogram of dyed paper after irradiation was made through a comparison with the chromatogram of CV irradiated in solution (figure 26). Except for peak 12 (due to pararosaniline), the same peaks were obtained both in solution and on paper, indicating that the same degradation products are formed. With the only exception of peak 8, a comparison of absorption spectra for all the peaks at issue confirms the analogy. As for CV irradiated on paper, the absorption spectrum of peak 8 is similar to the one of diamond green B, except for a shoulder around 570 nm (not shown). This might mean that the species responsible for peak 8 do not have three lone pairs of electrons (of nitrogen atoms) delocalized over the aromatic rings.

To summarize, except for peak 8, the same considerations made for CV in solution about peaks number 1 to 11 apply also for CV on paper (table 6).

As for the non colored degradation products, a sample of cotton linters paper dyed with CV and aged in a Xenotest exposure device revealed the presence of a chromatographic peak consistent with one of the minor peaks (number 2 in figure 29) found in the chromatogram of a reference sample of Michler's ketone. The species responsible for this peak is believed to be mono-demethylated Michler's ketone, although no mass data is available. Moreover, at least two species absorbing in the UV region below 300 nm were detected, but they could not be identified. Degradation

reactions leading to the fragmentation of the triphenylmethane skeleton of crystal violet were thus recognized also on paper.

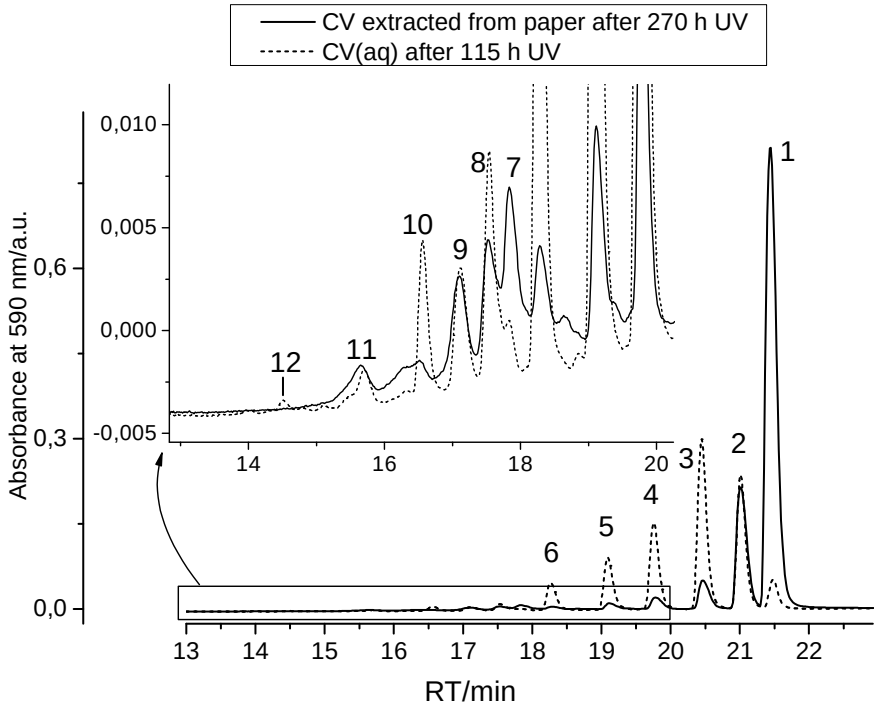

Figure 26: comparison between the chromatograms for CV extracted from paper after irradiation and for CV irradiated in solution.

1.2.2) FORS (Fiber Optics Reflectance Spectroscopy) analysis

A substantial fading was observed for CV on paper during irradiation with UV, as it can be seen from colorimetric L*a*b* values (table 8).

	before UV	16 h UV	32.5 h UV	58 h UV	126h UV	149.5h UV	176h UV	200h UV
L*	52,96	53,85	56,58	60,23	66,77	70,13	70,84	71,60
a*	21,08	19,99	13,53	10,10	6,09	4,50	3,10	3,03
b*	-62,10	-42,64	-37,98	-33,56	-29,00	-25,65	-23,96	-23,30

Table 8: L*a*b* values for CV on paper before and after different irradiation times.

The a* component decreased whereas b* and L* components increased upon irradiation, giving a duller and lighter color.

Reflectance and calculated[9] absorption spectra for CV on paper, before and after irradiation, are shown in figures 27 and 28 respectively. Upon irradiation, both a decrease in the intensity of absorption spectra and a change in spectral features were observed.

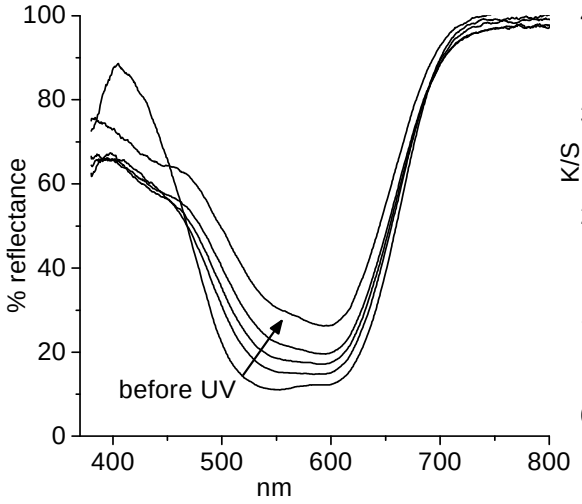

Figure 27: reflectance spectra for crystal violet on paper before and after different irradiation periods (16h, 32h, 58h and 126h).

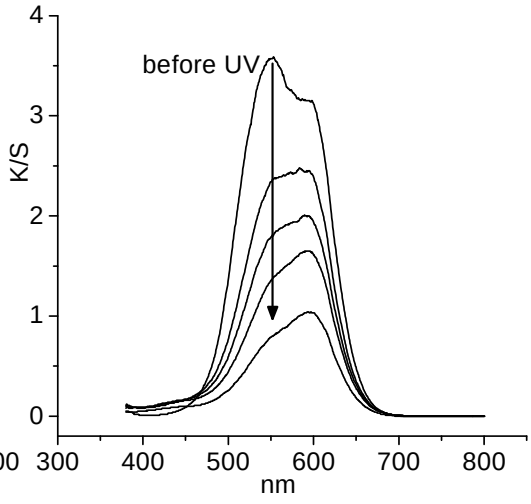

Figure 28: calculated absorption spectra for crystal violet on paper before and after different irradiation periods (16h, 32h, 58h and 126h).

The most significant change in spectral features occurred within the first 16 hours of irradiation: before irradiation the absorption spectrum showed an absorption maximum around 550 nm and a pronounced shoulder around 600 nm. After about 16 hours of irradiation, these two spectral features were barely distinguishable, while after 32 hours of irradiation the absorption maximum was at 590 nm and the shoulder around 550 nm. This behaviour has already been described by other authors for samples of CV in liquid solution and it has been explained as an effect of the aggregation of dye molecules [Duxbury], [Allen et al.], [Stork et al.]. In particular, the absorptions around 590 nm (α-band) and around 550 nm (β-band) were attributed to single monomers of CV and to CV dimers respectively. At higher dye concentrations larger aggregates are formed, causing a shift in the absorption maximum toward shorter wavelengths.

FORS therefore enabled both to measure the decrease in crystal violet concentration on paper upon irradiation and to evaluate the aggregation type for the dye. The latter, besides influencing the spectral features, plays a role also in determining the

[9] from reflectance spectra and according to eq. 13 in chapter one.

photochemical behaviour of dyes (as it was noted in chapter two). For this reason, the possibility of determining the aggregation type for CV on solid substrates with FORS makes this technique very interesting from a conservation point of view.

1.2.3) The role of Michler's ketone

The formation of Michler's ketone (or its demethylated derivatives), via oxidation at the central carbon atom of triarylmethane compounds, is of particular interest because Michler's ketone is known to act as a sensitizer for crystal violet degradation. Moreover, Michler's ketone might be present from the beginning in inks made with triarylmethane dyes because it was one of the possible reagents for the synthesis of this class of dyes. Consequently the effect of Michler's ketone on the degradation of crystal violet was taken into consideration.

Firstly, four samples of Michler's ketone at different concentration were analyzed with HPLC-PDA in order to get information about retention times and absorption spectra (the chromatogram for the most concentrate sample is shown in figure 29). Four peaks were attributed to the sample of Michler's ketone injected. Other minor peaks were present, but since their intensity did not depend on the concentration of the sample they were discarded as impurities from the column or the solvent.

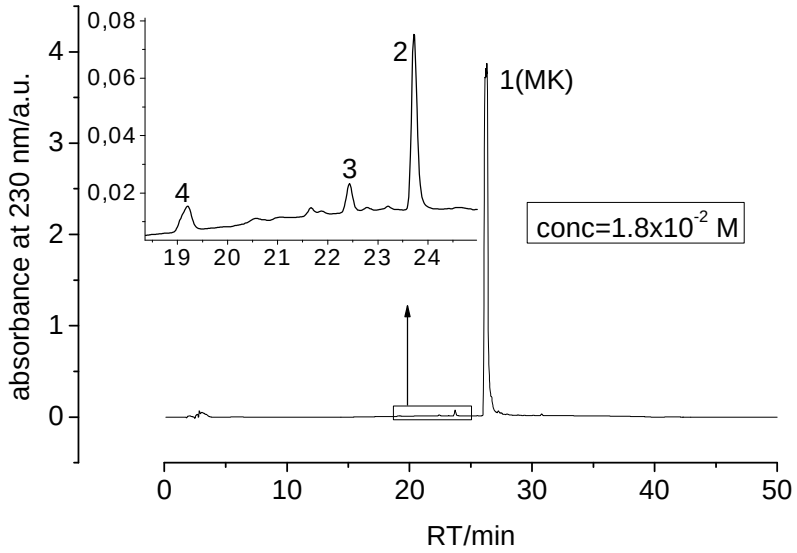

Figure 29: chromatogram of a reference sample of Michler's ketone in methanol ($1.8x10^{-2}$ M).

Absorption spectra and retention times for the four peaks in figure 29 are reported in figure 30. It has to be bear in mind that no mass data are available for these peaks and that the database of UV-Vis absorption spectra used at the ICN did not have reference

spectra of Michler's ketone or of its demethylated derivatives. Consequently, while peak 1 is positively due to Michler's ketone, for the others peaks it is only possible to hypothesize that (at least peaks 2 and 3) they correspond to demethylated derivatives of the ketone.

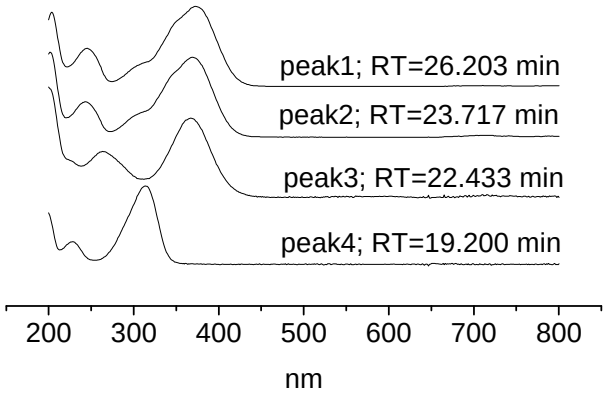

Figure 30: absorption spectra of the four peaks in the chromatogram of a reference sample of Michler's ketone.

Secondly, a sample of pure cellulose paper dyed with crystal violet and Michler's ketone was exposed to UV radiation for different time intervals and analyzed with HPLC-PDA. Interestingly, the area of the peak of Michler's ketone decreased during irradiation, showing that Michler's ketone was consumed along with the dye. A comparison of the (chromatographic) peak area of crystal violet versus irradiation time for samples of dyed paper in the presence or absence of Michler's ketone, is shown in figure 31. In the presence of Michler's ketone, the rate of consumption of crystal violet was higher than in the absence of the ketone.

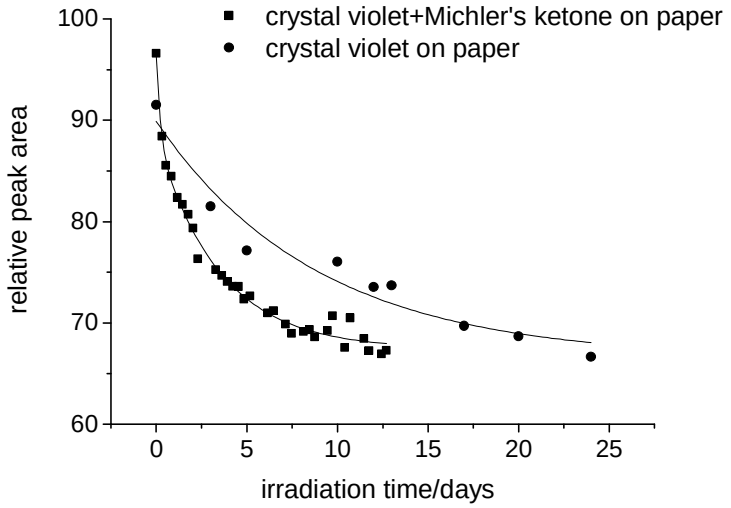

Figure 31: peak area of crystal violet versus irradiation time for samples of dyed paper in the presence or absence of Michler's ketone.

To conclude, it is possible to hypothesize that Michler's ketone (or some of its demethylated derivatives) is formed during degradation of crystal violet and successively involved in further degradation reactions. Moreover, inks made of triarylmethane dyes that were synthesized from Michler's ketone, can be considered more sensitive to light since traces of the ketone might be present in the ink.

2) Degradation of crystal violet in the presence of visible light alone.

The effect of exposure to visible light on the color of Crystal Violet on paper was taken into consideration in order to simulate actual indoor display conditions. Figure 37 shows a plot of the color change (ΔE) during illumination for three kinds of paper (cotton linters, lignin and printing paper). The same experiment was run in the presence of such an ink additive as gum arabic and the result will be discussed in more detail in section 3.

Interestingly, a strong discoloration of crystal violet was observed for all the samples even in the absence of UV radiation. This observation underlines the need of a better understanding of the photo-fading of drawings, writings or printings made of triarylmethane dyes.

3) Study of the degradation of crystal violet on different paper substrates and in the presence of different ink additives or common gaseous pollutants.

3.a) In this section, more realistic samples of paper than filter paper are taken into consideration. Cotton linters, lignin and printing paper were dyed or written with crystal violet (in the presence or absence of gum arabic) and aged with a Xenotest exposure device; samples of undyed paper were also aged. The products formed were analyzed with HPLC-PDA and the color change was measured before and during aging with FORS.

Figures 32B and 33 show the color change during aging with a Xenotest exposure device for all three kinds of paper, written or dyed with crystal violet (similar results were obtained with gum arabic as an additive. Not shown). Written samples (figure 32B) completely discolored after aging, reproducing the phenomenon observed in the menu by Van Gogh (figure 32A). As for dyed samples (figure 33), the color change was significant for all three samples, particularly for crystal violet on lignin and printing paper. It is worth noting that the areas of paper that were protected with metal masks during aging, did not fade significantly. Consequently, one can conclude that heat plays a minor role in the fading of crystal violet, if compared to light.

As for undyed paper, a more or less strong yellowing was obtained for lignin and printing paper respectively. On the contrary, cotton linters paper did not yellow.

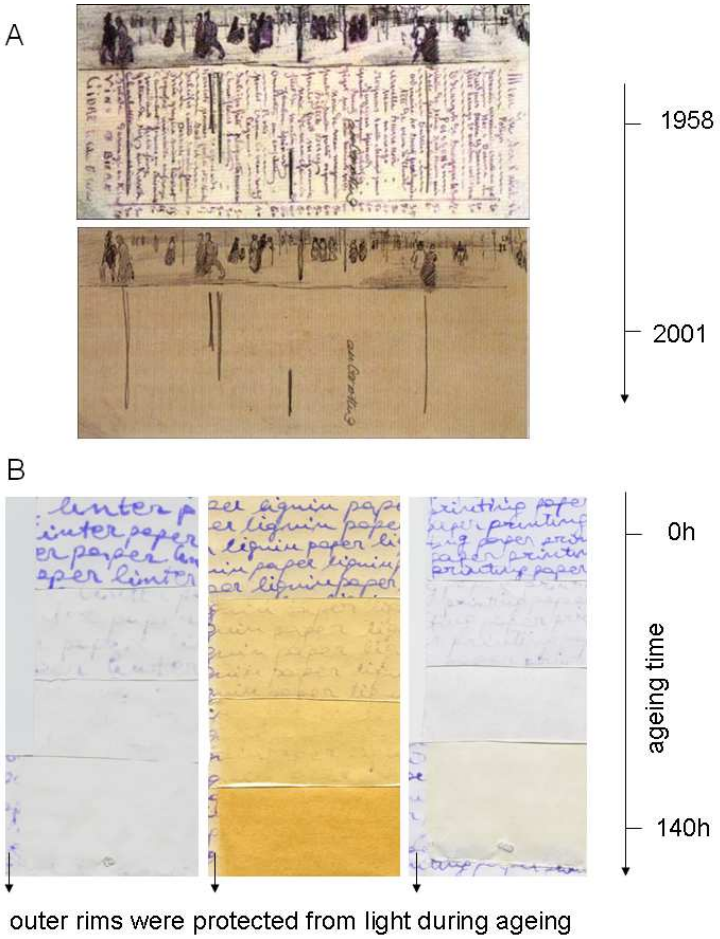

Figure 32: A. Menu drawn and written by Van Gogh in 1886 in Paris, as it appeared in a reproduction made in 1958 (top) and as it looked in 2001 (bottom). Van Gogh museum, Amsterdam. B. model samples of cotton linters, lignin and printing paper (from left to right) written with CV, before aging and after 7h, 14h and 140h with a Xenotest exposure device (from top to bottom).

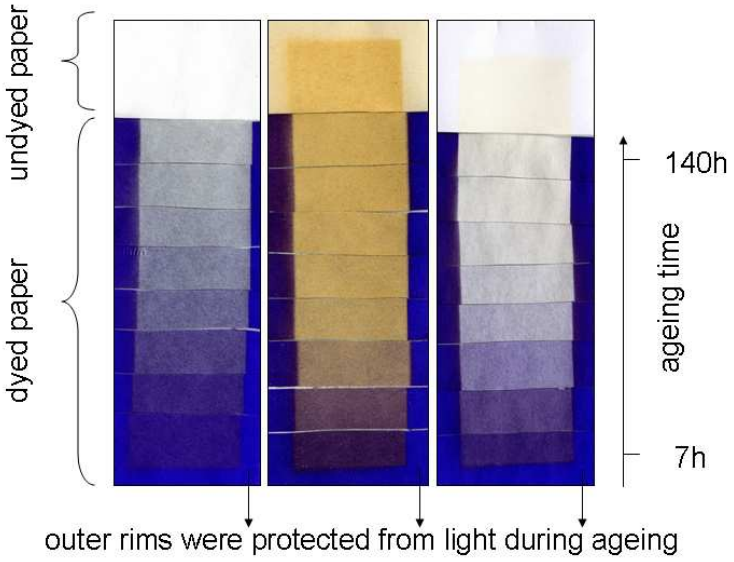

Figure 33: color change during the Xenotest exposure device for cotton linters, lignin and printing paper (from left to right) dyed with CV. Reference samples of undyed paper after 140h in the xenotest are also shown on top.

Samples of cotton linters, lignin and printing paper dyed with crystal violet and exposed to UV-Vis light for 140 hours were all treated with methanol and the extracted solutions were analyzed with HPLC-PDA. As expected, cotton linters paper showed the same chromatogram as model Whatman paper, demonstrating that exactly the same degradation products were formed. Interestingly, chromatograms for crystal violet on printing and lignin paper were also very similar to the one of Whatman paper, except for few differences. The most interesting was the formation, on printing paper, of a peak at 14.3 min with an absorption spectrum (figure 34) different from the ones found on Whatman paper. The same considerations apply to samples containing gum arabic, although the new peak at 14.3 min was much lower in intensity than in the absence of this additive. It is possible to hypothesize that brightners or sizing materials on printing paper are responsible for the formation of this additional species. Gum arabic might be able to prevent the dye from getting in contact with brightners and sizing materials.

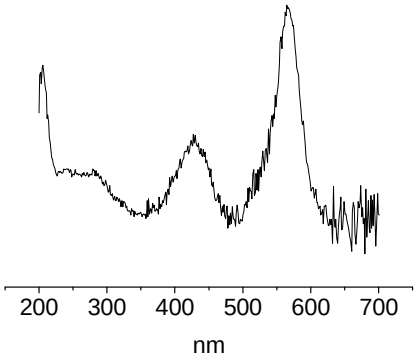

Figure 34: absorption spectrum of the peak at 14.3 min in the chromatogram of CV aged on printing paper.

Plots of the relative peak area (proportional to the relative concentration) of crystal violet versus aging time (in the Xenotest exposure device) is reported in figure 35 for all three kinds of paper, both in the presence and absence of gum arabic.

A reproducible trend was obtained both in the presence and absence of gum arabic: during the first hours of exposure, consumption of crystal violet on lignin paper was always slower than on cotton linters and printing paper whereas at longer exposure times, degradation of crystal violet was more pronounced on lignin paper. Interestingly, when crystal violet was aged on a pre-yellowed sample of lignin paper, a curve shape (figure 35 left, dotted line) similar to the ones corresponding to cotton linters and printing paper was obtained. This observation suggests that lignin does play a role in the degradation of crystal violet.

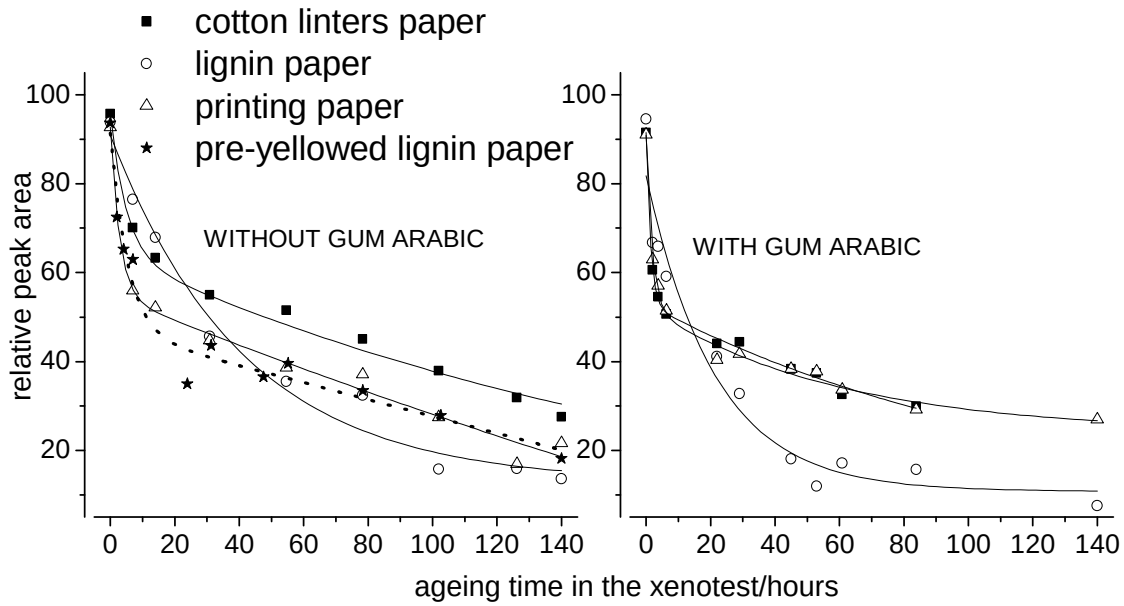

Figure 35: relative peak area of CV versus time, for different papers aged in a Xenotest exposure device, in the presence and absence of gum arabic.

Given that a reference sample of undyed lignin paper underwent a strong yellowing in a Xenotest exposure device, it is possible to hypothesize that during the first hours of irradiation, lignin competes with crystal violet for the absorption of light, thus slowing down crystal violet degradation. At longer exposure time, photo-oxidized lignin (e.g., yellow conjugated ketones) would enhance crystal violet degradation via a sensitization effect.

In conclusion, despite the consistency in the degradation products formed, degradation rates were different, depending on the paper substrate. On the long term, lightfastness[10] of crystal violet on lignin paper and cotton linters paper seems to be the worst and the best respectively.

The same samples were analyzed with FORS and the color change ΔE was calculated from the L*a*b* values. A plot of ΔE versus aging time in a Xenotest exposure device is reported in figure 36. Moreover, the color change due to micro-fading in the presence of visible light alone is reported in figure 37.

[10] A rigorous treatment would imply the measurement of the rates of consumption of CV on each substrate. Nevertheless, in this work the samples dyed with CV were prepared according to the same experimental procedure and aged together in the same Xenotest exposure device and therefore a qualitative comparison of lightfastness was proposed, by analogy with the blue wool test. The approximation was done that the different paper substrates absorbed the same quantity of dye.

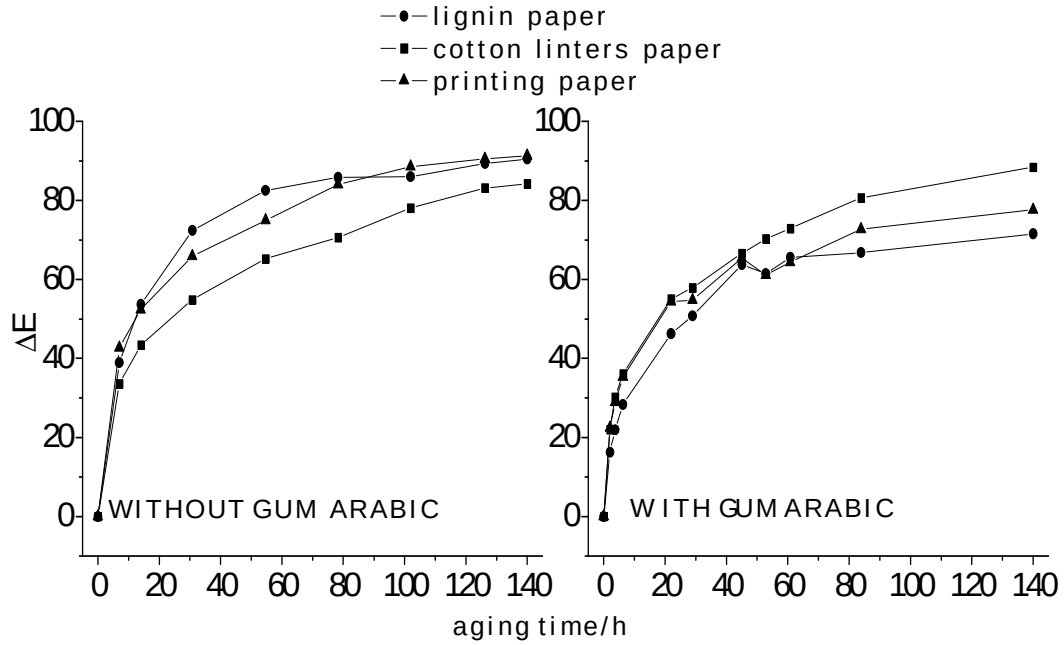

Figure 36: ΔE for CV on different papers during aging in a Xenotest exposure device.

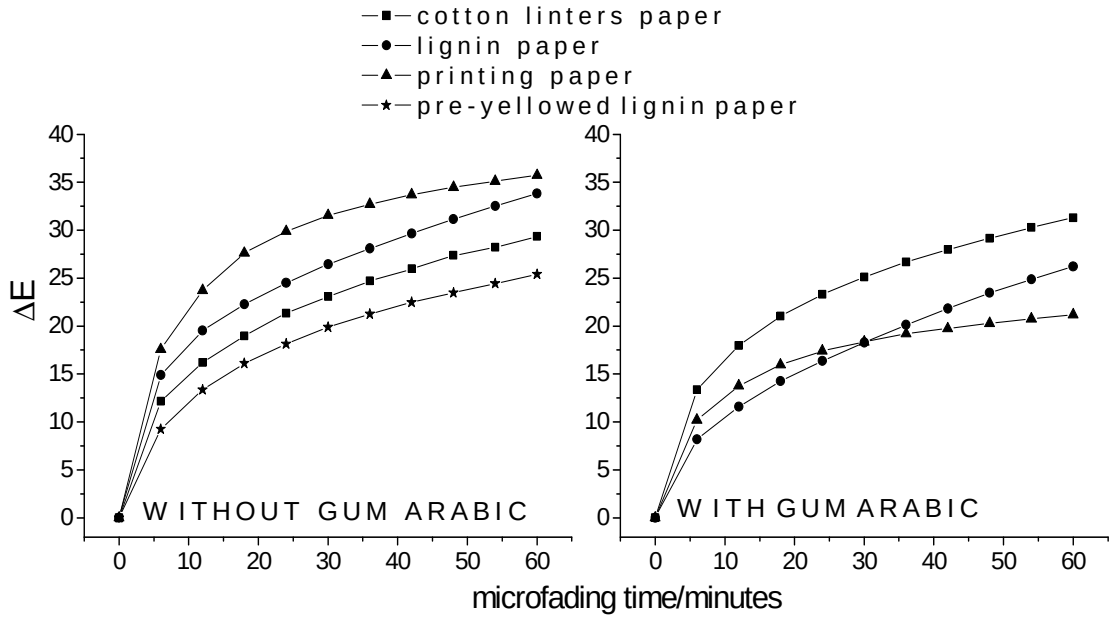

Figure 37: ΔE for CV on different papers during micro-fading.

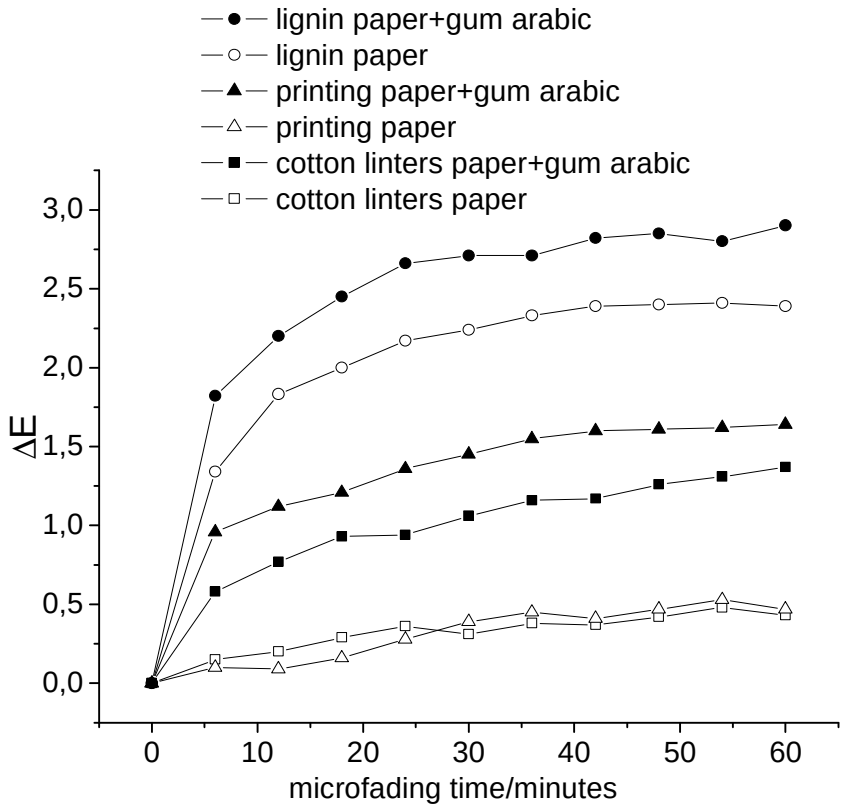

Figure 38: ΔE for different kinds of undyed paper during micro-fading.

In the absence of gum arabic, the smallest color change was measured for crystal violet on cotton linters paper, both for samples irradiated with UV-Vis light and Vis light. For crystal violet irradiated on lignin and printing paper, the color change curves obtained during exposure to UV-Vis light were similar. On the contrary, in the presence of visible light alone, different curves were obtained.

Interestingly, in the presence of gum arabic the color change of dyed cotton linters paper slightly increased whereas on lignin and printing papers it appreciably decreased, both for samples irradiated in a Xenotest exposure device (UV-Vis light) and with micro-fading-meter (Vis light). As a result, in the presence of gum arabic the biggest color change was measured for crystal violet on cotton linters paper.

In order to find an explanation for this behaviour, a test was run for crystal violet on lignin paper: the substrate was pre-yellowed in the Xenotest and only after this treatment it was dyed. The color change measured with the micro-fading-meter for this sample (figure 37 left) was very similar to the one obtained for crystal violet on lignin paper (not pre-yellowed) in the presence of gum arabic. Consequently, to a first approximation, it might be hypothesized that the decrease in ΔE for crystal violet on lignin paper (and possibly printing paper) is due to a less efficient yellowing of this

substrate in the presence of gum arabic. Trends of ΔE versus irradiation time for crystal violet on linter paper would be unaffected by the presence of gum arabic because linter paper does not yellow significantly. As a matter of fact, this hypothesis had to be reconsidered because micro-fading experiments on undyed samples of paper revealed that cotton linters, printing and lignin papers do yellow more in the presence of gum arabic (figure 38). Moreover, the extent of yellowing for all kinds of undyed paper, both in the presence and in the absence of gum arabic, was not high enough to explain the strong change in ΔE observed for dyed samples. Another hypothesis would be that lignin and printing papers contain compounds capable of enhancing crystal violet degradation, but not involved in any yellowing process. In this case, gum arabic would shield the dye from these compounds, as it was already hypothesized for the species responsible for the absorption spectra in figure 34. More studies would be required in order to verify this hypothesis.

Finally, in no case it was observed a browning of the ink: consequently, gum arabic can not currently be considered responsible for the brown discoloration occurred on some of Van Gogh's drawings.

However, since the presence of this additive was proved to play a role in the color change of the samples, a more comprehensive evaluation of the possible additives present in Van Gogh's inks would be necessary in order to shed light on the different kinds of discoloration observed on the artist's drawings and letters.

3.b) An ink prepared according to [Lehner] (figure 8) was applied on two sets of three kinds of paper (cotton linters paper, lignin paper and protein sized paper). The ink contained sucrose and oxalic acid as additives. The paper used for one of the two sets of samples was enriched with Fe(III) whereas the paper used for the other set was not. This choice is justified by the fact that Fe(III), commonly present on paper (it can be introduced with water or come from work machinery), is known for catalyzing radical reactions responsible for the degradation of paper.

In the presence of additional iron, both cotton linters paper and (especially) protein sized paper yellowed; moreover, when the ink was applied with a fountain pen, its color appeared different, depending on the presence or absence of iron (figure 39). For this reason, it was decided to study also reference samples of undyed cotton linters paper and protein sized paper containing various combinations of the same additives present in the ink (see section 3.c, page 126).

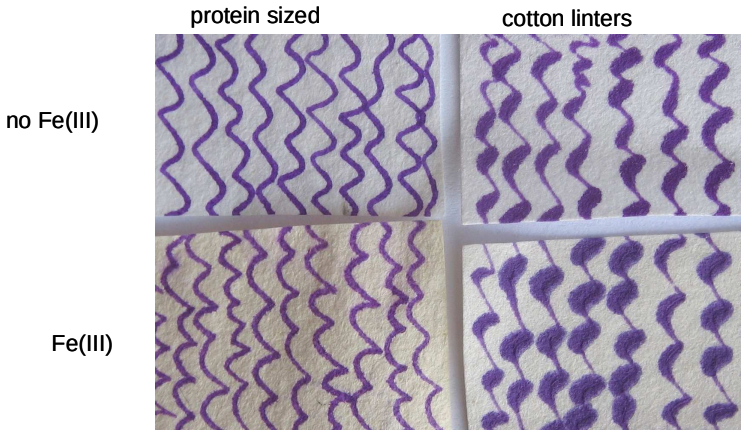

Figure 39: Lehner ink on protein sized paper (top left), on linter paper (top right), on protein sized paper enriched with Fe(III) (bottom left) and on linter paper enriched with Fe(III) (bottom right).

Both exposure to UV-Vis radiation (Xenon lamp) and to natural sun light caused a strong fading of all samples. On the contrary, thermal aging (24 h at 100 °C, no light) had a much smaller effect on the color of the samples, in agreement with what observed also for the other samples described so far.

Interestingly, both after exposure to natural sun light and UV-Vis radiation, the ink turned bluish-grey on cotton linters paper and brownish-grey on cotton linters paper enriched with Fe(III) (figure 40). The color difference between these two samples might be ascribed to the different colors of the two cellulosic substrates, white in the absence of Fe(III) and yellowish in the presence of Fe(III). A discoloration of this kind had never been observed before for the other samples of paper dyed with pure crystal violet. Currently, the sample in figure 40 (left) is the one that best resembles the discoloration occurred on the Montmajour drawing.

On protein sized paper the ink faded passing through a reddish color both after exposure to UV-Vis radiation and natural sun light, whereas on lignin paper it faded passing through a bluish color after exposure to UV-Vis radiation and through a reddish color after natural sun light.

At this point, it is worth drawing the attention of the reader to the reliability of artificial aging: indeed, exposure to UV-Vis radiation and to natural sun light had different effects on the discoloration of the ink on lignin paper. It would be therefore very important to plan monitoring studies of natural aging of museum objects over years.

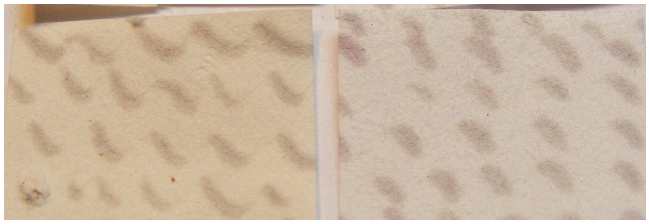

Figure 40: brownish-grey and bluish-grey discolorations obtained after exposure to natural sun light of ink (according to Lehner) on cotton linters paper with (left) and without (right) additional iron.

Undyed reference samples of cotton linters paper, lignin paper and protein sized paper, containing various combinations of the additives present in the ink studied, were also taken into consideration. Each sample was divided into 2 parts: one was exposed to natural sun light for 2 months (during summer) and the other was kept in the dark. As already described in section 3.b, the addition of Fe(III) to cotton linters paper and protein sized paper caused an homogeneous yellowing of paper. The effect was more pronounced on protein sized paper. After exposure to natural sun light, the yellowing of the samples enriched with Fe(III) became more evident, especially for those samples with no oxalic acid. In addition to this homogeneous yellowing, a bright yellow stripe appeared along an edge of cotton linters paper enriched with iron. The treatment with an aqueous solution of oxalic acid, caused a whitening of all the samples previously enriched with iron. This was most likely due to the removal of (part of) Fe(III) from paper (via complexation with oxalate anions) or of part of the sizing (for protein sized paper). After exposure to natural sun light, the sample of cotton linters paper enriched with Fe(III), oxalic acid and sucrose showed the formation of a brown area along an edge.

ATR-IR analysis (spectra in figure 41) was performed on all three kinds of paper before aging and before the treatment with additives. A typical IR spectrum of both cellulose paper or lignin paper (unsized and without fillers) is characterized by the following signals [Calvini et el. 2002] [Calvini et el. 2006]. At high frequencies, only a broad band (around 3300 cm^{-1}) due to the stretching of hydroxyl groups and a smaller band (2900 cm^{-1}) due to the stretching of the carbon-hydrogen bonds of CH_2 and CH_3, are visible. At low frequencies (between 500 cm^{-1} and 1000 cm^{-1}) there are many superimposed peaks, mainly due to C-H and C-OH stretchings, and not very informative. Nevertheless, a small peak is noteworthy around 810 cm^{-1} due to substituted aromatic rings or substituted aliphatic C=C and indicative of the presence of lignin, hemicelluloses or rosin. In some cases, it can also be present in oxidised and

aged cellulose. In the fingerprint region, between 1000 cm^{-1} and 1400 cm^{-1}, the absorbance of C-OH and C-H is very strong and masks any other signal. The most informative region of the spectrum lies in the range between 1400 cm^{-1} and 1900 cm^{-1} where many functional groups crowd in (figure 42).

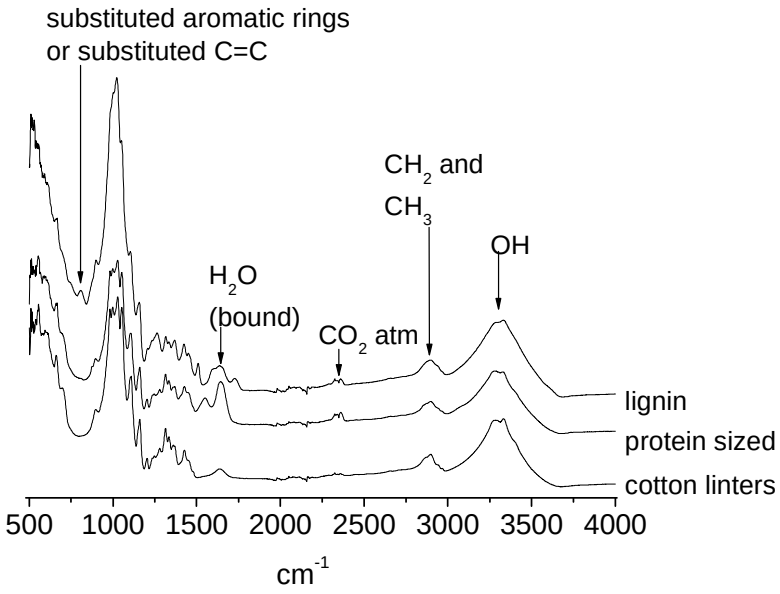

Figure 41: ATR-IR spectra of cotton linters, protein sized and lignin paper.

All samples showed a peak due to CH_2 bending (C_6 position in cellulose) around 1424-1428 cm^{-1} and a peak due to bound water around 1638-1644 cm^{-1}. Moreover, lignin paper showed a characteristic peak around 1509 cm^{-1} due to unconjugated aromatic rings and a peak at 1728 cm^{-1} due to unconjugated carbonyl groups. The former peak is considered a marker of the presence of lignin and the latter is present in oxidized lignin, cellulose and hemicelluloses. Finally, protein sized paper showed a peak around 1550 cm^{-1} due to N-H bending of the amide II of the peptide bond of proteins.

As for cotton linters paper enriched with Fe(III) and exposed to natural sun light, ATR-IR spectra were recorded both on the bright yellow stripe (figure 43, line B) and on the inner (less yellowed) surface (figure 43, line A). At a first glance the spectra look the same, but at a closer inspection a faint shoulder around 1730 cm^{-1} is visible in the spectrum of the bright yellow area. As already outlined earlier, this peak is due to carbonyl groups and it is indicative of the presence of oxycellulose. It is therefore possible to conclude that the presence of Fe(III) catalyzes the oxidation of cellulose, causing yellowing of paper. Although it was already known that yellowing is associated

to degraded (oxidized) paper, it was demonstrated that such a surface technique as ATR-IR is able to detect a higher concentration of carbonyl groups in a tiny yellowed area of the sample.

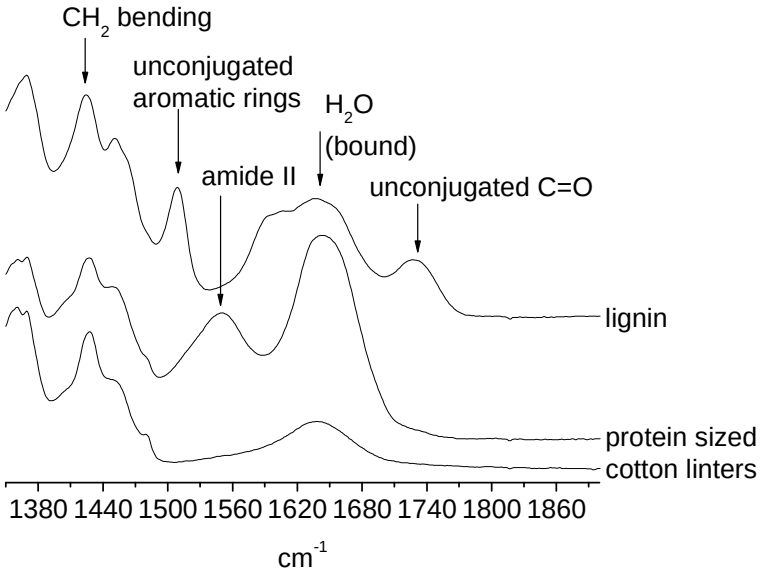

Figure 42: enlargement of the ATR-IR spectra of cotton linters, protein sized and lignin paper.

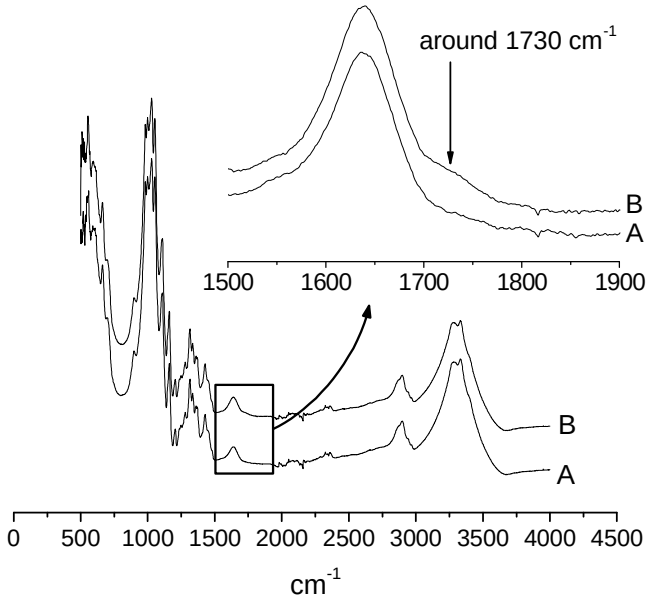

Figure 43: ATR-IR spectra of the bright yellow stripe (line B) and of the inner and less yellowed surface (line A) of cotton linters paper enriched with Fe(III).

ATR-IR analysis (spectra not shown) of the brown area previously described did not reveal any functional group useful for the identification of the brown compound(s).

As for protein sized paper, it was not possible to detect with ATR-IR any appreciable effect of aging. In particular, it was not observed a higher concentration of C=O in the

yellowed areas, although the yellowing was more pronounced than for cellulose paper. In this case, yellowing is more likely due to the formation of colored metal-protein complexes than to oxidation of cellulose. On the contrary, aqueous treatments (used to enrich paper with additives) had an effect on ATR-IR spectra of this kind of paper. Indeed, the intensity of the amide II band was lower for treated samples (figure 44), thus confirming the hypothesis that protein sizing is partly removed during aqueous treatments.

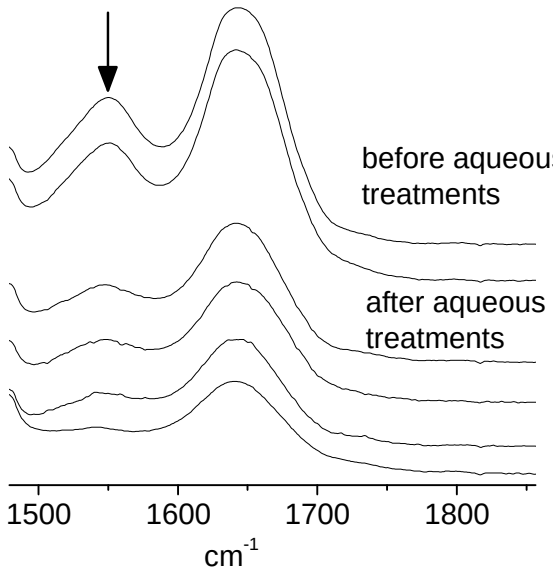

Figure 44: effect of aqueous treatments on ATR-IR spectra of protein sized paper. The amide II band (indicated with an arrow) decreased in intensity after the treatments.

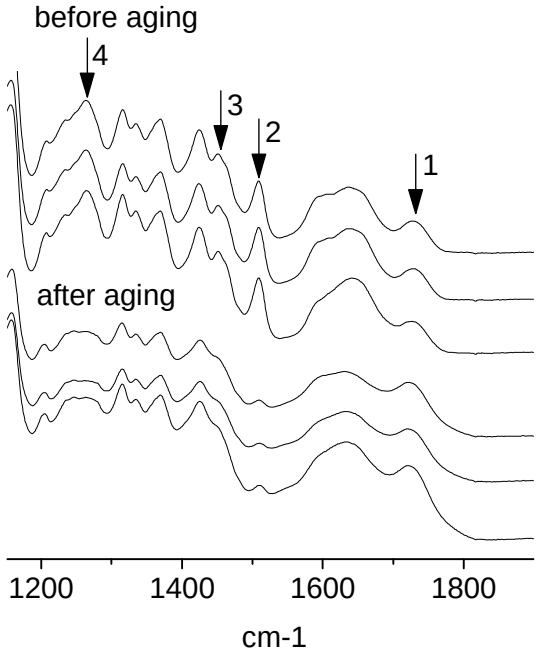

Figure 45: effect of exposure to natural sun light on ATR-IR spectra of lignin paper. The bands that underwent a change after aging are indicated by arrows.

Finally, lignin paper showed a strong yellowing after exposure to natural sun light, in particular in the presence of sucrose or oxalic acid. ATR-IR spectra were not significantly affected by the presence of additives. Contrary to what observed for protein sized paper, with ATR-IR it was possible to distinguish between aged and unaged samples of lignin paper (figure 45). After aging, the relative intensity of the C=O peak (number 1 in figure 45) increased with respect to the peak of bound water, and the peak characteristic of lignin (number 2) sensibly decreased. The peak previously attributed to substituted aromatic rings or substituted C=C group (around 810 cm^{-1}, not shown) and the unknown peaks number 3 and 4 also decreased after aging.

3.c) The effect of two common pollutants such as NO_2 and O_3 on crystal violet and on the ink made with crystal violet was studied. Exposure to ozone did not affect significantly the color of the samples, except for a lightning of the ink, observed on cotton linters paper both in the presence and absence of Fe(III). On the contrary, exposure to NO_2 caused a strong darkening both of crystal violet and of the ink on all samples, except cotton linters paper dyed with pure crystal violet.

Let us first consider samples dyed with pure crystal violet (figure 46). Before exposure, samples were purple colored (not shown) on all substrates. On protein sized paper and lignin paper, the dye discolored to dark blue after exposure whereas it faded to light bluish-grey on cotton linters paper.

Figure 46: pure crystal violet on samples of lignin paper (left), protein sized paper (middle) and cotton linters paper (right) after exposure to NO_2. On the bottom of the sample in the middle, the original purple color is still visible.

As for the ink in the absence of additional Fe(III), after exposure it turned dark grey, dark greenish-blue and dark blue on cotton linters paper, protein sized paper and lignin paper respectively. Undyed lignin paper also yellowed after exposure. In the presence of Fe(III), the ink turned black on cotton linters paper whereas on protein sized paper the color was similar to what observed in the absence of Fe(III), but less saturated as if the concentration of the dye was lower.

So far, it has been possible to analyze with LC-MS the sample of Crystal Violet on cotton linters paper exposed to NO_2. Both absorption spectra and mass spectra consistent with Crystal Violet and its mono- and bi-demethylated derivatives were detected. Therefore, it can be concluded that a demethylation mechanism is active also during exposure to this gaseous pollutant. Moreover, a species responsible for an absorption spectrum that had never been observed before (for samples of Crystal Violet exposed to UV or visible light) was detected (figure 47). Its maximum of absorption was around 630 nm, consistently with the bluish color of the sample; the shape of the spectrum suggested the presence of a triarylmethane dye having one of the lone pairs of electrons on nitrogen atoms not delocalized over the aromatic rings (as it was also the case for diamond green and N-oxides of Crystal violet).

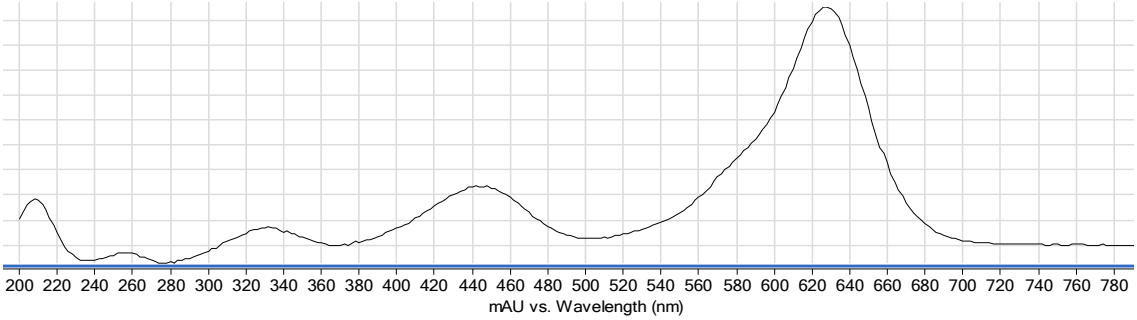

Figure 47: Absorption spectrum of the peak at 27.7 min in the chromatogram of a sample of cotton linters paper dyed with Crystal Violet and exposed to NO_2.

The mass spectrum corresponding to this species showed two peaks, the main one located at a value of m/z of 387.21838 and the second one (almost half the size of the other one) at 357.22070. The main peak is consistent with the nitrosoamine shown in figure 48. The resonance form on the right would explain the (DG-like) shape of the absorption spectrum.

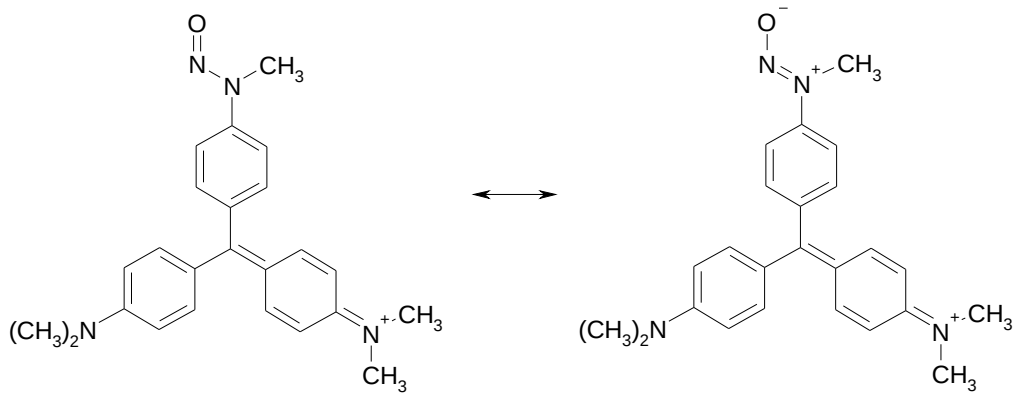

Figure 48: two resonance forms of the species responsible for the absorption spectrum in figure 49.

As a further confirmation of this attribution, the difference between the main mass peak and the secondary one is equal to 29.99768 m/z, which correspond to the mass of the N=O fragment. Some species absorbing in the UV or visible range were also detected, but it has not been possible to identify them yet.

To conclude, it should be underlined the importance of an efficient monitoring of environmental conditions in the display and storage areas of museums. Indeed, although the concentration of NO_2 used was about ten times higher than then of polluted urban areas, a prolonged exposure to lower concentration might induce severe discoloration effects.

4) EPR characterization of crystal violet, pararosaniline and diamond green radical cations

4.a) Figure 49 shows the EPR spectra at 290K of undyed cellulose paper and of crystal violet on cellulose paper, after exposure to UV-Vis radiation. In the absence of crystal violet, after irradiation an EPR signal was detected due to the formation of organic radicals of cellulose. The presence of crystal violet caused a significant increase of the EPR signal and for this reason it was hypothesized the formation of radicals of the dye. The line shapes of the two normalized EPR spectra (figure 49, right) were similar, although not identical.

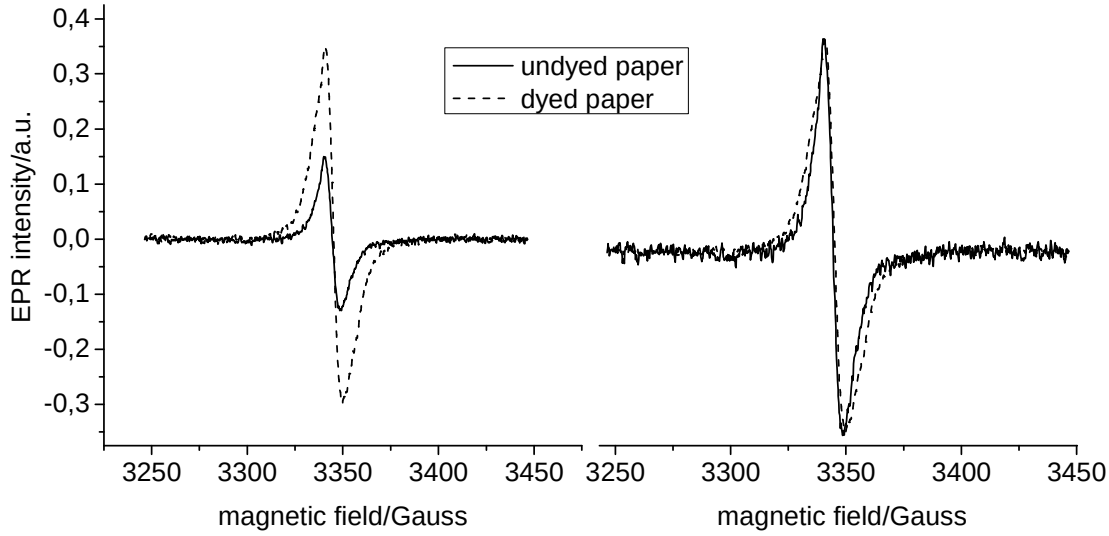

Figure 49: EPR spectra (left) and normalized EPR spectra (right) at 290K of undyed cellulose paper (solid line) and of cellulose paper with crystal violet (dashed line), both after exposure to UV-Vis radiation.

In order to know more about the role of crystal violet in the formation of radicals on paper, a more extensive EPR study of the dye on paper and in solution was carried out. In particular, it was of interest to understand if the higher intensity of the signal detected in the presence of crystal violet, was due to the formation of radicals of the dye or of cellulose. The structures of radicals formed during photo-oxidation of cellulose have already been described in [Confortin] and are reported in figure 50. The structures of the radical dications formed by oxidizing crystal violet, pararosaniline and diamond green are shown in figure 51 [Stanoeva et al.]. It should be noted that for these radical dications many other resonance forms exist, also with the unpaired electron on one of the nitrogen atoms. In this way, hyperfine coupling between the unpaired electron and the nitrogen atom is possible.

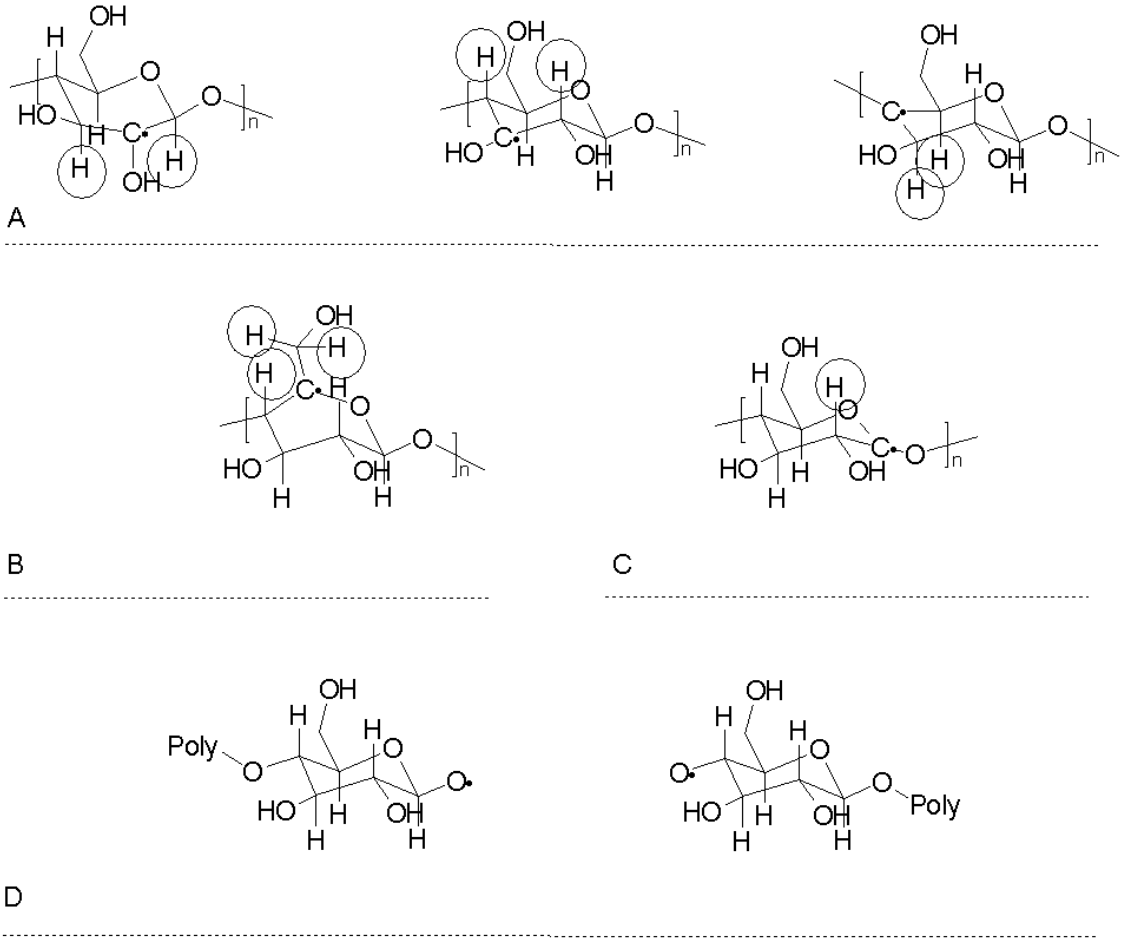

Figure 50: structures of the radicals formed upon exposure to UV-Vis of cellulose paper. Hydrogen atoms marked with a circled are those involved in hyperfine couplings with the unpaired electron. Poly denotes the rest of the polymer.

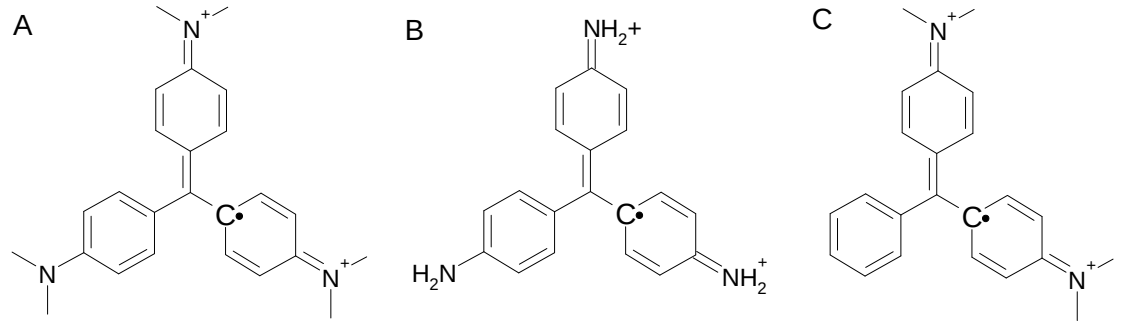

Figure 51: structures of the radical dications of crystal violet $[CV]^{\cdot 2+}$ (A), pararosaniline $[PR]^{\cdot 2+}$ (B) and diamond green $[DG]^{\cdot 2+}$ (C).

Consequently, it is possible to distinguish between radicals of cellulose and radical dications of crystal violet, pararosaniline and diamond green thanks to the hyperfine coupling of the unpaired electron with nitrogen atoms of these three dyes. To this purpose, Electron Spin-Echo Envelope Modulation (ESEEM) spectra of dyed paper

after irradiation were recorded, but no hyperfine coupling constant consistent with the presence of nitrogen atoms was revealed.

4.b) As an additional test, radical dications of crystal violet ($[CV]^{\cdot 2+}$), pararosaniline ($[PR]^{\cdot 2+}$) and diamond green ($[DG]^{\cdot 2+}$) were synthesized and analyzed with EPR spectroscopy, in order to compare their spectra with the one obtained for the sample of crystal violet on paper exposed to UV. EPR spectra of the radical dication $[CV]^{\cdot 2+}$ at 290K and 200K are shown in figure 52 and a simulated spectrum, based on the structure proposed in [Stanoeva et al.], is reported in figure 53 (for the experimental spectrum at 290K). The EPR spectrum at 290K was characterized by a very complex hyperfine structure and a line width of about 20 G. In the EPR spectrum at 200K, the hyperfine structure was no longer visible and the line width was larger (about 30 G).

The simulated spectrum obtained was very satisfactory and gave evidence of the formation of the radical dication $[CV]^{\cdot 2+}$. The characteristic spectral feature of the experimental spectrum is due to the high delocalization on the unpaired electron over the aromatic rings of the radical cation of crystal violet. Thanks to this highly delocalized structure, there is a large number of hyperfine couplings between the unpaired electron and the nuclei of hydrogen and nitrogen. This is the origin of the characteristic spectral feature of the radical dication of crystal violet. In particular, in agreement with [Stanoeva et al.], three groups of magnetically equivalent protons and a group of magnetically equivalent nuclei of nitrogen were identified, with hyperfine coupling constants of 0.64 G, 0.298 G, 0.121 G and 0.617 G respectively. The number of equivalent nuclei belonging to each group was 12, 4, 4 and 2 respectively. On the basis of this result, it was possible to state that the unpaired electron is delocalized over two of the rings. The 12 equivalent protons belong to the hydrogen atoms of the methyl groups whereas the two groups of 4 equivalent protons belong to the hydrogen atoms in ortho and meta positions of the rings.

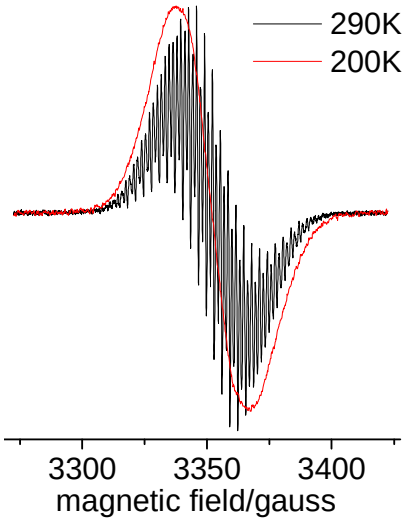

Figure 52: EPR spectra of the radical dication of crystal violet at 200K and 290K.

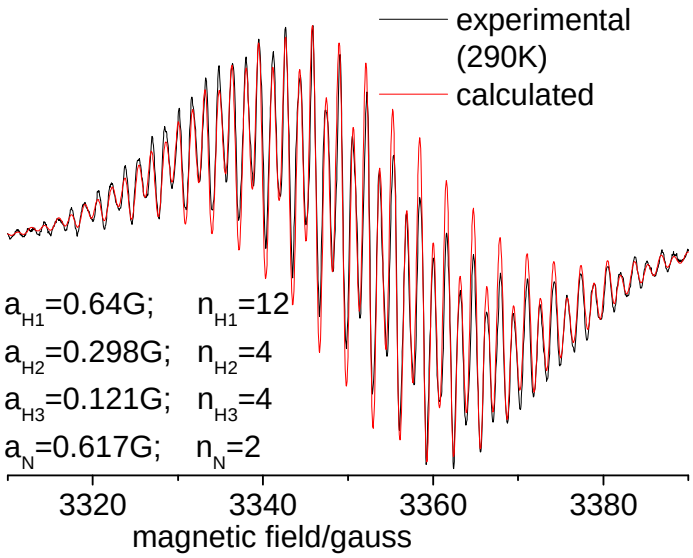

Figure 53: experimental and calculated EPR spectra of the radical dication of crystal violet at 290K.

EPR spectra of radical dications $[DG]^{\cdot 2+}$ and $[PR]^{\cdot 2+}$ at different temperatures are shown in figure 54 and 55 respectively.

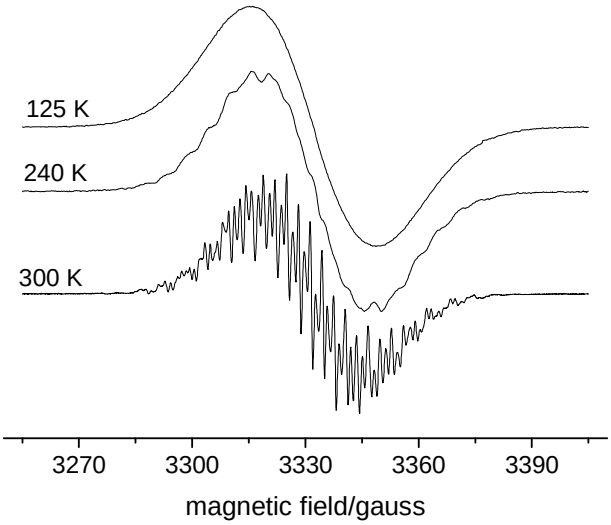

Figure 54: EPR spectra of the radical dication of diamond green at 125K, 240K and 300K.

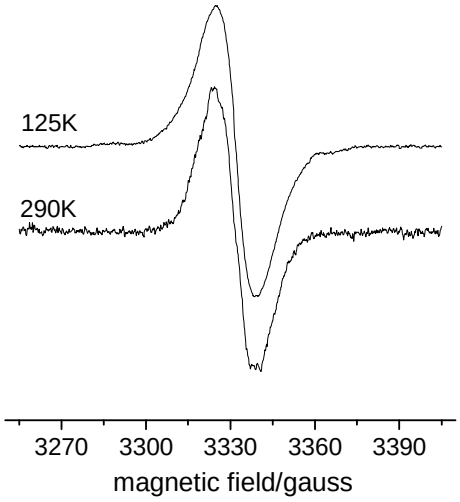

Figure 55: EPR spectra of the radical dication of pararosaniline at 125K and 290K.

Also the hyperfine structure of $[DG]^{\cdot 2+}$ at 300K showed a very complex hyperfine structure which merged into a single band at lower temperature, in agreement with what was observed before. On the contrary, the EPR spectrum of $[PR]^{\cdot 2+}$ consisted of a single band both at room temperature and low temperature.

A comparison between the EPR spectra of $[CV]^{\cdot 2+}$ and CV irradiated on paper is now possible. At room temperature the spectral features were completely different, thus suggesting the presence of different radical species in the two samples. Nevertheless, it should be noted that we are comparing a solid state spectrum (crystal violet on paper) and a spectrum of a liquid ($[CV]^{\cdot 2+}$ in HFP/TFA 10:1 (v:v)) and that the different spectral features might be ascribed to this reason. Thus, the EPR spectrum of CV irradiated on paper was also compared to the spectrum of $[CV]^{\cdot 2+}$ in frozen solution at 200K (figure 56), but the spectra were still very different.

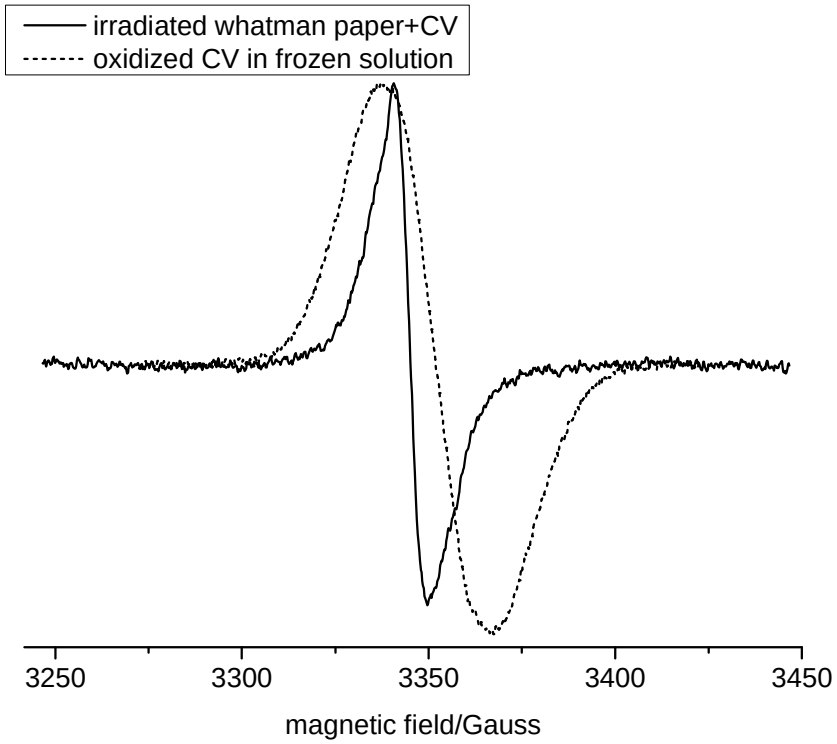

Figure 56: comparison between the normalized EPR spectra of CV irradiated on paper (dotted line) and of $[CV]^{\cdot 2+}$ in frozen solution at 200K (solid line).

To summarize, such experimental observations as the absence of hyperfine couplings with nitrogen atoms in the sample of crystal violet irradiated on paper, the similar line shapes of crystal violet irradiated on paper and of undyed irradiated paper and the inconsistency of the line shapes of $[CV]^{\cdot 2+}$ and crystal violet irradiated on paper, suggested the presence of radicals of cellulose rather than of the radical dication $[CV]^{\cdot 2+}$ on irradiated dyed paper. The small difference between the EPR spectra of CV irradiated on paper and of irradiated undyed paper (figure 49, right) might be due to the formation of various cellulose radicals in different concentration ratio in the presence or absence of CV. Therefore it can be hypothesized that CV acts as a sensitizer for the

formation of radicals of cellulose, thus playing a role in the degradation of paper. A possible mechanism for the sensitization might involve the reaction between a photo-excited state of CV and molecular oxygen to give the radical dication of CV and the superoxide anion $O_2^{\bullet -}$. The latter would then remove an hydrogen atom from cellulose, yielding OOH^- and a radical of cellulose. As an alternative, the photo-excited triplet state $^3CV^*$ might produce singlet oxygen $^1O_2$ which in turn would react with cellulose giving peroxides (and hence radicals). Consequently, in the presence of CV, radicals of cellulose would be obtained also during irradiation with visible light (which is not absorbed by undyed cellulose), and hence the sensitizing effect of the dye. Indeed, the formation of $^1O_2$ and of the superoxide anion $O_2^{\bullet -}$ has already been detected on irradiated paper dyed with triarylmethane dyes [Brezová et al.].

Given the results of chapter three, where the slow component of the transverse relaxation time of protons of paper ($T_{2,S}$) was demonstrated to be a marker of the state of conservation of this material, I decided to study with NMR-MOUSE the effect of Crystal Violet on the photo-induced aging of paper. To this purpose, two samples of cellulose paper, one dyed with Crystal Violet and the other left undyed, were aged with a Xenotest exposure device. Successively, the transverse relaxation times of both of them were measured, but no significant difference could be noted. It is possible that the sensitizing effect of Crystal Violet (revealed by the presence of an higher than normal amount of radicals) is not strong enough to have a significant effect on nuclear relaxation times.

4.c) Two samples of cellulose paper dyed with crystal violet were exposed to UV, either in the presence or in the absence of molecular oxygen (O_2). The same was done for two samples of undyed cellulose paper. Interestingly, even in the absence of oxygen a discoloration of dyed paper, from deep purple to lighter purple, was observed. In the presence of oxygen, though, the color change was bigger. Consequently, it was possible to infer that CV undergoes photo-degradation reactions also in the absence of oxygen. This information is of particular interest for conservators, if considered that anoxic protection is one of the conservation methods in use in museums.

A comparison of the EPR spectra of cellulose paper both dyed with CV and undyed, in the presence or absence of oxygen and before and after exposure to UV-Vis radiation is shown in figure 57.

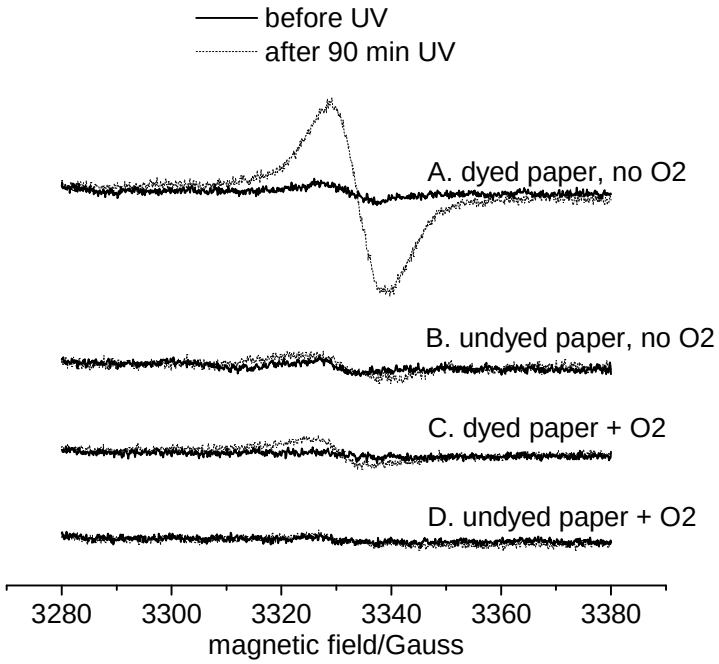

Figure 57: EPR spectra of both undyed and dyed cellulose paper, in the presence or absence of oxygen and before and after exposure to UV.

Before exposure to UV, no EPR signal was visible (except for a very weak signal for the sealed quartz tubes due to sealing process). In the absence of oxygen, after exposure to UV-Vis radiation the EPR signal obtained for the dyed sample was higher than the signal of undyed cellulose paper. The hypothesis that CV acts as a sensitizer for the formation of cellulose radicals might therefore hold true also in the absence of oxygen. Triarylmethane dyes have been reported to act as oxidizing agents under anaerobic conditions, where the reaction may involve either an electron or hydrogen atom abstraction by the dye [Duxbury]. Moreover, it was demonstrated that photo-excited triarylmethane dyes can abstract hydrogen atoms from ethanol giving ethoxy radicals [Brezová et al.]. It is therefore possible to hypothesize that CV irradiated on paper may abstract hydrogen atoms from the substrate, thus giving cellulose radicals. As an alternative, Feichtmayr and Schlag suggested that a one-step electron transfer from the counterion X^- to the photo-excited dye cation $*D^+$ may yield the radical species $*D^{\cdot}$ and $X^{\cdot}$ [Duxbury]. In solid substrates, the proximity between the dye cation and the counterion would promote this mechanism. The radicals formed would subsequently react with the paper substrate to give radicals of cellulose. To summarize, also in anoxic conditions CV would be able to produce radicals of cellulose during irradiation with visible light (which is not absorbed by undyed cellulose), and hence the sensitizing effect of the dye.

It is worth noting that in the absence of oxygen a higher amount of radicals was detected both for dyed and undyed paper, but this does not necessarily mean that the amount of radicals formed (and the degradation extent) was higher. Simply, in the presence of oxygen, radicals are quickly scavenged. Indeed, the color change of the sample of crystal violet on paper was smaller in the absence than in the presence of oxygen as it was possible to see also to the naked eye.

5) Preliminary study of the color change of various colorants aged on paper.

According to historical sources, other recipes for purple inks were in use besides those based on methyl violet. The oldest recipes consisted in mixing a blue and a red pigment or dye, e.g. indigo and cochineal (Mitchell und Hepworth, 1904, p. 114). Other recipes suggested to react logwood and copper (II) (e.g. Cooley's Cyclopædia of Practical Receipts, 1856) or (to get a purplish black) logwood and chromium (VI)[11]. There is evidence for the use of both chromium and copper logwood in some of Van Gogh works.

Therefore it was decided to carry out photo- and thermal- aging tests of some colorants (on paper) that might have been used in purple drawings or letters, as an alternative to methyl violet or in mixture with it. The color change of the samples was studied with the aim of assessing if any purple ink would undergo a change in hue upon aging rather than simply fade to a lighter and less saturated color. The colorants chosen were the following: indigo, indigo carmine, cochineal carmine (ink), copper logwood (synthesized according to two routes) and chromium logwood. Chemical structures of indigo (a pigment) and indigo carmine (a dye) are shown in figure 58A and B. Cochineal carmine consists of complexes of carminic acid (figure 58C) with Fe(III) and Al(III) whereas the color of logwood inks is due to complexes of hematein (figure 58D) with metal cations such as Cr(VI) and Cu(II) [Kazuko et al.] [Centeno et al.].

Pictures of the samples both before (A) and after thermally-induced (B) and photo-induced (C) aging are shown in table 9. Reflectance spectra for all samples are shown in figures 59 and 60 and colorimetric L*a*b* values are enlisted in table 10.

[11] Birgit Reissland, private communication.

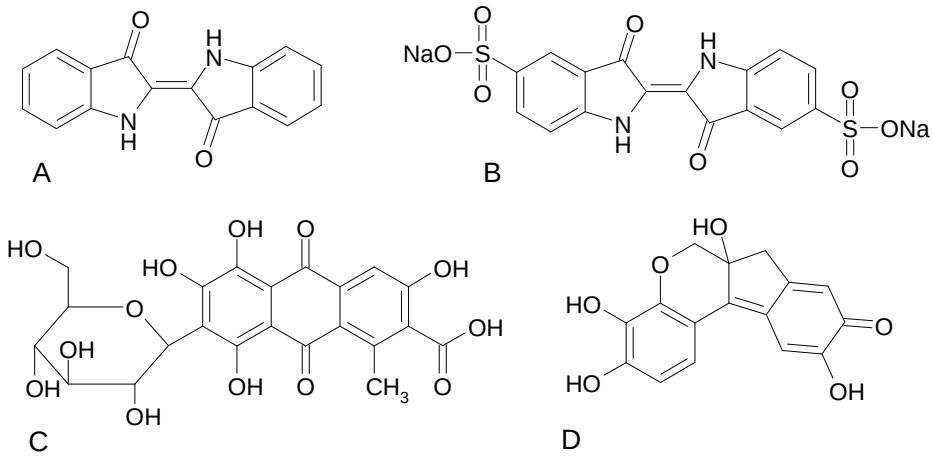

Figure 58: molecular structures of indigo (A), indigo carmine (B), carminic acid (C) and hematein (D).

Colorants	Pictures before (A) and after thermally-induced (B) and photo-induced (C) aging	Colorants	Pictures before (A) and after thermally-induced (B) and photo-induced (C) aging
indigo	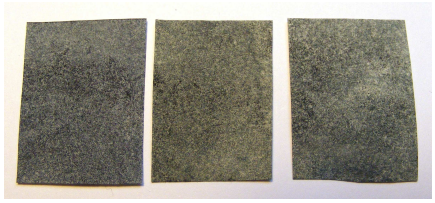 A B C	copper logwood (synthetic route 1)	C  B A
indigo carmine	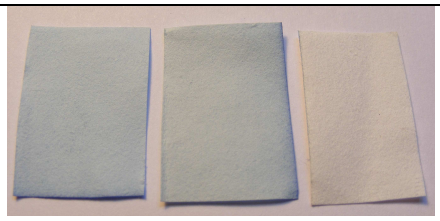 A B C	copper logwood (synthetic route 2)	C  B A
cochineal carmine ink	 A B C	chromium logwood	C  B A

Table 9

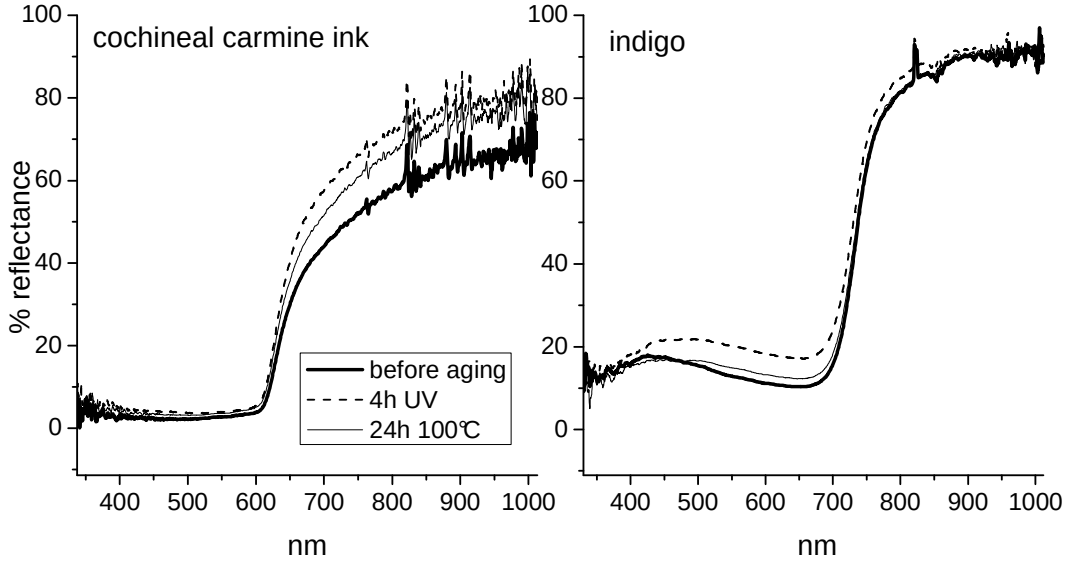

Figure 59: reflectance spectra of samples of paper dyed with different colorants, before aging (thick solid line) and after exposure to UV-Vis radiation (dotted line) or thermal aging (thin solid line).

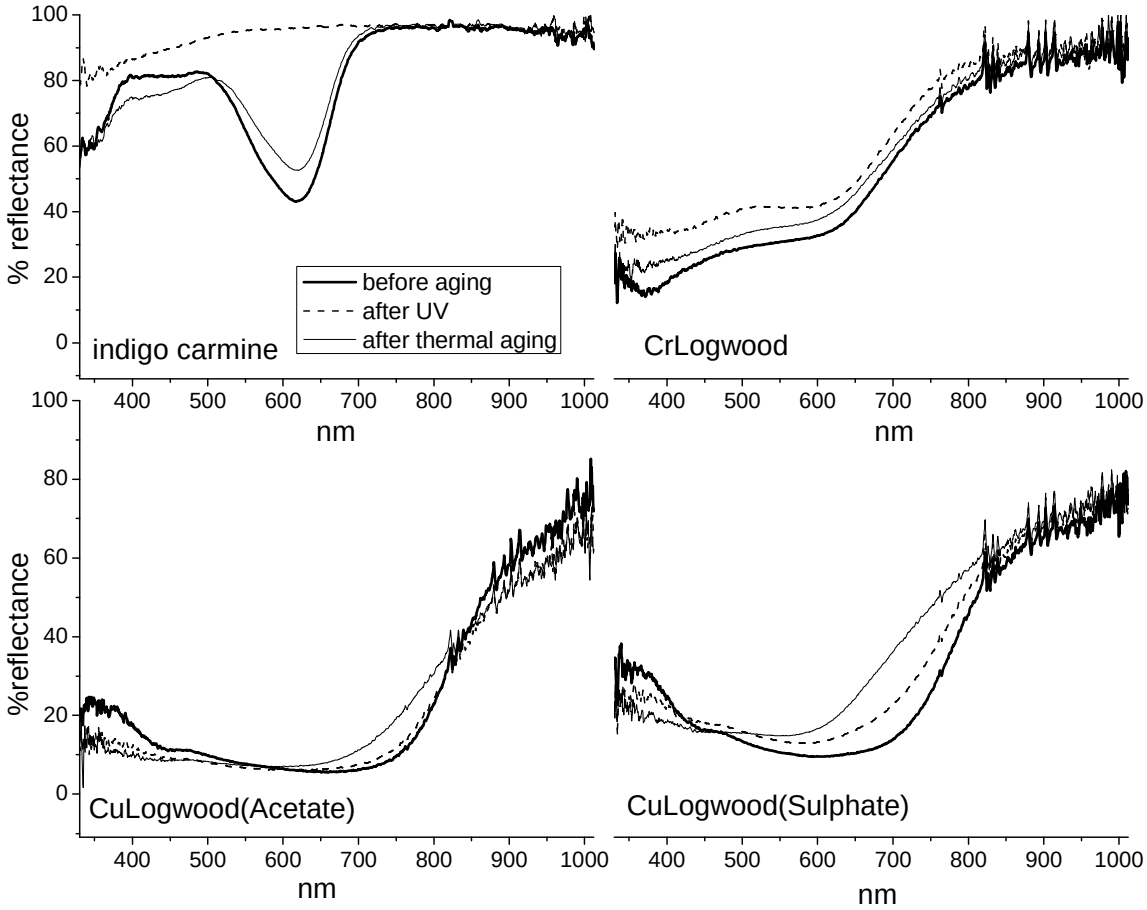

Figure 60: reflectance spectra of samples of paper dyed with different colorants, before aging (thick solid line) and after exposure to UV-Vis radiation (dotted line) or thermal aging (thin solid line).

Colorants	Before aging	After photo-induced aging	After thermal aging
indigo	L*= 42.6; a*= -1.7; b*= -9.7 hue-angle=-99,8° chroma=9,8	L*= 51,7; a*=-3,4; b*=-2,8 hue-angle= -141,1° chroma=4,4	L*= 45,3; a*=-3,3; b*=-4,3 hue-angle= -127,4° chroma=5,4
indigo carmine	L*= 83,4; a*=-11,6; b*=-15,4 hue-angle= -127,0° chroma=19,3	L*=98,0; a*=-0,6; b*=3,4 hue-angle= 99,9° chroma=3,4	L*= 86,3; a*=-10,4; b*=-7,0 hue-angle= -146,0° chroma=12,6
cochineal carmine	L*= 28,6; a*=34,7; b*=19,9 hue-angle=29,8 ° chroma=40,0	L*=34,0; a*=38,1; b*=16,7 hue-angle= 23,7° chroma=41,5	L*=32,3; a*=36,2; b*=18,1 hue-angle= 26,6° chroma=40,5
copper logwood (SO_4^{2-})	L*= 52,5; a*=-4,4 ; b*=0,4 hue-angle=175,2 ° chroma=4,4	L*= 54,1; a*= 2,8; b*=3,4 hue-angle= 50,6° chroma=4,4	L*= 52,4; a*= 6,2; b*=4,7 hue-angle= 37,5° chroma=7,8
copper logwood (AcO^-)	L*= 32,4; a*=-5,4; b*=-13,2 hue-angle= -112,2° chroma= 14,3	L*= 30,9; a*=-1,4; b*=-9,0 hue-angle= -98,8° chroma= 9,2	L*= 32,5; a*= -0,2; b*=-4,7 hue-angle= -91,9° chroma= 4,7
chromium logwood	L*=63,4; a*=5,1; b*=8,9 hue-angle=60,3 ° chroma=10,3	L*=71,1; a*=2,5; b*=5,4 hue-angle= 64,9° chroma=6,0	L*=67,2; a*=5,4; b*=9,5 hue-angle=60,5 ° chroma=10,9

Table 10

As for cochineal carmine ink, at the naked eye no visible color change was detectable either after thermal- or photo-aging. Accordingly, the reflectance spectra of this dye did not show significant changes in the visible range after aging tests (figure 59, left).

As for indigo, only a little discoloration was observed after thermal aging whereas, after photo-induced aging, lighter spots unevenly distributed over the surface of the sample appeared. Indigo carmine slightly discolored after thermal aging whereas it discolored almost entirely after photo-induced aging, as it ca be easily seen from the reflectance spectra in figure 60 (top left). Interestingly, in a previous work by other authors [Sousa et al.], indigo carmine irradiated (335 nm and 610 nm) in the presence of oxygen showed a high lightfastness, both in aqueous solution (quantum yield of reaction=$9x10^{-6}$ or lower) and in aqueous gels (quantum yield of reaction=$2x10^{-3}$ or lower). In dimethylformamide, indigo carmine and indigo irradiated (335 nm) in the presence of oxygen showed similar quantum yields of reaction ($3x10^{-3}$ and $8x10^{-3}$ respectively). The strong discoloration observed in the present work for indigo carmine irradiated (UV-Vis) on paper is therefore of interest and might be due to the interaction with the cellulose substrate. As discussed in the previous work [Sousa et al.], oxygen based radicals can attack the central double bond of indigo and indigo carmine, thus

degrading the dyes. It is possible to hypothesize that oxygen-based radicals formed during irradiation of cellulose are responsible for the strong discoloration of indigo carmine observed in this work. As for indigo, since it was not possible to obtain a very well dispersed solution, the dye deposited on paper had probably a lower surface to volume ratio than indigo carmine. For this reason the interaction with oxygen-based radicals was likely lower than for indigo carmine, and hence the little effect of irradiation on the colour of indigo on paper.

Copper logwood was produced in aqueous solution starting from copper acetate or copper sulphate, according to different historical recipes. Two different blue shades were obtained starting from copper acetate or sulphate. These two versions of copper-logwood also showed different behaviour upon artificial aging. After photo-induced aging, copper logwood from copper acetate discolored to a slightly different blue color whereas copper logwood from copper sulphate turned purplish-brown. Interestingly, after thermal-aging copper logwood from copper acetate again became of a slightly different blue shade whereas copper logwood from copper sulphate turned brown. Interestingly, both kinds of copper logwood showed a larger change in spectral features after thermal aging than photo-induced aging (figure 60, bottom), contrary to what observed for the other colorants. A possible explanation of this behaviour is that the color change observed for copper logwood samples after thermal aging might be due to a modification of the geometry of logwood complexes with Cu(II) or a modification of the kind of ligands involved rather than to a fragmentation of the colorant complex (e.g. the loss of water molecules at 100 °C might play a role).

Finally, although the aqueous solution of chromium logwood showed purple shades, on paper the color obtained was brown. After photo-induced aging the color of the dye on paper became lighter, whereas thermal-aging caused a discoloration to a different brown.

This preliminary study was designed with the aim of gaining qualitative information on the colors obtainable from thermal and photo-degradation of dyes that might have been used for the purple ink on van Gogh drawings and letters. The results of these preliminary analyses will be used for shedding light on the origin of the brown discoloration occurred on the Montmajour drawing. For this reason, contrary to what was done for samples of paper dyed with CV, in this case the concentrations of the solutions of colorants used to dye paper were not controlled (in some cases they were unknown).

6) HPLC-PDA analysis of the purple ink from 'Montmajour'

Both the paper and the traces of purple ink of the drawing entitled Montmajour (1888, Vincent Van Gogh) were analyzed.

The analysis of the paper[12], revealed the presence of short softwood fibers and no lignin. On one side of the sample, starch was identified; probably it belonged to the adhesive that was used to hinge the drawing with Japanese paper.

As for the dye, the result of HPLC-PDA analysis of a dyed fiber of paper taken from a purple area of the Montmajour drawing is shown in figure 61. The chromatogram of a reference sample of cellulose paper dyed with crystal violet and exposed to prolonged UV radiation is also shown for comparison. Significantly, the peak positions were clearly reproducible for the historical sample and the model sample (except for the retention times in the range from 21.5 to 25 minutes, where some extra peaks were present in the historical sample) giving evidence of the reliability of the model samples used. In particular, a comparison between the absorption spectra of the peaks of the Montmajour sample and of the reference sample revealed the presence of crystal violet (peak 1[13]), mono- (peak 2), bi- (peak 3), tri- (peaks 4 and 5), tetra- (peak 6), penta- (peak 10) demethylated crystal violet and pararosaniline (peak 12). Such a mixture can be explained either as the result of Crystal violet degradation on paper or as the result of the use of an ink containing (some of) the mentioned dyes. Only in the range from 17 to 18 minutes, although there were still a very good reproducibility of peak positions, there was no correspondence as for the absorption spectra of the historical and model samples.

A for the extra peaks in the range from 22 to 25 minutes, visible in the chromatogram of the Montmajour sample, they have never been observed in aged samples of pure crystal violet. Nevertheless, their absorption spectra were very similar to the spectra of crystal violet or of its demethylated derivatives. Therefore, it can be concluded that the extra peaks were likely due to triarylmethane dyes present from the beginning in the ink used by Van Gogh. Significantly, HPLC-PDA analysis of 10 historical (from the middle of the XX century) methyl violet samples (from the ICN dye collection) revealed in at least 7 cases the presence of chromatographic peaks at retention times higher than that of crystal violet. Interestingly enough, some of these peaks had similar retention times

[12] Analysis performed by personnel[0] of the Van Gogh Museum (unpublished result).

[13] HPLC numbering system is used here.

as some of the extra peaks detected in the Montmajour sample. At this point, a comparison between the absorption spectra of the matching peaks was carried out and for at least 4 dyes of the ICN collection the matching with the Montmajour sample was satisfactory. The dyes were the following: Methyl Violet 2B Farbenfabriken Fr. Bayer & Co (6320), Methyl Violet 3B Farbenfabriken Fr. Bayer & Co Elberfeld (7065), Methyl Violet 2B 200 imperial chemical industries limited, hexagonhouse, blackley, Manchester (7081) and Methyl Violet PV imperial chemical industries limited, hexagonhouse, blackley, Manchester (6559). The extra peaks, for which a matching of the absorption spectra was found, are those labelled as A, B, C and D in figure 61 (right).

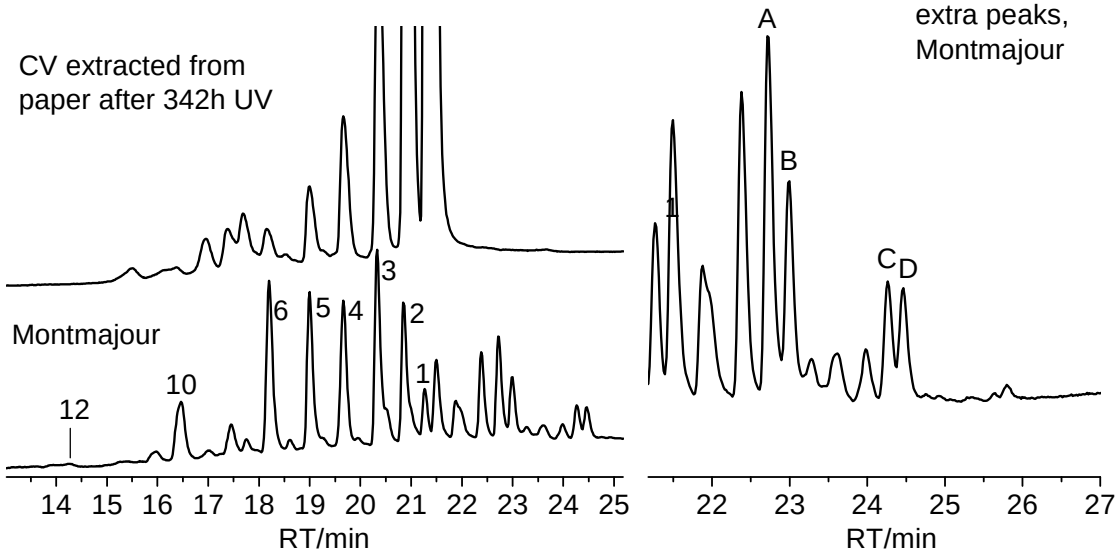

Figure 61: comparison between the chromatograms of a sample of purple ink from the Montmajour drawing (bottom, left) and of a model sample of CV on cellulose paper after exposure to UV (top, left). Enlargement of the extra peaks detected for the Montmajour sample (right).

In figure 62, a comparison between the chromatogram of the Montmajour sample and of Methyl Violet 3B (7065) is shown[14]. As it can be seen from figure 62 (right), in the sample of dye from the ICN collection four peaks (marked with arrows) at retention times similar to those of peaks A, B, C and D were present.

[14] The intensity of the chromatogram of methyl violet 3B was rescaled to make the comparison easier.

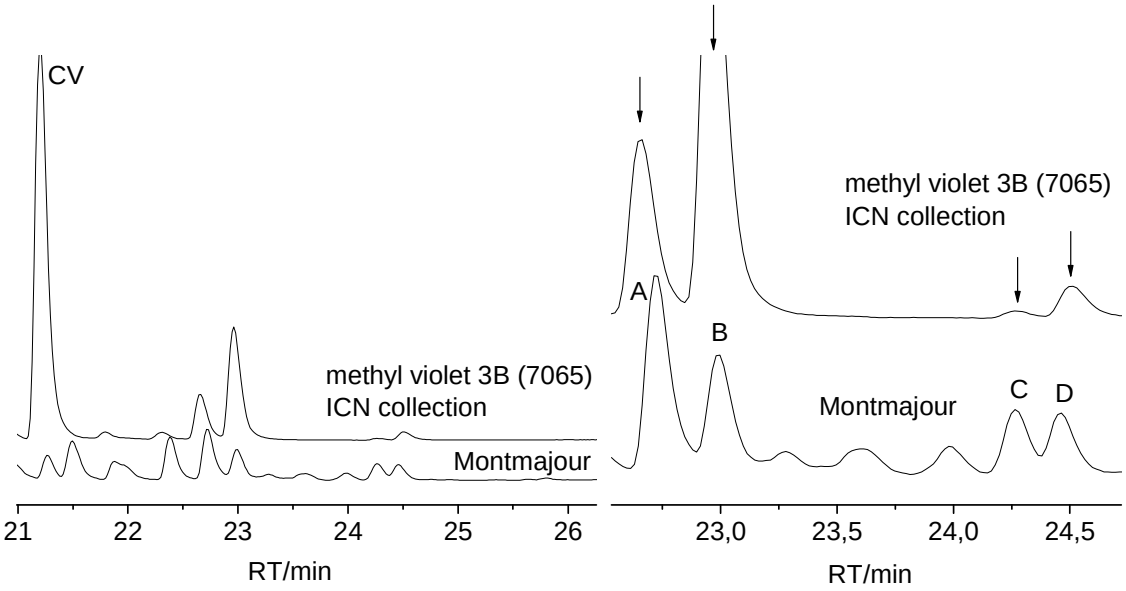

Figure 62: comparison between the chromatograms of the Montmajour sample and of Methyl Violet 3B (left). Only the range of retention times higher that that of CV is shown (i.e. the range where extra peaks were detected). Enlargement showing the correspondence of some of the extra peaks of the historical and model samples (right).

In figure 63, a comparison between the absorption spectra of the peaks at issue is shown and it can be seen that the matching between the spectra, especially for peaks A, B and D, is very good.

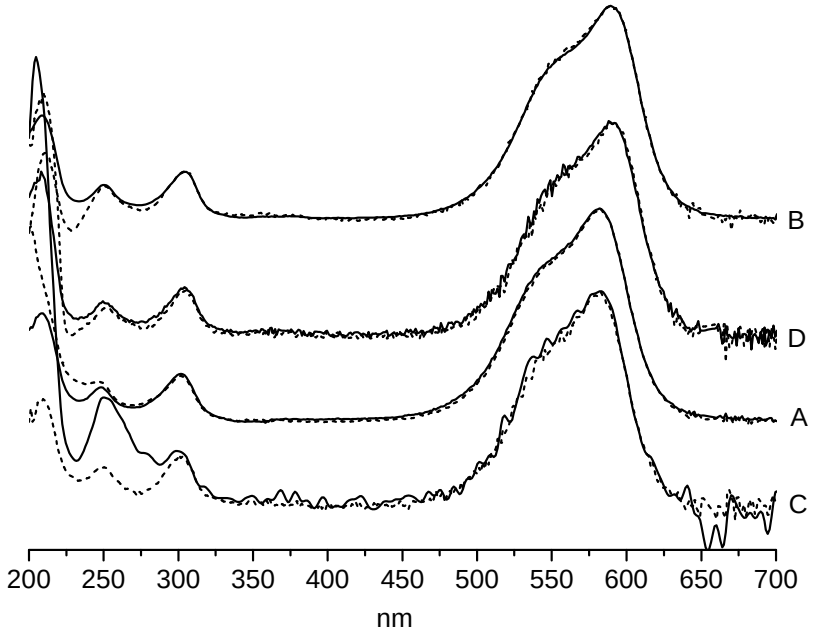

Figure 63: comparison between the absorption spectra of some of the extra peaks (A, B, C and D) in the Montmajour sample (dotted line) and in the model sample (solid line).

Although the absorption spectra at issue are very similar also to the spectra of Crystal Violet and its demethylation products, there was no matching as for retention times;

however, this similarity suggested that the extra peaks are due to dyes of the triarylmethane class. Ethyl violet has been taken into consideration as a possible species responsible for these extra peaks, but the results of LM-MS analysis ruled out this hypothesis.

To conclude, it is possible that the extra peaks found in the Montmajour drawing are due to unknown dyes already present in the methyl violet mixture used to prepare the ink, rather than to degradation products of Crystal Violet.

The fact that methyl violet mixtures (at least from Farbenfabriken Fr. Bayer & Co and from imperial chemical industries limited, hexagonhouse, blackley, Manchester) did contain some other minor components besides crystal violet and its demethylated derivatives, is an important piece of information that was obtained from the analysis of the dyes from the ICN collection. Another important information is that two samples of the same kind of product (Methyl Violet 3B) from the same brand (Farbenfabriken Fr. Bayer & Co Elberfeld) did have in fact slightly different formulations. The chromatograms of the two samples are shown in figure 64, where it can be seen that the extra peaks (at values of retention time higher that 22 minutes) that were observed for the sample number 7065, were not present in the sample number 4051. This is to underline the existing uncertainty about dye (and ink) recipes, also when the trade name and brand of a product are known.

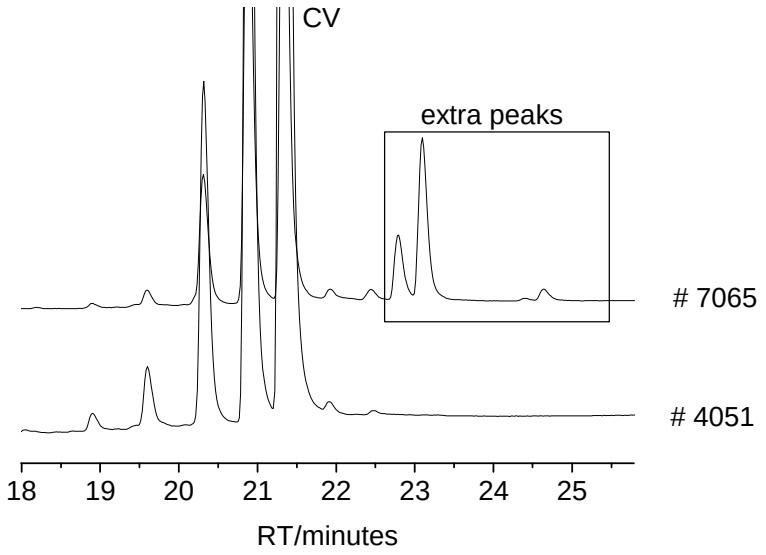

Figure 64: chromatograms of two samples (number 7065 and 4051 according to the ICN collection) of Methyl Violet 3B from the same brand (Farbenfabriken Fr. Bayer & Co Elberfeld).

As for the brown discoloration of the ink occurred on the Montmajour drawing, three main reasons can be invoked. First of all, the ink used might have contained some dye(s) that turned brown upon aging. In turn, aging might be due to many reasons, among others exposure to light, pollutants, humidity or heat. Secondly, the ink might have contained additives responsible for the discoloration. Finally, there might have been present some impurities in paper (such as Fe(III)) able to react with the ink and yield colored products. To complicate the scenario, it is also possible that interactions between two or more components took place, leading to the brown color visible nowadays.

As it has already been said previously, the analysis of Montmajour samples revealed also the presence of dyes other than crystal violet and its demethylated derivatives. Nevertheless, they are likely to be of the triarylmethane class and, so far, none of the triarylmethane dyes studied in this work (crystal violet, pararosaniline and diamond green) turned brown upon light exposure on paper.

Moreover, the presence of Fe(III) was detected with XRF whereas no copper or chromium were found on the Montmajour drawing. As a consequence, the brown color could not have been caused by chromium logwood and copper logwood.

Based on the model samples studied in this work, it is possible to hypothesize that the brown discoloration is due to the presence of additives. Indeed, model samples of ink (made of methyl violet according to a recipe by Lehner) on cellulose paper looked similar to the color of the Montmajour drawing after they were exposed to UV-Vis radiation or sun light (figure 40). This was especially true for the (more yellowed) sample of paper enriched with additional Fe(III). It should be underlined that the brownish-grey color of the sample enriched with Fe(III) might also be ascribed to the superimposition of two colored layers; that is, the bluish-grey color of the faded ink (observed on the sample with no additional iron) might look brownish if superimposed to a yellowish background (the yellowed paper containing additional Fe(III)).

Nevertheless, it should be underlined that no information about the original ink recipe is available and consequently the ink used by Van Gogh might have contained different additives from the ones in the reconstructed ink.

Finally, given the effect of NO_2 on crystal violet, it can not be excluded that the discoloration of the Montmajour drawing was also due to exposure to environmental pollutants.

7) FORS analysis of letters written with purple ink.

Three letters (private collection, Birgit Reissland) showing purple or bluish writings or stamps were analyzed with FORS. In order to focus the analysis on such small dyed areas as ink strokes, a direct reflectance probe was used instead of the integrating sphere. The first one was a letter from the Dutch Ministry of Foreign Affairs dating back to the 1889 and showing bluish purple writings and stamp whereas the second and third ones were personal letters from the 1871 (written in purple) and (possibly) from the 1875 (written in purplish blue) respectively.

Letter one was analyzed both on the purple stamp (sampling denoted PS) and on a light purple area of the writings (sampling denoted LPW). Letter two and three were analyzed once, on the purple writings (sampling denoted PW) and the purplish blue writings (sampling denoted PBW) respectively. The reflectance spectra obtained are shown in figures 65 and 66, together with the reflectance spectrum of a model sample of cotton linters paper written with Crystal Violet. The reflectance spectrum of an undyed area of the paper of each letter (or the model sample) was subtracted as blank.

As for letter one and two, the ink used for writing showed reflectance spectra (LPW and PW) very similar to the one of the model sample of Crystal Violet (CV). As for the purple stamp (PS) on letter one, the intensity of the reflectance spectrum obtained was very low, since the ink layer was very pale. Nevertheless, it suggested the presence of purple dyes of the triarylmethane class.

HPLC-PDA analyses[15] confirmed the presence of Methyl Violet both in the ink of the stamp and of the writings of letter one. As for letter two, the concentration of the sample analyzed with HPLC-PDA was very low and enabled to obtain a very noisy spectrum which was, however, consistent with Methyl Violet.

As for letter three, the reflectance spectrum was not as similar to the one of the reference as in the cases just described. The width of the spectrum is much larger than the model one and the maximum of reflectance is blue shifted, in agreement with the bluish color of the writings. It is worth noting that particularly large spectral widths were also observed for samples of paper dyed with a high concentration of Crystal Violet. It is therefore possible that in this case the ink manufacturer used a mixture of concentrate Methyl Violet or Crystal Violet with other blue dyes, with the aim of obtaining a deep blue hue. HPLC-PDA analysis revealed the presence of species with

[15] Performed at the ICN by Art Néss Proaño Gaibor.

absorption spectra consistent with Methyl Violet. However, one should bear in mind that triarylmethane dyes with structures very similar to Methyl Violet (such as for example Ethyl Violet, a bluer dye than Crystal Violet, having six ethyl groups instead of methyl groups) have absorption spectra very similar to Crystal Violet.

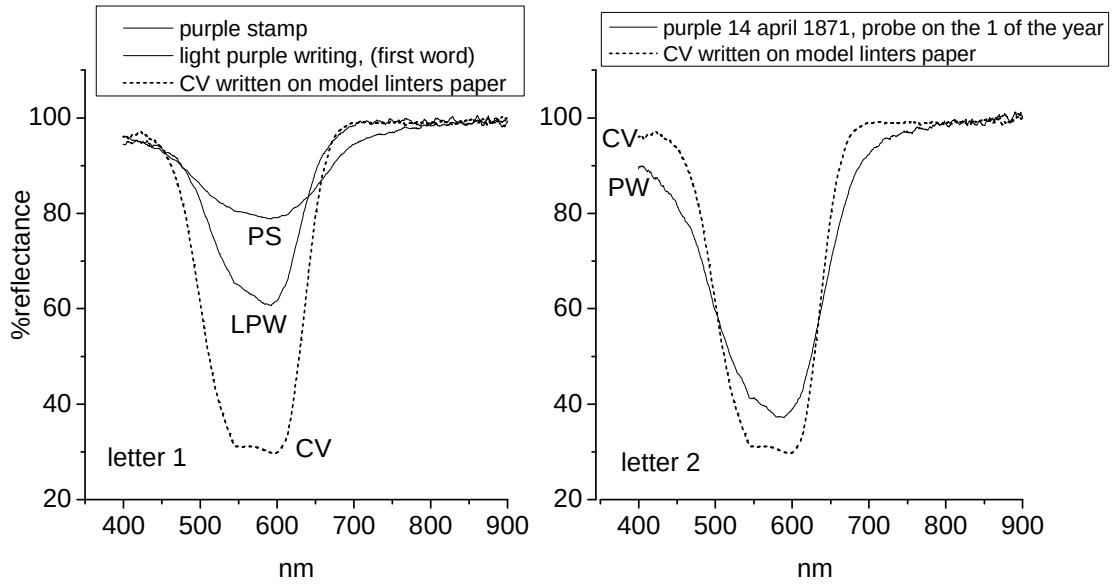

Figure 65: reflectance spectra of purple writings (LPW and PW) and a purple stamp (PS) on two letters from the XIX century and of a reference sample of cellulose paper dyed with CV (dotted line labelled CV).

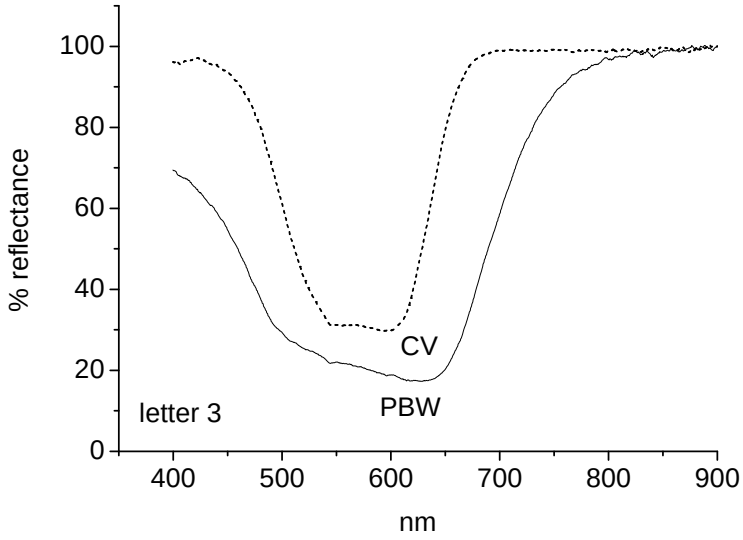

Figure 66: reflectance spectra of purplish blue writings (PBW) on a letter (possibly) from the XIX century and of a reference sample of cellulose paper dyed with CV (CV).

From the historical samples analyzed in the present work, it is possible to conclude that the use of methyl violet inks was common, if not very diffused, during the last

decades of the XIX century. The issue of the poor lightfastness of triarylmethane dyes is therefore very pressing and would deserve full attention on the part of conservators and conservation scientists.

CONCLUSION

The photoinduced degradation of Crystal Violet was studied both in aqueous solution and on paper via HPLC-PDA, LC-MS and FORS.

As for the dye in solution, during UV irradiation the sample showed a color shift form purple to reddish. HPLC-PDA combined with LC-MS enabled to detect the degradation products formed: the photo-fading of Crystal Violet was demonstrated to be due to demethylation reactions (leading to colored products) and oxidation at the central carbon atom giving rise to colorless (or imperceptibly colored) aromatic ketones (such as Michler's ketone or its demethylated derivatives). A series of demethylation products from Crystal Violet (hexamethylated pararosaniline) to pararosaniline (fully-demethylated Crystal Violet) were detected in contrast with [Duxbury], where it was reported that one methyl group per nitrogen atom at most would be removed during degradation. There was no evidence for deamination reactions. Moreover, a group of absorption spectra different from the ones of Crystal Violet or its demethylated derivatives, were detected. The hypothesis was made that they are due to N-oxide derivatives of Crystal Violet.

It was also demonstrated that, in the presence of Michler's ketone, the rate of consumption of Crystal Violet on paper exposed to UV is higher. Michler's ketone was also consumed during the reaction.

As for Crystal Violet on paper, contrary to what observed in solution, the color of the dye turned from deep purple (before irradiation) through light blue to almost invisible. Nevertheless, with the experimental conditions adopted, degradation products detected for CV on Whatman paper were the same as for CV in solution. Moreover, FORS enabled to express in term of colorimetric L*a*b* values the color change of CV on paper and to detect the change in concentration and in aggregation type for CV during irradiation. The complete fading of the ink observed on a Menu drawn and written by Van Gogh when he was in Paris in 1886 was therefore reproduced.

In an attempt to study more realistic samples than Whatman paper, also other substrates (cotton linters paper, lignin paper and printing paper) were taken into consideration and the degradation of crystal violet was demonstrated to produce the same degradation products (although at different rates) as on Whatman paper. Only one minor difference was observed for printing paper: on this substrate, Crystal Violet formed an unknown compound that had not been observed for the other kinds of paper. Moreover, an initial retardant effect of lignin on the rate of consumption of Crystal

Violet was observed: the hypothesis was proposed that the reactions that lead to the yellowing of lignin compete with Crystal Violet for the UV radiation, thus (initially) slowing down dye fading. Indeed, on a pre-yellowed sample of lignin paper the effect of lignin was not observed.

The color change of Crystal Violet on paper was also studied during micro-fading tests with visible light alone and it was demonstrated that visible light is also involved in the degradation of this dye. This information is of fundamental importance for planning, for example, an exhibition of the Van Gogh drawings made with triarylmethane dyes. The same tests were also run in the presence and absence of such an ink additive as gum arabic. In its absence, the color change on printing and lignin paper was higher than on cellulose paper whereas in its presence the contrary was observed. Although an explanation for this behaviour has still to be found, this observation is of interest in the field of conservation science since it demonstrates the importance of studying more realistic samples where the interaction among different components (e.g. paper substrates, ink additives) can lead to different results with respect to (simplified) model samples. To this regard, multidisciplinary studies on artist's working practice and on materials used would be very effective and could be of much help for scientists.

Always in an attempt to study more realistic samples, an ink was reconstructed according to a recipe described in [Lehner] and its photo-fading was studied on different paper substrates and in the presence or absence of additional Fe(III). The choice of studying the effect of Fe(III) was due to the fact that Fe(III) is commonly present on paper (it can be introduced with water or come from work machinery) and it is also known for catalyzing radical reactions, responsible for the degradation of paper. Interestingly, the color of ink strokes on cellulose paper after exposure both to UV-Vis radiation and natural sun light was bluish-grey or brownish-grey in the absence or in the presence of additional iron respectively. This kind of discoloration had never been observed on the samples of paper dyed with pure crystal violet described so far. Again, this observation underlines the importance of studying real museum objects, in order to reproduce targeted model samples. In this regard, it would be necessary to boost accessibility to museum collections so that scientists can analyze real objects in their real environment.

As for Fe(III), its presence on undyed paper was associated to the formation of yellow stains whose ATR-IR spectra shown an higher than normal concentration of carbonyl groups.

Samples of both pure crystal violet and of ink on paper were also exposed to common gaseous pollutants such as NO_2 or O_3. The effect of NO_2 on the color of the samples was much more drastic than that of O_3: the latter did only cause a slight lighting of the color of dyed cotton linters samples whereas the former was responsible for a significant fading of pure Crystal Violet on cotton linters paper, for the discoloration to dark blue of the pure dye on lignin paper and protein sized paper and for a severe darkening of the ink on paper. A blue colored nitrosoamine was identified on dyed cotton linters paper.

EPR studies on samples of crystal violet on paper both in the presence and in the absence of oxygen demonstrated that crystal violet strongly enhances the formation of radicals upon irradiation with UV. A comparison between the EPR spectra of these samples and of the radical cation of crystal violet (and related dyes such as diamond green and pararosaniline) suggested the formation of radicals of cellulose rather than of crystal violet, during irradiation of dyed samples of paper. Crystal violet would therefore acts as a sensitizer for the formation of radicals of cellulose during irradiation. This effect was observed both in the presence and in the absence of oxygen.

Moreover, it was demonstrated that the degradation of crystal violet on paper occurs also in the absence of oxygen, although in this case the color change was smaller than in the presence of oxygen. This finding is of particular interest if considered that anoxic protection is in use in museums.

In addition to the research on the fading of crystal violet, a preliminary study of the color change of other dyes and pigments used for making purple inks (indigo, indigo carmine, cochineal carmine ink, copper logwood and chromium logwood) was carried out. The most noteworthy examples of discoloration were observed for indigo carmine and copper logwood (synthesized from copper sulphate). Interestingly, the former was fugitive to UV-Vis radiation on cellulose, contrary to what is observed in aqueous solution [Sousa et al.]. The latter, turned purplish-brown or brown after photo-induced or thermal aging respectively.

Finally, in this work the analyses of three historical letters from the XIX century and of the drawing by Van Gogh (Arles, 1888) entitled Montmajour, are presented. The presence of methyl violet was revealed both in the drawing and on at least two of the

letters, thus confirming the diffusion of this mixture of dyes as an ink component during the last decades of the XIX century.

As for the Montmajour drawing, the causes of the brown discoloration of the original purple ink were investigated. First of all, the composition of the traces of purple ink protected under the frame was studied: Methyl Violet, possibly Fuchsine and other still unknown triarylmethane dyes were detected. On the contrary, the presence of copper or chromium logwood inks was excluded. Secondly, the composition of the paper was taken into account: it appeared to be softwood paper containing Fe(III) but no lignin.

Currently, the proposed hypothesis is that the brown color is due to two concomitant effects: the discoloration of the ink to a neutral color (possibly bluish grey) and the yellowing of the paper substrate. The superimposition of these two colors would result in a brown color. The participation of gaseous pollutants in the degradation occurred can not be excluded with certainty, though.

To conclude, the knowledge of the kind of products formed during ink fading and their concentration ratios may give interesting information about the original dye used for preparing the ink and consequently about the original color for example of a drawing. Nonetheless, it is important to bear in mind that Crystal Violet was often produced (and used) in a mixture with variously demethylated derivatives and, consequently, a better knowledge of historical recipes would be required in order not to misinterpret the results of compositional analyses of historical inks. Moreover, it would be fundamental to have better insight into the effects of natural aging processes, since accelerated aging tests often produce ‘unnatural’ effects. To do so, it would be necessary to monitor artworks during exhibitions and storage over years, in order to study the behavior of real objects in their real environment.

REFERENCES

[Abbott et al.] Abbott L C, MacFaul P, Jansen L, Oakes J, Smith J R L and Moore J N 2001 Spectroscopic and photochemical studies of xanthene and azo dyes on surfaces: cellophane as a mimic of paper and cotton *Dyes pigments* **48** 49-56.

[Allen] Allen N S 1994 Photofading and Light Stability of Dyed and Pigmented Polymers *Polymer degradation and stability* **44** 357-374.

[Allen et al.] Allen N, McKellar J F 1980 Photochemistry of dyed and pigmented polymers *Applied Science Publisher LTD* London.

[Arieli et al.] Arieli D, Vaughan D E W, Goldfarb D 2004 New Synthesis and Insight into the Structure of Blue Ultramarine Pigments *J. Am. Chem. Soc.* **126** 5776-5788.

[Attanasio et al.] Attanasio D, Platania R 2000 ESR Spectroscopy as a Tool for Identifying Joining Fragments of Antique Marbles: The Example of a Pulpit by Donatello and Michelozzo *Journal of Magnetic Resonance* **144** 322–329.

[Bangert et al.] Bangert R, Aichele W, Schollmeyer E, Weimann B and Herlinger H 1977 Photooxidation von Malachitgrun und Kristallviolett *Melliand Textilberichte* **5** 399-404.

[Blümich et al. 2003] Blümich B, Anferova S, Sharma S, Segre A L, Federici C 2003 Degradation of historical paper: non-destructive analysis by the NMR-MOUSE J. Magn. Reson **161** 204-209.

[Blümich et al.2010] Blümich B, Casanova F, Perlo J, Prosciutti F, Anselmi C and Doherty B 2010 Noninvasive Testing of Art and Cultural Heritage by Mobile NMR *Accounts of Chemical Research* Vol **46** No 6 761-770.

[Brailsford et al.] Brailsford J R, Woods J 1968 Electron spin resonance in cadmium sulphide *J. Phys. C: Solid State Phys.* **1** 1213.

[Braun et al.] Braun A M, Maurette M T, Oliveros E 1991 Photochemical Technology *Wiley John Wiley & Sons* Chichester New York Brisbane Toronto Singapore.

[Brezová et al.] Brezová V, Pigošová J, Havlínová B, Dvoranová D and Ďurovič M 2004 EPR study of photochemical transformations of triarylmethane dyes *Dyes and Pigments* **61** 177-198.

[Calvini et el. 2002] Calvini P, Gorassini A 2002 FTIR-Deconvolution Spectra of Paper Documents *Restaurator* 48-66.

[Calvini et al. 2006] Calvini P, Gorassini A, Chiggiato R 2006 Fourier Transform Infrared Analysis of Some Japanese Papers *Restaurator* **27** 81-89.

[Campanella et al.] Campanella L, Casoli A, Colombini M P, Marini Bettolo R, Matteini M, Migneco L M, Montenero A, Nodari L, Piccioli C, Plossi Zappalà M, Portalone G, Russo U, Sammartino M P 2007 La chimica per l'arte *Zanichelli* Bologna.

[Capitani et al.1996] Capitani D, Segre A L, Attanasio D, Blicharska B, Focher B, Capretti G 1996 ^{1}H NMR relaxation study of paper as a system of cellulose and water *Tappi J.* **79** 113-122.

[Capitani et al. 2002] Capitani D, Proietti N, Ziarelli F, Segre A L 2002 NMR study of water–filled pores in one of the most widely used polymeric material: the paper *Macromolecules* **35** 5536-5543.

[Casieri et al.] Casieri C, Bubici S, Viola I, De Luca F 2004 A low-resolution non-invasive NMR characterization of ancient paper *Solid State Nucl. Mag.* **26** 77-85.

[Centeno et al.] Centeno S A, Ropret P, Del Federico E, Shamir J, Itin B, Jerschow A 2010 Characterization of Al(III) Complexes with Hematein in Artistic Alum Logwood Inks Journal of Raman Spectroscopy **41** 445-451.

[Christie] Christie R M Colour Chemistry *RSC Paperbacks*.

[Clark et al. 1978] Clark R J H, Cobbold D G 1978 Characterization of Sulfur Radical Anions in Solutions of Alkali Polysulfides in Dimethylformamide and Hexamethylphosphoramide and in the Solid in Ultramarine Blue, Green and Red *Inorganic chemistry* vol **10** No 11 p. 3169.

[Clark et al. 1983] Clark R J H, Dines T J, Kurmoo M 1983 On the Nature of the Sulfur Chromophores in Ultramarine Blue, Green, Violet and Pink and of the Selenium Chromophore in Ultramarine Selenium: Characterization of Radical Anions by Electronic and Resonance Raman Spectroscopy and the Determination of Their Excited-State Geometries *Inorg. Chem.* **22** 2766-2772.

[Confortin] Confortin D 2007 Spettroscopie EPR e NMR Applicate ai Beni Culturali. Analisi del Degrado della Carta *Master Thesis*.

[Conn] Conn H J 1922 An Investigation of American Gentian Violets *Report of Committee on Bacteriological Technic*.

[Creighton] Creighton H J M *Assistant Professor of Chemistry in Swarthmore College, Swarthmore, Pa., USA* 1919 A Method for Making Methyl Violet.

[Cuttle] Cuttle C 1996 Damage to Museum Objects Due to Light Exposure *International Journal of Lighting Research and Technology* **28** (1) 1-9.

[Delamare et al.] Delamare F, Guineau B Colour, Making and Using Dyes and Pigments *New Horizons Thames & Hudson.*

[Druzik] Druzik R 1985 Ozone: The Intractable Problem *Western Association for Art Conservation* **7** No 3 pp.3-9.

[Duxbury] Duxbury D F 1993 The photochemistry and Photophysics of Triphenylmethane Dyes in Solid and Liquid Media *Chemical Reviews* **93** 381-433.

[Feller 1994] Feller R L 1994 Accelerated Aging. Photochemical and Thermal Aspects *Research in Conservation, The Getty Conservation Institute*.

[Feller 2001] Feller R J 2001 Color Science in the Examination of Museum Objects. Non Destructive Procedures *Tools for Conservation, The Getty Conservation Institute*.

[Florian] Florian M-L E 2007 Protein facts. Fibrous Proteins in Cultural and Natural History Artifacts *Archetype Publications*.

[Giamalva et al.] Giamalva D H, Kenion G B, Church D F, Pryor W A 1987 Rates and Mechanisms of Reaction of Nitrogen Dioxide with Alkenes in Solution *Journal of the American chemical Society* **109** 7059-7063.

[Gordon et el.] Gordon P F and Gregory P 1983 Organic chemistry in colour *Springer-Verlag* Berlin Heidelberg New York London Paris Tokyo.

[Grosjean et al. 1989] Grosjean D, Whitmore P M, Cass G R, Druzik J R 1989 Ozone Fading of Triphenilmethane Colorants: Reaction Products and Mechanisms *Environmental Science Technology* **23** 1164-1167.

[Grosjean et al. 1992] Grosjean D, Salmon L G, Cass G R 1992 Fading of Organic Artists' Colorants by Atmospheric Nitric Acid: Reaction Products and Mechanisms *Environmental Science and Technology* **26** 952-959.

[Halliburton et al.] Halliburton L E, Giles N C, Garces N Y, Ming Luo, Chunchuan Xu, Lihai Baic, Boatner L A 2005 Production of native donors in ZnO by annealing at high temperature in Zn vapor *Applied Physics Letters* **87** 172108 - 172108-3.

[Havlinova et al.] Havlinova B, Jancovicova V, Brezova V, Ceppan M and Turanova M 2006 Study of aging of arylmethane dyes by UV-Vis spectroscopy *Restaurator* **27** 24-34.

[Huang et al.] Huang M, Russo R, Fookes B G and Sigman M E 2005 Analysis of Fiber Dyes By Liquid Chromatography Mass Spectrometry (LC-MS) with Electrospray Ionization: Discriminating Between Dyes with Indistinguishable UV-Visible Absorption Spectra *Journal of Forensic Science* Vol 50, No 3 526-534.

[Ischenko et al.] Ischenko V, Polarz S, Grote D, Stavarache V, Fink K, Driess M

2005 Zinc Oxide Nanoparticles with Defects *Advanced functional materials* **15** 1945-1954.

[Joosten et al.] Joosten I, van Bommel M R, Hofmann-de Keijzer R, Reschreiter H, 2006 Micro Analysis on Hallstatt Textiles: Colour and Condition *Microchimica Acta* **155** 169-174.

[Kazuko et al.] Kazuko Shirai, Masaru Matsuoka 1996 Structure and Properties of Hematein Derivatives *Dyes and Pigments* Vol **32** No 3 159-169.

[Larsen] edited by Larsen R 2002 Microanalysis of Parchment *Archetype Publications Ltd.*

[Lehner] Lehner S 1909 Die Tintenfabrikation 6th ed., *A Hartlebens Verlag, Wien und Leipzig* p. 170.

[Minolta] Precise Color Communication. Color Control from Feeling to Instrumentation *Minolta*.

[Nakamura et al.] Nakamura R and Hida M 1982 Photoreaction of crystal violet in solution *Sen-I Gakkaishi* **38** 183-90.

[Neevel] Neevel J G 1992 The Biacetyl-Azo Dye System: a Model System to Investigate Oxidative Dye Fading *PhD thesis*.

[Neevel et al.] Neevel J G, van Bommel M 2008 Non-invasive analysis of Van Gogh's drawing inks ICOM *committee for conservation, 15th triennial conference New Delhi, preprints volume I*

[Proost et al.] Proost K, Janssens K, Wagner B, Bulska E, Schreiner M 2004 Determination of Localized Fe^{2+}/Fe^{3+} Ratios in Inks of Historic Documents by Means of μ-XANES *Nuclear Instruments and Methods in Physics Research B* **213** 723-728.

[Reife et al.] Reife A, Freeman H S 1996 Environmental Chemistry of Dyes and Pigments *Wiley-Interscience Publication*.

[Reinhardt et al.] Reinhardt C; Anthony S Travis 2000 Heinrich Caro and the Creation of Modern Chemical Industry *Dordrecht; Boston: Kluwer Academic Publishers*.

[Saunders et al.] Saunders D, Kirby J 1996 Light-Induced Damage: Investigating the Reciprocity Principle *ICOM Committee for Conservation*

[Sharma et al.] Sharma S, Casanova F, Wache W, Segre A, Blumich B 2003 Analysis of historical porous building materials by the NMR-MOUSE *Magnetic Resonance Imaging* Vol. **21** 249-255.

[Sousa et al.] Sousa M M, Miguel C, Rodrigues I, Parola A J, Pina F, Seixas de Melo J S and Melo M J 2008 A photochemical study on the blue dye indigo: from solution to ancient Andean textiles *Photochemical and Photobiological Sciences* **7** 1353-1359.

[Stanoeva et al.] Stanoeva T, Neshchadin D, Gescheidt G, Ludvik J, Lajoie B, Batchelor S N 2005 An Investigation into the Initial Degradation Steps of Four Major Dye Chromophores: Study of Their One-Electron Oxidation and Reduction by EPR, ENDOR, Cyclic Voltammetry, and Theoretical Calculations *Journal of Physical Chemistry A* **109** 11103-11109.

[Stork et al.] Stork W H J, Lippits G J M, Mandel M 1972 Association of crystal violet in aqueous solutions *J. Phys. Chem.* **76** 1772-75.

[Turro] Turro N J Modern Molecular Photochemistry *University Science Books*.

[van den Berg] van den Berg J D J 2002 Analytical Chemical Studies on Traditional Linseed Oil Paints *PhD thesis*.

[van Gogh] The complete letters of Vincent van Gogh, 3 vols., Greenwich, Conn. 1958, p. 512.

[Vellekoop et al.] Vellekoop M, van Heugten S, with the assistance of Hageman M and Zwikker R, translated by Hoyle M, 'Vincent van Gogh Drawings, volume 3, Antwerp and Paris 1885-1888', *Van Gogh Museum*, Amsterdam.

[Viola et al.] Viola I, Bubici S, Casieri C, De Luca F 2004 The Codex Major of the Collectio Altaempsiana: a non-invasive NMR study of paper *J. Cult. Herit.* **5** 257-261.

[Whitmore et al. 1989] Whitmore P M, Cass G R 1989 The Fading of Artists' Colorants by Exposure to Atmospheric Nitrogen Dioxide *Studies in Conservation* **34** 85-97.

[Whitmore et at. 1999] Whitmore P M, Pan X, Bailie C 1999 'Predicting the fading of objects: identification of fugitive colorants through direct nondestructive lightfastness measurements', *JAIC* **38** 395-409.

[Zollinger] Zollinger H 2003 Color Chemistry, Syntheses, Properties, and Applications of Organic Dyes and Pigments *Third, revised edition Wiley-VCH.*

RINGRAZIAMENTI
ACKNOWLEDGMENTS

Vorrei ringraziare la Prof.ssa Marina Brustolon, per avermi dato la possibilità di continuare a lavorare nel campo dei beni culturali per questi tre anni di dottorato. La ringrazio anche per aver reso possibile l'esperienza per me importantissima di trascorrere un anno all'estero e di lavorare in un istituto di ricerca, il Netherlands Institute for Cultural Heritage (ICN, Amsterdam), completamente dedicato alla studio e alla conservazione dei beni culturali. Voglio ringraziare anche il Dott. Lorenzo Franco, il Dott. Alfonso Zoleo per il loro costante aiuto in laboratorio e nell'analisi dei dati. E poi tutti gli altri colleghi del laboratorio EPR di Padova, il Dott. Antonio Barbon, il Dott. Marco Ruzzi, il Dott. Marco Bortolus (grazie per le continue consulenze sul funzionamento degli spettrometri ;)), la Dott.ssa Claudia Bortolussi (grazie per tutti i bandi che mi mandi!!) e il Dott. Alberto Collauto.

Ringrazio inoltre il Prof. Paolo Pastore e la Dott.ssa Gabriella Favaro dell'Università di Padova, per avermi dato la possibilità di approfondire presso il loro gruppo le analisi cromatografiche iniziate all'ICN e per aver sempre avuto la disponibilità di discutere insieme delle problematiche legate alla mia ricerca e dei risultati sperimentali ottenuti.

Ringrazio infine la fondazione Aldo Gini, per la borsa di studio concessami per trascorrere un periodo di studio presso l'ICN.

I wish to thank Han Neevel and Maarten van Bommel for the great opportunity they gave me, of working in such a research institute as the ICN. I would also like to thank all the other people I met when working at the ICN. In particular, I thank Art Néss Proaño Gaibor for sharing with me his results of the HPLC-PDA analysis of the ink of some letters containing methyl violet (Birgit Reissland, private collection) and Birgit Reissland for her advice on my research activity and for arranging a fascinating visit at the storage area of the van Gogh museum.

Many thanks also to the Van Gogh Museum, for the permission to reproduce the images of the Montmajour drawing (Arles, 1888) and of a Menu (Paris, 1886) by van Gogh.

Finally, I wish to thank Daniel Burge and Nino Gordeladze of the Image Permanence Institute, Rochester Institute of Technology, New York, for the NO_2 and O_3 exposures.